



UNIVERSITEIT VAN PRETORIA
UNIVERSITY OF PRETORIA
YUNIBESITHI YA PRETORIA

Investigation of the effects of welding parameters on the tensile strength and fatigue life of the structural welded joints S355J2+N steel plate

by

Vusimuzi Patrick Moloji

Submitted in partial fulfilment of the requirements for the degree
Master of Mechanical Engineering

University of Pretoria

Department of Mechanical and Aeronautical Engineering

2023

Supervisor: Professor P.S. Heyns

Abstract

Title: Investigation of the effects of welding parameters on the tensile strength and fatigue life of the structural welded joints S355J2+N steel plate

Author: Vusimuzi Patrick Moloi

Student Number: 16360631

Supervisor: Professor P.S. Heyns

University: University of Pretoria

Department: Mechanical and Aeronautical Engineering

Degree: Master of Mechanical Engineering

The railway industry wants to obtain structural welded joints that have optimum weld strength and fatigue life. Since the variance of welding parameters producing welding defects and weak structural integrity, there are uncertainties in the selecting the welding parameters that produce a good structural welded joint with the necessary weld quality. This necessitates the optimisation of the welding parameters to produce welded joints with improved mechanical properties.

The impact of various welding parameters (i.e. wire-feed speed (WFS), voltage and travel speed) on the ultimate tensile strength (UTS) and fatigue life of S355J2+N single V butt weld produced by metal inert gas (MIG) robotic welding was experimentally investigated. The design of experiments (DOE) approach was used to optimise the welding parameters to ensure the reliability of the experimental results. A removable ceramic weld backing bar was used to improve weld root penetration and minimise the risk of lack of fusion. To ensure weld quality and reliability of the experimental results the flush ground welded joints were used to minimise the geometric notch effect. A minimum number of two specimens for each number of experiments were tested to ensure the correct evaluation of welds. The magnetic particle testing (MT) technique was used to detect the welding defects that might have an impact on the material properties of the welded joints. Analysis of variance (ANOVA) was used to precisely demonstrate which welding parameters had the greatest impact on the performance output of the welded joint and to determine interactions between welding parameters.

It was observed that varying the welding parameters had an impact on the weld quality. An increase in voltage and travel speed at lower WFS are the primary contributing factors to weld defects. Only the defect-free specimens were tested to avoid making the experimental results inconclusive for statistical analysis. According to the ANOVA results, voltage and travel speed interact to affect the welded joint's UTS. Increasing voltage increases the UTS of the welded joints at the higher ranges of travel speed, while decreasing the UTS in the lower and medium range of travel speed. The most influential welding parameter that affects the UTS of the welded joint is travel speed. The fatigue life of the welded joint is affected by interactions between WFS and travel speed, as well as the voltage and travel speed. Increasing WFS increases the fatigue life at the medium range of travel speed. When welding at lower speed, the fatigue life duration becomes longer as the voltage increases. The fatigue life of the welded joint is significantly influenced by the WFS. The optimal welding parameters for the welded joint is A2B1C1 (i.e. WFS at level 2, voltage at level 1 and travel speed at level 1) for better UTS and fatigue life.

This research reduces uncertainties in the selection of optimum settings of welding parameters of a MIG welded joint. The welding parameters that significantly affect the welded joint mechanical properties performance were identified. The optimum welding parameters selection for UTS and fatigue life can

be developed. Undesirable welding defects that affect the structural integrity of the welded joint can be minimised by an improved selection of welding parameters.

Key terms: Welding parameters, Metal inert Gas (MIG), Tensile strength, Fatigue life, Design of Experiments (DOE), Analysis of Variance (ANOVA)

Acknowledgements

I would like to acknowledge and thank the following people for their contribution to this work:

- Prof. Stephan Heyns for his patience and guidance throughout the period of this study.
- Dr. Velaphi Matjeke for his mentoring, guidance and support in ensuring that funding for this research project is available.
- Mr. Stephan Bellingan for his assistance with tensile and hardness testing.
- Mr. Rion Venter, Mr. Johan Kruger and Miss Mari Hanekom for their assistance in cutting and extraction of testing specimens.
- Mr. Koena Ramoroka for his assistance with magnetic particle inspection.
- Mr. Hanni Miller for his assistance with robotic MIG welding.
- Mr. Herman Booysen for his assistance with fatigue testing.
- My wife Nokulunga and friends for their continuous support throughout my study.
- Transnet Engineering for providing me with the opportunity to further my engineering skills and knowledge by pursuing my master's degree in mechanical engineering.

Table of Contents

1.	Introduction.....	1
1.1.	Background.....	1
1.2.	Problem statement.....	2
1.3.	Literature review.....	2
1.3.1.	Significance of welding parameters on the mechanical properties of welded joints	2
1.3.2.	The impact of heat input on weld strength.....	5
1.3.3.	Metallurgical characteristics and the impact of heat input on the welded joints	5
1.3.4.	Effect of welding geometry on a welded joint’s mechanical properties	6
1.3.5.	Influence of shielding gasses on mechanical properties of welding joints	8
1.3.6.	Selection of filler wire for welding S355J2+N	9
1.3.7.	Structural steel plate for purposes of rolling stock manufacturing	10
1.3.8.	Effect of HAZ and filler material on fatigue strength.....	11
1.3.9.	Failure of welded joints.....	13
1.3.10.	Fracture behaviour of welded joints.....	13
1.4.	Scope of research	16
1.5.	Chapter outline.....	17
2.	Basic Theory	19
2.1.	Static and fatigue loading of welded joints.....	19
2.1.1.	Mean and amplitude stress effect.....	19
2.1.2.	The relationship between ultimate tensile strength and fatigue strength	21
2.2.	Testing standards and data validation method	22
2.2.1.	Welded joint geometry.....	22
2.2.2.	Test methods	25
2.2.3.	Precision of test results	26
2.2.4.	Significance of robotic welding in minimising experimental variability.....	27
2.2.5.	Non-destructive testing	28
2.2.6.	Analysis of variance (ANOVA).....	30
2.3.	Conclusion	34
3.	Research methods and material.....	35
3.1.	Material and welding parameters selection.....	35
3.2.	Welded joint specimen geometry.....	36
3.3.	Experimental welding procedure	37
3.3.1.	Welding procedure.....	37

3.3.2.	Tensile testing experimental setup.....	40
3.3.3.	Fatigue testing experimental setup.....	41
3.3.4.	Stereoscope and hardness measurement	45
3.4.	Conclusion	46
4.	Results and discussion	47
4.1.	Effect of the welding parameters on ultimate tensile strength and fatigue life.....	47
4.2.	Analysis of variance results	50
4.2.1.	Effect of welding parameters on ultimate tensile strength of the welded joints	50
4.2.2.	Main effects and interaction effects plots of ultimate tensile strength on welded joints	51
4.2.3.	Effect of welding parameters on fatigue life of the welded joints	54
4.2.4.	Main effects and interaction effects plots of fatigue life on welded joints	55
4.2.5.	Discussion of ANOVA results	58
4.3.	Failure of welded joints.....	58
4.3.1.	Failure analysis of tensile tested specimens.....	59
4.3.2.	Failure analysis of fatigue tested specimens	60
4.3.3.	Macrostructural examination	61
4.3.4.	Hardness test	62
4.4.	Non-destructive testing	63
4.5.	Effect of welding parameters on UTS and fatigue life of the welded joints.....	65
4.6.	Conclusion	67
5.	Conclusion and recommendation.....	68
5.1.	Conclusion	68
5.2.	Contribution and limitations	69
5.3.	Recommendations for future work	69
6.	References.....	71
	Appendix A: Manufacturing process of welded joint specimen.....	77
	Appendix B: Experimental results and analysis summary.....	83

List of Figures

Figure 1: Bead and penetration shapes for various shielding gases (Shoeb, 2013).	8
Figure 2: Effect of welding on fatigue strength (Maddox, 2000)	11
Figure 3: An illustration showing the weldment areas in relation to the equilibrium Fe-C binary phase diagram (Li et al., 2018).	12
Figure 4: Three modes of crack surface displacements (Schijve, 2008).....	14
Figure 5: Ductile fracture modes of the welded joint (Kazasidis and Pantelis, 2017).....	14
Figure 6: Constant amplitude alternating stress curve (Budynas–Nisbett, 1997).....	20
Figure 7: Fatigue strength curve for constant amplitude stress ranges (Maddox, 2000)	21
Figure 8: Fatigue strength vs ultimate tensile strength (Maddox, 2000)	22
Figure 9: Specimens for transverse tensile test (AWS B4.0, 2016).....	23
Figure 10: Specimens for longitudinal tension test (AWS B4.0, 2016).....	24
Figure 11: Test specimen for plates (BS EN ISO 4136, 2012).....	25
Figure 12: Half skip distance for calibration of angle-beam probe.....	28
Figure 13: Principle of magnetic particle testing (Zolfaghari, Zolfaghari and Kolahan, 2018).....	29
Figure 14: Geometry of welded joint.....	37
Figure 15: Yaskawa Motoman XRC robot	38
Figure 16: Details of butt-welded joint specimens extracted from the welded plate	39
Figure 17: Experimental tensile testing	40
Figure 18: Experimental fatigue testing.....	42
Figure 19: Fatigue strength curve for direct stress range (Hobbacher, 2008).....	43
Figure 20: Fatigue loading diagram	44
Figure 21: Data logger cyclic loading.....	45
Figure 22: Mounted specimens for macrostructural examination.....	46
Figure 23: Mounted specimens for hardness test.....	46
Figure 24: Ultimate tensile strength and fatigue life vs. wire-feed speed diagram for constant travel speed (Level 1).....	49
Figure 25: Ultimate tensile strength and fatigue life vs. wire-feed speed diagram for constant travel speed (Level 2).....	49
Figure 26: Ultimate tensile strength and fatigue life vs. wire-feed speed diagram for constant travel speed (Level 3).....	49
Figure 27: Interaction plots for wire-feed speed, voltage and vice versa for mean of UTS	52
Figure 28: Interaction plots for wire-feed speed, travel speed and vice versa for mean of UTS.....	52
Figure 29: Interaction plots for voltage, travel speed and vice versa for mean of UTS.....	52
Figure 30: Effect of welding parameters on the mean of ultimate tensile strength on each level	53
Figure 31: Interaction plots for wire-feed speed, voltage and vice versa for mean of N_f	56
Figure 32: Interaction plots for wire-feed speed, travel speed and vice versa for mean of N_f	56
Figure 33: Interaction plots for voltage, travel speed and vice versa for mean of N_f	56
Figure 34: Effect of welding parameters on the mean of N_f on each level.....	57
Figure 35: Specimen failure in gauge test section	59
Figure 36: Stress - strain plot for three test specimens: 1A, 1B and 1C of the first experiment.....	59
Figure 37: Shear bands mode of fracture for tensile test	60
Figure 38: Fatigue tested specimen showing the location of fracture.....	60
Figure 39: Welded joint 3A	61
Figure 40: Welded joint 11C.....	62
Figure 41: Welded joint 27A	62

Figure 42: Hardness profile measurements of three selected experiments	63
Figure 43: Effect of welding parameters vs. welding defects on each level	65
Figure 44: Waterjet cut steel plates	77
Figure 45: Tacked plate	77
Figure 46: Fixture arrangement for fixing specimen	78
Figure 47: Welding pendant.....	78
Figure 48: Programming SKS Q80 controller	79
Figure 49: Robot welding	79
Figure 50: Root run.....	80
Figure 51: Welded plate.....	80
Figure 52: Welding parameters graphs for root run and capping run	81
Figure 53: MT preparation.....	81
Figure 54: MT performed on the welded.....	82
Figure 55: Manufactured specimens	82
Figure 56: Stress - strain plot for three test specimens of experiments number 1 to 6	83
Figure 57: Stress - strain plot for three test specimens of experiments number 7 to 14	84
Figure 58: Stress - strain plot for three test specimens of experiments number 15 to 20	85
Figure 59: Stress - strain diagram for three test specimens of experiments number 21 to 27	86
Figure 60: Welded joint 3A	89
Figure 61: Welded joint 11C.....	89
Figure 62: Welded joint 27A	89

List of Tables

Table 1: Chemical composition for steel grade S355JR and S355J2.....	11
Table 2: Precision condition	26
Table 3: Input welding parameter	36
Table 4: Nominal mechanical properties of S355J2+N base plates and welding material	36
Table 5: Welding parameters design of experiment	38
Table 6: Experimental results for UTS and fatigue life	48
Table 7: Summary results of analysis of variance for ultimate tensile strength of the welded joints ...	50
Table 8: Summary results of analysis of variance for number of cycles to failure	54
Table 9: Non-destructive testing	64
Table 10: Ultimate tensile strength and number of cycles to failure	66
Table 11: Ultimate tensile strength data analysis.....	87
Table 12: Number of cycles to failure data analysis	88

Abbreviations and Acronyms

Abbreviation	Description
AISI	American Iron and Steel Institute
Amp	Amperes
ANOVA	Analysis of Variance
AR	As rolled
ASTM	American Society for Testing and Material
AWS	American Welding Society
BS	British Standard
CG-HAZ	Coarse Grained-Heat Affected Zone
cm	Centimetre(s)
DOE	Design of Experiments
EBW	Electron Beam Welding
EN	European Standard
FAT	FAT class; Design Fatigue Strength according to IIW
FG-HAZ	Fine Grained-Heat Affected Zone
GMAW	Gas Metal Arc Welding
GRA	Grey Relational Analysis
GTAW	Gas Tungsten Arc Welding
HAZ	Heat Affected Zone
HCF	High-Cycle Fatigue
HI	Heat Input
HSS	High Strength Steel
IC-HAZ	Inter Critical-Heat Affected Zone
IIW	International Institute of Welding
ISO	International Organization for Standardization
LBW	Laser Beam Welding
LCF	Low-Cycle Fatigue
m	Metre(s)
MAG	Metal Active Gas
MIG	Metal inert Gas
mm	Millimetre(s)
MMA	Multipass Manual Metal Arc
MPa	Megapascal(s)
MS	Means of Squares
MSA & MSB	Between Mean of Squares
MSE	Within Means of Squares
MT	Magnetic Particle testing
+N/G3	Normalized
NDT	Non-Destructive Testing
OFW	Oxyacetylene Welding
PM	Parent Material
PQR	Procedure Qualification Record
RSW	Electric Resistance Spot Welding

S/N	Signal-to-Noise
SAW	Submerged Arc Welding
SN	Stress-Life
SS	Sum of Squares
SS(AB)	Factors & Levels Interaction Sums of Squares
SSA & SSB	Between Sums of Squares
SSE	Error Sum of Squares
SST	Total Sum of Squares, The Sum of MSA, MSB and MSE
TIG	Tungsten inert Gas
UHSS	Ultra-High Strength Steel
UTS	Ultimate Tensile Strength
V	Volts
WFS	Wire-Feed Speed
WM	Weld Metal
WPS	Welding Procedure Specification
YS	Yield Strength

English Letters and Symbols

Symbol	Definition
H_a	Alternative hypotheses
A	Cross-sectional area
df	Degrees of freedom
$N_{c,new}$	Design value of number of cycles
$F_{dynamic}$	Dynamic load
$ab(r - 1)$	Error degrees of freedom
X_i	Experimental result for the i^{th} experiment
m	Exponent of $S - N$ curve /Slope
F	F statistics (F-ratio)
\bar{X}	Grand mean
HI	Heat input
\bar{A}_i	Average of all response values associated with i^{th} level factor A
\bar{B}_j	Average of all response values associated with i^{th} level factor B
X_{ij}	j^{th} experiments result for i^{th} experiment
X_{ijk}	k^{th} observation when A is at level i and B is at level j
F_{max}	Maximum static load
\bar{X}	Mean of n experiments
P -value	Measure of probability
F_{min}	Minimum static load
R	Nominal load stress ratio
H_0	Null hypotheses
N	Number of cycles
N_c	Number of cycles at 2×10^6
N_f	Number of cycles to failure
n_i	Number of experiments for the i^{th} experiment
a	Number of levels of factor A
b	Number of levels of factor B
r	Number of replications per cell
k	Number of tested experiments levels
n	Number of the experiments tested
L_c	Parallel length
F_{static}	Static load
Σ	Sum
L_t	Total length of the test specimen
f_u	Ultimate tensile strength
s^2	Variance of n experiments
I	Current
V	Voltage
S	Travel speed
b_1	Width of shoulder
b	Width of the parallel length
f_y	Yield strength

Greek Symbols

σ_a	Amplitude stress
$\Delta\sigma_{c,new}$	Design value of stress range
σ_a	Load mean stress
σ_{max}	Maximum stress under cyclic loading
u_k	Mean of factors
σ_{min}	Minimum stress under cycle loading
α	Significant level in hypothesis test
ε_u	Strain at ultimate tensile strength
ε_y	Strain at yield strength
$\varepsilon - N$	Strain-life
$\Delta\sigma_c$	Stress range

Element Symbols

Ar	Argon
CO_2	Carbon dioxide
C	Carbon
Cu	Copper
Mn	Manganese
N	Nitrogen
O_2	Oxygen
P	Phosphorus
Si	Silicon
S	Sulphur

1. Introduction

1.1. Background

The fabrication of most rolling stock components is accomplished by welding (Madyira, Kumba and Kaymakci, 2017). According to the structural design requirements of the bogie frame, welded joints are critical points in the structure of the bogie frame (BS EN 13749, 2011). Cast components are currently replaced by fabricated components in most engineering applications, particularly in the railway industry, since casting is expensive for the production of limited numbers of components, compared to fabrication. Modern practice encourages rolling stock companies to automate their manufacturing processes. Automated welding is highly repeatable, reduces reworks, increases production, and lowers labour costs.

The metal inert gas (MIG) is extensively used in the railway industry to join a variety of ferrous and nonferrous material. It is widely used for its adaptability and simplicity of adjusting the method to robotic automation with its all-position capabilities (Basim *et al.*, 2017). The welding parameters like wire-feed speed (WFS), voltage and travel speed have a substantial impact on the welded joint's quality. According to published research, the welding parameters have an impact on the welding joint's weld quality (Karadeniz, Ozsarac and Yildiz, 2007; Ibrahim *et al.*, 2012; Madyira, Kumba and Kaymakci, 2017).

Optimum weld performance and economy may be attained while maintaining the welded component's safety and durability, according to the rolling stock designers (Maddox, 2000). Welding changes the microstructures of the material and makes it inhomogeneous, which has the potential of altering the ultimate tensile strength (UTS) and fatigue life of the welded joint. The UTS and fatigue life of steel welded joints are affected by variations in welding parameters such as WFS, voltage, and travel speed. The increase in welding defects like cracks and pore sizes was identified with the variation of welding parameters (Madyira, Kumba and Kaymakci, 2017). It is necessary to select welding parameters correctly that will produce welds of high quality. The conservative design allowable range values of welding parameters approved by the welding engineer allow variation of welding parameters that produce unnecessarily welding defects and weakens the welded joint. This research will identify the optimum welding parameter values with high-quality results of the welded joint.

The effect of microstructural changes on the welded joint depends upon the welding method, welding parameters, joint design, thickness, filler metal, shielding gas, and welder skill. Understanding the metallurgical characteristics of structural steel S355J2+N and its microstructural changes during welding will assist in providing a sound joint like or better than the parent material (PM) of the welding joint. Excellent weld quality means that the welded joint does not fracture on the weldment but on the PM. The welding parameters must be selected such that they produce a good quality weld with less heat input (HI) required to produce fusion and lower thermal distortion (Basim *et al.*, 2017). These will improve productivity and maintenance costs by minimising premature failure of the welded structures.

The mechanical properties of structural steel S355J2+N welded joints were tested in this research employing robotic MIG welding. Welding parameters such as WFS, voltage and travel speed were evaluated. The aim of the experiment was to investigate the influence of these welding parameters on the mechanical properties of the welded joints.

1.2. Problem statement

Rolling stock components such as fabricated bogies and wagon chassis are produced by the MIG process. These components are designed to withstand static, quasi-static and dynamic loads that may occur while they are in use without developing defects that will cause sudden fracture, irreversible deformation, and fatigue cracks. Fabricated bogies are expected to endure 8×10^6 cyclic loads without fatigue failure. Fatigue cracks may occur after 8×10^6 to 1×10^7 cyclic loads but without the likelihood of a total failure.

There is a limited amount of reliable ultimate tensile strength and fatigue data currently available regarding the effect of welding parameters such as WFS, voltage and travel speed of the welded joint produced by the MIG technique. The welding parameters are normally optimised, based on improving the weld strength. However, there is limited data on optimised welding parameter selection that takes into consideration the weld strength and fatigue life of the welded joint. The welding parameters range specified on the welding procedure specification (WPS) allows variation of welding parameters. Variations of welding parameters produce welding defects and weak structural integrity on the welded components. Obtaining reliable experimental tensile strength and fatigue data of the welded joint is an essential step in selecting the optimum welding parameter combinations and is fundamental to manufacturing.

1.3. Literature review

This section presents a discussion of recent work done on the topic by other scholars and identifies what has not been reported. This section goes into extensive detail on the variables impacting the mechanical properties of the welded joint. In sections 1.3.1 and 1.3.2, it is addressed how important welding parameters and HI are to the mechanical properties of welded joint. Sections 1.3.3 and 1.3.4 explore the mechanical properties of welded joints in terms of their metallurgical characteristics and the impact that welding geometry has on them. The influence of shielding gas and filler material for MIG welding is discussed in sections 1.3.5 and 1.3.6. The selection of the structural steel for purposes of rolling stock manufacturing is discussed in section 1.3.7. The effect of the heat-affected zone (HAZ) and filler material on fatigue strength is discussed in section 1.3.8. Failure and fracture behaviour of welded joints are discussed in sections 1.3.9 and 1.3.10.

1.3.1. Significance of welding parameters on the mechanical properties of welded joints

Fusion welding is a process that has many input welding parameters which are current, voltage, travel speed, electrode size, gas flow rate, shielding gas composition and welding position. The correct welding parameters must be selected in order to get the optimum welding strength of the welded joint. The structural integrity of the welded joint is affected by the welding parameters (Sankar, Lawrence and Jayabal, 2018). The strength of the welded joint is improved by optimising the welding parameters namely current, travel speed, voltage, electrode size, gas flow rate, shielding gas composition and welding position (Basim *et al.*, 2017; Vanaja, 2017; Reddy Vempati, Brahma Raju and Venkata Subbaiah, 2018). These welding parameters are investigated using different welding processes to improve the welding strength of welded joint steel.

The production of rolling stock components is mostly achieved through MIG welding. The development of the most productive and high quality fusion welding method is being led by MIG welding (Ibrahim *et al.*, 2012). The variation of welding parameters determines the weld quality of the welded joint. Ibrahim *et al.* (2012) used robotic MIG welding for examining the welding parameters that influence the penetration, microstructure, and hardness of the 6 mm thick mild steel of welded joint. Current, voltage, travel speed, and CO_2 as shielding gas were taken as welding parameters. Ghazvinloo and Shadfar (2010) investigated the impact of MIG robotic welding parameters, which include current, voltage and travel speed on the fatigue life, impact energy, and bead penetration of aluminium welded joints. It was observed that weld metal's (WM) fatigue life decreases with increasing HI, although its impact energy increases initially before drastically decreasing. AISI 310 steel's tensile strength and hardness were studied by Sankar, Lawrence and Jayabal (2018) in relation to MIG welding parameters. Grey relational analysis (GRA) based on Taguchi was used to examine the significant impacts of welding parameters like current, voltage and gas flow rate. The ultimate tensile strength of the welded joint was found to improve with higher travel speed and lower current.

Jagtap *et al.* (2017) used an experimental design technique to investigate how welding parameters affect the UTS and yield strength (YS) of welded steel plates (IS 2062 grade). To accomplish MIG welding, the following parameters were used: current, WFS and the number of passes. It was observed that increasing current beyond its moderate value decreases mechanical properties. Shinde *et al.* (2017) used response surface methods to examine how MIG welding parameters affected the UTS and YS of mild steel plates that were butt-welded using CO_2 as shielding gas. The variation of the welding parameters including current, voltage and the flow rate of shielding gas was investigated. Since reduced grain size structures have greater strength, it was established that welded joints created with low HI should be used to obtain optimal strength of welded joints (Shinde *et al.*, 2017). Kumar, Khurana and Yadav (2016) examined the impact of the MIG welding process parameters that include current, travel speed, and gas flow rate utilising CO_2 as shielding gas on the bead geometry. The optimal bead geometry was determined using grey relation analysis based on Taguchi method, and its findings indicated that the travel speed is the most essential welding parameter.

Mishra, Panda and Mohanta (2014) looked at how welding parameters such as current, voltage, and travel speed affect the penetration depth of welded joints made of AISI 1020 steel. The penetration was observed to be affected by current and travel speed. The impact of welding parameters on the fatigue life of railway bogie welded joints was examined by Madyira, Kumba and Kaymakci (2017). An optical microscope was used to check the manufactured joints for defects like cracks and porosity when travel speed and welding angle were varied. The Paris law was used to predict how welding variables would affect fatigue life. It was shown that when travel speed increased welding defects such as crack and pore sizes also increased. Hussain *et al.* (2010) employed gas tungsten arc welding (GTAW) to examine the impact of travel speed on the tensile strength of the welded joint of aluminium. The UTS of the welded joint was found to be reduced as the travel speed increased, which also caused more welding defects.

The MIG welding process has been researched in order to optimise the welding parameters to enhance the welding strength of the welded joint connection of the steel (Ibrahim *et al.*, 2012; Vanaja, 2017; Sankar, Lawrence and Jayabal, 2018). Bęczkowski and Gucwa (2014); Basim *et al.* (2017); Biswas *et al.* (2018) experimental investigated the impact of welding variables on the mechanical properties of dissimilar welded joints using gas metal arc welding (GMAW). The welded dissimilar materials have completely different metallurgical characteristics that make it challenging to join with fusion melting methods without compromising the welded joint's structural integrity. The weldability of dissimilar

metals is depending on many factors (Biswas *et al.*, 2018), however is connected by the solid-state welding method without any difficulties (Celik and Ersozlu, 2009; Mercan, Aydin and Özdemir, 2015).

The mechanical properties of stainless steel and medium carbon steel welded joints have been examined by Biswas *et al.* (2018) utilising MIG welding variables current, voltage, and travel speed gas flow rate. Based on analysis of variance (ANOVA) and Taguchi's signal-to-noise (S/N) ratio analysis, it was shown that the current has a substantial influence on the mechanical properties of the welded joints. Other welding parameters which include voltage, travel speed, and gas flow rate are not statistically significant for UTS.

The quality of welding may be influenced by the atmosphere environment. During fusion welding, shielding gas is necessary to protect the weld pool from atmospheric gases. The welded specimen may react with oxygen in the atmosphere once heated during welding and results in porosity in the weld if the weld pool is not shielded from atmospheric gases. Therefore, it is usually necessary to use a shielding gas of some kind to keep air out of the molten weld pool (Kaçar and Kökemli, 2005). GMAW and GTAW need a shielding gas to develop a controlled atmosphere. The flux-cored arc welding (FCAW) method utilises continuous flux-cored filler material to develop the controlled atmosphere. The distinction between these processes is that the GMAW and GTAW generate slag, however FCAW does not generate slag.

The impact of a controlled environment on the arc weldment properties of MIG and metal active gas (MAG) welding was investigated by Kaçar and Kökemli (2005). The particular type of gases utilised in the welding technique determines the difference between MIG and MAG welding. MIG welding uses inert gases as the shielding and MAG welding uses active shielding gases. The metal active gas mixtures have been developed primarily for welding steels. Kaçar and Kökemli (2005) designed a controlled environment enclosed space for the gas metal arc welding method (CAGMAW) using identical welding parameters to the GMAW. The mechanical and metallurgical properties of each weldment of the traditional GMAW method and CAGMAW method were evaluated. Various temperatures were used during the experiments. It has been observed that the weldments that are made by GMAW have a wide HAZ compared to the CAGMAW. The microstructure of GMAW has been shown to have significant gas porosity and inclusion whereas in CAGMAW no inclusion within the WM was observed. The results obtained indicated that the GMAW method exhibited lower tensile strength weldments compared to the CAGMAW process. Each welded joint of the COGMAW and GMAW process was acceptable as a result of all test specimens being broken from the PM.

In steel with a 2.5 mm thickness that was welded using robotic gas arc welding processes, Karadeniz, Ozsarac and Yildiz (2007) reported the impact of varying welding parameters on welding penetration. The welding variables like current, voltage and travel speed were investigated. The most significant elements influencing the level of weld quality, productiveness and cost of welded joint are the MIG welding parameters (Kim *et al.*, 2003; Karadeniz, Ozsarac and Yildiz, 2007; Ibrahim *et al.*, 2012).

Weld geometry is an essential variable in the design and manufacturing of the welded joints in the fabrication industries (Karadeniz, Ozsarac and Yildiz, 2007). The current should be precisely controlled when welding thin components because it has the significant influence on melting capacity, weld geometry and depth of penetration (Karadeniz, Ozsarac and Yildiz, 2007; Ibrahim *et al.*, 2012; Mishra, Panda and Mohanta, 2014). A very high current causes high penetration and a very low current results in insufficient penetration (Karadeniz, Ozsarac and Yildiz, 2007). The depth of penetration was shown to increase as current increased (Karadeniz, Ozsarac and Yildiz, 2007). It has also been observed that

the voltage has a substantial impact on the depth of penetration, but not as significantly as the current (Karadeniz, Ozsarac and Yildiz, 2007). In comparison to other welding parameters, current was shown to be the most significant variable. It has an impact on the current density, which in turn impacts the rate at which the filler and PM melt (Bęczkowski and Gucwa, 2014).

Exceptionally low travel speed causes accumulation of welding metal on the PM due to a large welding pool and results in low penetration. The depth penetration increases linearly as travel speed increases until it reaches the optimum value and begins to decrease linearly afterward point (Karadeniz, Ozsarac and Yildiz, 2007). It is important to prevent over-penetration as a result of its waste of material and rise in production cost (Karadeniz, Ozsarac and Yildiz, 2007).

1.3.2. The impact of heat input on weld strength

It has been proven by many scholars that HI influences the strength of the weld joint (Kumar and Shahi, 2011; Kazasidis and Pantelis, 2017). The structural integrity of the weld joint and the weld quality may both be improved by carefully selecting welding variables including current, voltage, and travel speed. Current (I), voltage (V), travel speed (S) and arc efficiency (η) all contribute to the calculation of heat input (HI) (BS EN 1011-1, 1998). Prior to calculating heat input the travel speed needs to be determined using equation (1.1).

$$\text{Welding speed } (S) = \frac{\text{length of weld}}{\text{Time to weld}} \quad (1.1)$$

$$\text{Heat Input } (HI) = \eta \frac{IV}{S} \quad (1.2)$$

It is evident from equation (1.2) that increased current, voltage, and decreasing travel speed all results in an increase in HI. It decreases by decreasing current, and voltage and increasing travel speed. Weld strength is substantially influenced by welding parameters like current and travel speed, although voltage has a much less impact (Patil and Waghmare, 2013; Vanaja, 2017; Sankar, Lawrence and Jayabal, 2018). The UTS of the welded joint is increased by increasing the travel speed and decreasing the current (Vanaja, 2017; Sankar, Lawrence and Jayabal, 2018). The UTS increases at low HI but decreases at high HI (Ghazvinloo and Shadfar, 2010; Sankar, Lawrence and Jayabal, 2018).

1.3.3. Metallurgical characteristics and the impact of heat input on the welded joints

Single pass and multipass welding joints have completely different metallurgical characteristics. Kolhe and Datta (2008) examined and compared the similarities and differences between several multipass submerged arc welding parameters of a steel butt welded joint. To ensure that the welded joints are free from defects, image analysis software was used to analyse the HAZ microstructure characteristics. Various HIs of the multipass submerged arc welding welded joint specimens were conducted to evaluate the hardness, fracture toughness and HAZ of the weld joint. It was observed that the level of HI can control the percentage of phases like ferrite, martensite and austenite content in the microstructure of welded structure (Kolhe and Datta, 2008). According to observations, submerged arc welding (SAW) causes a continual variation in the thermal cycle of the weld joint with each and every pass (Kolhe and Datta, 2008).

There is limited information regarding the variation of welding parameters for comparison between single-pass and multipass welding. The effect of HI is different between the single pass and multipass welded joint. However, single-pass welding is limited to a certain range of thicknesses depending on the amount of HI provided to achieve the thickness of the weld. It is challenging to achieve a good weld size of a thick design joint in a single pass without welding defects. To provide understanding of how HI affects the welded joint, it is vital to evaluate the impact of multipass compared to single pass. The HI in the multipass welded joint is high compared to a single pass. The prior runs serve as pre-heating for the following weld deposits (Murti *et al.*, 1993). Increased HI in multipass welded joints results in slow cooling rates subsequently reduces the hardness and UTS of the HAZ and WM.

Kazasidis and Pantelis (2017) used the robotic metal-cored arc welding (MCAW) process to examine the impact of HI on the microstructure, hardness and UTS of the welded joints. It was observed that the welded joint's strength is decreased by the excessive HI. It was also observed that when the HI decreases, the quantity of beads inside the weld region increases. The UTS and the YS of the welds decline as HI increases up to a certain level and then stabilise. Kumar and Shahi (2011) investigated how HI affected the microstructure and mechanical properties of welded joints made of AISI 304 steel using GTAW process. According to their research, welded joints with medium and high HI had lower UTS than welded joints made with low HI.

The type of weld joint determines how HI affects the UTS and fatigue life of the welded joint. The butt weld joint and lap weld joint have different weld bead geometry, load distribution and microstructure. The crack initiation in welded joints initiates in the weld toe or weld root, irrespective of the weld joint type. Basak, Pal and Shome (2016) examined how the welding parameters affected the microstructure, shear strength, fatigue life and weld geometry of the MIG brazed galvanized dual-phase steel lap joints. Basak, Pal and Shome (2016) reported that weld joint strength increases with increasing HI to a certain extent and then decreases with increasing HI. It was also observed that the fatigue life of the weld joint increases with increasing HI depending on weld geometry.

The HI has a significant impact on the mechanical properties of the welded joint. If HI is not controlled the welded material becomes prone to different metallurgical issues. The influence of HI and cumulative fatigue damage on the mechanical properties of MIG welded joints of dissimilar stainless steel plates was examined Flores *et al.* (2016). It was observed that yield stress is lower in welded joints with high HI compared to low HI and reported that UTS decreases as HI increases. Amraei *et al.* (2019) examined the impact of HI and cooling rate on the mechanical properties of MIG butt-welded made of various grades of high and ultra-high-strength steels (HSS/UHSS) including S700, S960 and S1100. According to Amraei *et al.* (2019), increasing the welding HI, reduces strain at UTS (ϵ_u), UTS to YS ratio $\left(\frac{f_u}{f_y}\right)$ and the ratio of strain at the YS to UTS $\left(\frac{\epsilon_u}{\epsilon_y}\right)$ of the weldments.

1.3.4. Effect of welding geometry on a welded joint's mechanical properties

The joint type significantly affects in depth penetration of the welded joint. Butt joint geometries can take a variety of shapes, including square, closed square, single-bevel, single-J, double-bevel, double-J, single-V, single-U, double-V and double-U. The square and closed square joints are simple and economical however are limited by joint thickness. The other joints are mostly used for thicker joints due to their geometry which makes welding accessible and ensures the strength of the welded structure.

The welded joint's mechanical properties were examined using root gaps of zero and two millimetres (Ullah *et al.*, 2019). It was shown that the welded specimens with root gaps yielded better UTS compared to zero *mm* root gaps. The 2 *mm* root gap provides accessibility for welding to achieve a suitable depth penetration of the root run. It was observed that the microstructure of the 2 *mm* root gap welded joint has a coarse grain structure compared to the zero *mm*. The welded joint with root gaps consumes more filler material, which causes the cooling process to take longer. The 2 *mm* root gap welded joint provides increased HI, which enhance the blending of PM with filler material and produces more columnar grain structures. In consequence of the presence of additional filler material in the root gap, the specimen with a 2 *mm* root gap exhibits higher average hardness than one with a zero *mm* root gap. The better welded joint configuration selection should have a root gap to give better weld in-depth penetration.

According to reports (Kim *et al.*, 2003; Shoeb, 2013), the bead geometry has a significant impact on the strength of a welded joints. Shoeb (2013) developed a model that predicts the required weld bead geometry and shape to identify the best welding parameters combination to enhance the weld strength. The effects of GMAW parameters like voltage, travel speed and current on bead width, bead height, depth of penetration, and HAZ width have been demonstrated by Mishra, Panda and Mohanta (2014); Kumar, Khurana and Yadav (2016). The welding parameters were optimised using the Taguchi technique combined with GRA. It has been demonstrated that travel speed and voltage are most essential welding variables that influence bead width, bead height, depth of penetration and HAZ width have been shown to be travel speed and voltage . Shoeb, (2013); Sankar, Lawrence and Jayabal (2018) examined how the welding parameters affected the shape of the weld beads. It was observed that the weld bead height and the width decreased, the voltage increased, and the weld penetration increased. It was also observed that when the gas flow rate increases the bead penetration and bead breadth remain constant, and the height increases (Shoeb, 2013).

The relationship between weld bead geometry and microstructure and the fatigue characteristics of HSS butt welds was examined (Ahiale and Oh, 2014). Ahiale and Oh (2014) compared the microstructure and fatigue behaviours of HSS butt weld joints with and without weld beads. They observed that all the specimens with beads had significantly less fatigue life than those without beads. Experimental research was conducted to determine the impact of weld geometry on the fatigue life of fillet welded cruciform joints that are not load-bearing (Lee *et al.*, 2009). According to Chang Hee Suh, Rac Gyu Lee, Sang Kyun Oh, (2011), the influence of bead geometry has a substantial impact on the fatigue life of welded joints. All butt weld failures with weld beads occurred at the weld toe because of stress concentration caused by the bead's geometric discontinuity (Lee *et al.*, 2009; Ahiale and Oh, 2014). Excessive bead penetration in height and width introduces a notch effect which could cause the failure of the welded joint. To improve the fatigue performance of the welded structure the optimum bead geometry must be obtained, or the bead must be ground flat equal to the thickness of the PM.

Zhao *et al.* (2012) studied the butt welds ground flush's fatigue behaviour under super-long life regime. It was discovered that the crack sources of butt weld ground originate from tiny scratches from machining traces on the surface of the specimen. The internal defects of the welded joint have less impact on fatigue life compared to machining scratches on the surface of the specimen. It was also discovered that the fatigue fracture of the ground flush butt-welded joints occurred at fusion line.

1.3.5. Influence of shielding gasses on mechanical properties of welding joints

To safeguard the weld pool throughout fusion welding against the arc atmospheric gases, shielding gas is required. MIG welding uses either argon or helium or carbon dioxide or a mix of argon and helium or a mix of argon and carbon for protecting the molten weld pool. The shielding gas chemically reacts with the molten weld pool. Therefore, it is important to select the shielding gas based on the attributes that affect how well the welding process works, which include (Singh, 2022):

- Chemical interaction of the gas with the distinct elements in the PM and filler material; thermal characteristics of the gas.
- The impact of each gas on the way metal is transferred.

Shielding gas selection must take into account a gas's thermal conductivity, or capacity to transfer thermal energy (Shoeb, 2013; Singh, 2022). The weld's thermal energy will travel further through the weld if its thermal conductivity is high (Singh, 2022). Helium and carbon dioxide have substantially greater thermal conductivities than argon (Shoeb, 2013). The method of metal transfer and depth of penetration of welded joint are determined by shielding gases. Figure 1 shows various shielding gases and their produced weld penetration.

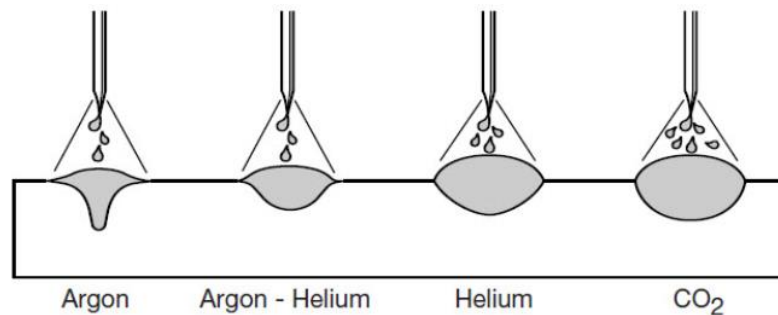


Figure 1: Bead and penetration shapes for various shielding gasses (Shoeb, 2013)

Welds with a wider penetration profile and greater depth of penetration are produced by using shielding gasses having a greater thermal conductivity, which include 100% helium or 100% carbon dioxide. Low thermal conductivity shielding gases like 100% argon (*Ar*), have shallower penetration profiles that are more tapered in the centre. The gas mixture of argon and helium results in a broader penetration profile and a better depth of penetration. The weld bead geometry is impacted by the shielding gas. The WM properties are relatively dependent on the weld bead geometry.

Inert gas like argon, carbon dioxide, helium, and oxygen are the most common shielding gases used in MIG welding. Argon is comparatively expensive compared to carbon dioxide, helium, and oxygen. One of the reactive gases that can be utilised without the addition of inert gas is carbon dioxide. Argon gas can also be utilised without the addition of inert gas in its pure form. The benefits of the different shielding gases and how they affect the HI are as follows (Singh, 2022):

- Argon facilitates more effective arc starting and arc stability due to its ability to transfer thermal energy at a lower level.
- When more HI is required, helium is employed as shielding gas. As a result of its high thermal conductivity this will require more voltage compared to argon to maintain a good arc stability.

- Argon/Helium combination is used when high thermal conductivity, better arc starting, and arc stability are required.
- Carbon dioxide is used when wider and deep penetration is required.
- Argon/Carbon combination is generally used for welding carbon steel using MIG welding process. It produces wider weld penetration compared to finger-like penetration of argon/oxygen mixture.

The GMAW process was used to investigate how HI and shielding gas affected the hardness, UTS, and impact strength of 2.25 Cr-Mo steel for welded joints (Pawaria *et al.*, 2013). Variation of the HI was achieved by varying current, voltage, and travel speed. Two mixtures of shielding gases were used such as 90%Ar + 10%CO₂ and 90%Ar + 8%CO₂ + 2%O₂. It has been shown that tests with low HI produce better results than tests with high HI, and shielding gas has little to no effect on the strength of welded joint (Pawaria *et al.*, 2013).

Chotai (2011) investigated the effect of four welding variables like current, travel speed, voltage, and shielding gas using the MIG welding process. The effect of shielding gas was studied by varying various combinations of shielding gas like 97.5% Ar + 2.5%CO₂, 90% Ar + 10%CO₂, 82% Ar + 18%CO₂ and 75% Ar + 25%CO₂. It was observed that variation of the welding variables namely current, travel speed, voltage and changing the composition of shielding gas produces changes in penetration. In addition to safeguarding the molten metal pool and maintaining arc stability, shielding gas utilised in the process also influences the weld's characteristics, bead geometry and depth of penetration. The increase in carbon dioxide content increases the depth of penetration. Sittichai, Santirat and Sompong (2012) examined the impact of welding parameters like current, travel speed, and shielding gas mixture on the mechanical properties of stainless steel AISI 304 with GMAW. The findings of the laboratory tests showed that the shielding gas mixture affects the UTS and percentage of elongation.

The shielding gas should be selected based on its properties that affect the performance of the welding processes. It was proven by many scholars that the composition of shielding gas does influence the weld bead geometry, HAZ and strength of the welded joint (Shoeb, 2013). It might be necessary to incorporate the impact of change in the composition of shielding gas in the HI formulation. The degree of thermal diffusivity, which depends on thermal conductivity, affects the HAZ. The welded material with higher thermal conductivity cools quickly and results in reduced HAZ. The welded material with lower thermal conductivity retains heat for a longer period and produces wider HAZ.

1.3.6. Selection of filler wire for welding S355J2+N

Solid wire electrodes are used in MIG welding. The different electrode diameter sizes and classification influence the weld depth of penetration. The smaller diameter electrode needs a lower amount of current density to achieve a better weld depth of penetration than the larger diameter electrode. The size of the electrode diameter influences the energy input. The important factors to consider for filler wire selection in MIG welding are (Jenney and O'Brien, 1969, 1991):

- The mechanical properties and chemical composition of the PM
- The use of shielding gas
- The design of the weld joint
- And the relevant criteria

Based on its chemical composition, solid wire electrodes are divided into many categories. Thermal differences in the WM, HAZ, and PM may result from variations in the filler material and PM's chemical composition (Ragu Nathan *et al.*, 2015). Under-matched filler metal cause a softening effect in the WM which leads to a reduction in the mechanical properties of the welded structure (Ahiale and Oh, 2014). The shielding gas employed should be within a specific group to match solid wire electrode mechanical properties. The welding voltage depends on the choice of shielding gas employed. It is evident that the solid wire electrode's chemical composition and HI have a significant impact on the WM's microstructure (Ragu Nathan *et al.*, 2015; Ullah *et al.*, 2019). Stoschka *et al.* (2013) studied how the fatigue behaviour of butt joints was affected by various combinations of filler material and shielding gas. The influence of the filler material was found to be negligible in the finite life region, however, exhibited an increase in endurance stress range. The effect of shielding gas showed an impact on the fatigue strength of the welded butt joint.

In this study, a mild steel solid wire electrode, not plated with copper, will be used to aid electrical conductivity and to prevent oxidation by employing the shielding gas that is within the specific group to match solid wire electrode mechanical properties. Generally, copper-plated wires are used to prevent rust and to improve the current to pass easily (Bęczkowski and Gucwa, 2014). The impact of the copper content of the plated electrodes on the mechanical and microstructure characteristics of multipass of the low alloy steel welded joints using manual metal arc (MMA) welding was investigated by Avazkonandeh-Gharavol, Haddad-Sabzevar and Haerian (2009). Three experimental copper plated electrodes with the final WM which has the variation of copper content of 0.14, 0.53 and 0.94 wt.% were investigated. It was observed that as the level of copper on the WM increases the microstructure becomes finer and the amount of acicular ferrite increases. The yield and UTS increase along with the copper content.

The proper selection of the filler wire should be taken into consideration in order to be able to optimise the melting temperature ranges of the metals, thermal conductivities, coefficient of thermal expansion, WM-PM integration, and joint design (Bęczkowski and Gucwa, 2014).

1.3.7. Structural steel plate for purposes of rolling stock manufacturing

Low carbon mild steel was selected for manufacturing the experimental test specimens because it has many applications across a wide range of industries namely, rolling stock, automotive, construction, manufacturing and mining. The structural steel plates are produced in four grades (i.e. S275JR, S355JR, S335J0, S335J2, and S355K2) in two yielding strength levels (i.e. 275 MPa, 355 MPa) with different temperatures (i.e. JR (20°C), J(0°C) and J2/K2(-20°C)) and condition such as AR (as rolled), +N/G3(normalized) (BS EN 10025-2, 2004). The S355J2+N structural steel plate was used in this study for specimen fabrication due to its benefits of low internal tensile residual stresses and improved mechanical properties like hardness and machinability. S355J2+N structural steel plate is high-strength steel with a fine-grained microstructure which provides a uniform structure and good bending qualities.

The S355J2+N structural steel plate has better benefits compared to S355JR because it has less carbon content. It has better cold-forming properties compared to S355JR and both the structural steel plate (i.e. S355JR and S355J2+N) properties are controlled by carbon content. The carbon content has a substantial effect on the mechanical properties of the welded joint. However, higher carbon content increases the hardenability of the welded joint and results in the risk of cold cracking during cooling

(Bęczkowski and Gucwa, 2014). S355J2+N structural steel plate has excellent weldability because it has less carbon content (Kalpakjian and Schmid, 2013). Table 1 displays the chemical composition of S355JR and S355J2 as specified by BS EN 10025-2 (2004).

Table 1: Chemical composition for steel grade S355JR and S355J2

Steel name	Carbon	Silicon	Manganese	Phosphorus	Sulphur	Nitrogen	Copper
S355JR+AR	0.24	0.55	1.6	0.035	0.012	0.012	0.55
S355J2+N	0.20	0.55	1.6	0.025	0.022	-	0.55

1.3.8. Effect of HAZ and filler material on fatigue strength

The microstructure of the welded joint and unwelded material are not similar (Jagtap *et al.*, 2017). Compared to welded materials, unwelded materials have a higher fatigue strength. The fatigue strength of an unwelded material correlates with its material strength, but it is different for a welded joint. According to Maddox (2000), an increase in material strength has no effect on the fatigue strength of a welded joint, but does have an effect on the fatigue strength of an unwelded joint. The test findings demonstrated that when YS of steel increases, so does the fatigue strength of the PM (Laitinen, Valkonen and Kömi, 2013).

Fatigue failure is governed by the fatigue crack initiation process which is more easily formed in the welded joint due to weld discontinuities like weld toe intrusions and welding defects compared to an unwelded joint. This results in the contrasts between the fatigue behaviour of welded and unwelded material. The presence of a weld generally reduces the fatigue strength of the welded joint (Dowling, 2005). Figure 2 shows the S-N curves for different fatigue failure designs. It is evident from Figure 2 that unwelded structures have better fatigue life compared to welded structures or structures with geometric discontinuity.

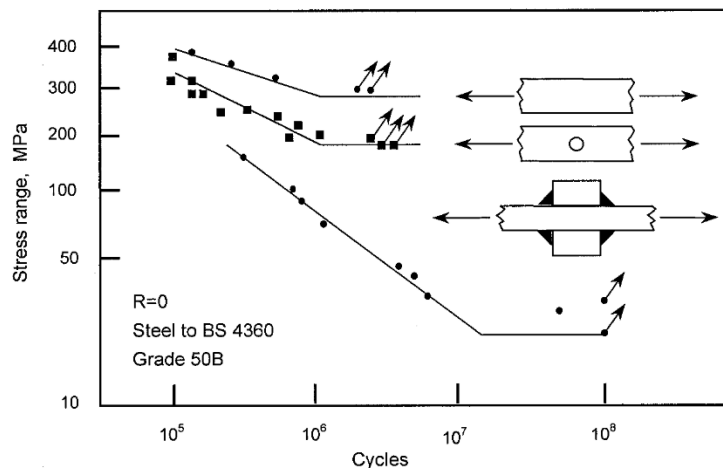


Figure 2: Effect of welding on fatigue strength (Maddox, 2000)

To investigate the failure of the welded joint, it is important to comprehend the properties of the weldment microstructure. It is known that the microstructure of a weld consists of three regions (i.e. a WM, a HAZ and a PM). The material properties of the welded joint are impacted by welding and the cooling rate after welding which develops an inhomogeneous microstructure. The inhomogeneous microstructure is developed due to grain structure formation. The width of the HAZ depends on the HI and the cooling time of the welded material (Pirinen, 2013). The phase diagram is used to illustrate the

correlation between the weld's highest temperature and the main phase transformation temperatures in Figure 3 below. The grain shape distribution for the butt transverse weld is depicted in Figure 3, where the HAZ microstructure characteristics are classified into coarse-grained (CG-HAZ), fine-grained (FG-HAZ) and inter-critical (IC-HAZ). It was observed that the failures normally start within the IC-HAZ region (Li *et al.*, 2018). The inter-critical zone is between fine-grained and PM which is made up of partly austenitized grains and over-tempered martensite laths (Wang, Kannan and Li, 2016). The hard martensite formed in the IC-HAZ makes the structure to be brittle and the brittle structure is susceptible to crack initiation.

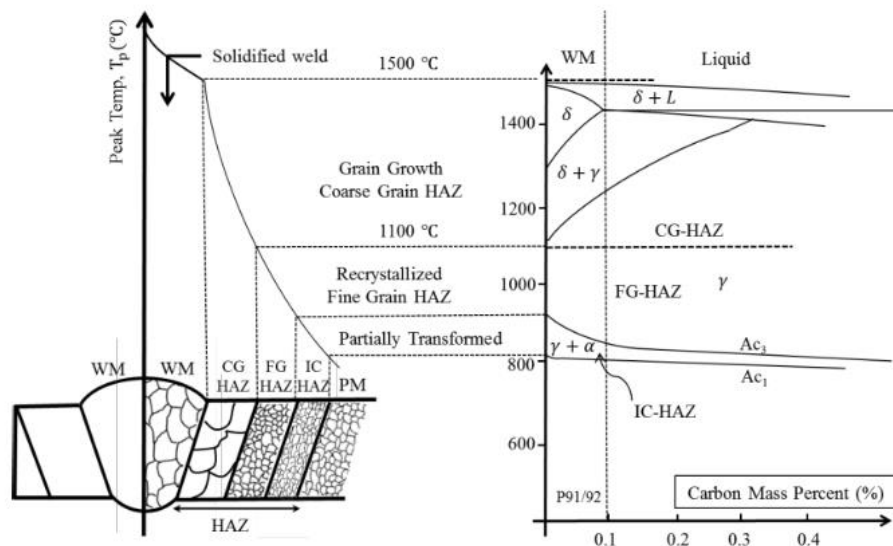


Figure 3: An illustration showing the weldment areas in relation to the equilibrium Fe-C binary phase diagram (Li *et al.*, 2018)

The hardness at the weld zone and HAZ are generally greater as compared to other zones of the welded joint specimens (Jagtap *et al.*, 2017). The grain size and hardness are directly affected by HI. According to research by Jagtap *et al.* (2017), as HI increases, the microstructure of the material becomes more ferrite-dominated and less pearlite-dominated, which results in a decrease in tensile strength. The relationship between the hardness and the UTS is generally linearly proportional, when the hardness increases the tensile strength increase as well. According to a microstructural analysis of welded joints with a root gap of 0 mm and 2 mm, the development of acicular ferrite is what gives the joints their improved mechanical characteristics (Ullah *et al.*, 2019). It was observed that higher HI causes a coarser grain structure in the WM due to a slower cooling rate (Ragu Nathan *et al.*, 2015). However lower HI causes fine structure due to a faster cooling rate.

Temperature changes in the PM and WM during welding have a significant impact on the material properties, residual stresses, and geometrical and shape accuracy of welded structural fabrication (Long *et al.*, 2009). The temperature variation during welding and subsequently cooling results in unavoidable distortions and residual stresses in the welded joint and PM. These affect the weld quality of the welded structures which may result in premature failure.

Structural steel elements like carbon increase the hardenability of the steel and result in the risk of cold cracking (Bęczkowski and Gucwa, 2014). The thicker structural steel plate should be preheated and the specified inter-pass temperature should be maintained to avoid unnecessarily cold cracking.

1.3.9. Failure of welded joints

Failure of a welded joint might be caused by the presence of defects in the weldment, lamellar tearing, residual stresses, hot cracking, and a bad microstructure due to welding parameters variation, under-matched shielding gas, or filler wire to the welded material. Microstructural variations across a weld joint due to temperature variation also cause failure of the welded joint. The most common failure of welding structures is fatigue failure (Callister, 2017). To ensure good quality and reliable welded joints, the joint should be designed such that the welder has adequate access to the joint design to ensure good fusion, particularly at the weld root of the joint. The impact of weld bead geometry and shape on fatigue life has been discussed in detail in section 1.3.4.

The WM is often stronger than the PM. The failure of the welded joint should occur in the PM or the HAZ. If it occurs in the WM, that indicates that there might be welding defects in the WM. In some cases, it might be due to under-matched filler metal or shielding gas and cause softening effect on the WM which lead to a reduction in the mechanical properties of the welded structure. The weld geometry affects the stress distribution of the welded joint and introduces high local stress concentration at the weld toe. The crack initiation principally occurs in highly stressed areas. A complete fusion or a fully penetrating weld at the root of a weld joint is vital for weld strength. Ottersböck *et al.* (2016) looked at how undercuts and other weld flaws affected the fatigue strength of UHSS butt welded joints. It was observed that the shape of the undercut substantially influences the crack formation stage. The undercut-defective specimen compared to the defective free specimen showed a distinct decrease in fatigue strength.

The fatigue strength of the welded joint is significantly affected by the surface finish quality (Laitinen, Valkonen and Kömi, 2013). Laitinen, Valkonen and Kömi (2013) observed that the rougher surface roughness and cut edges are the main factors affecting fatigue crack propagation. Marines *et al.* (2003) observed that machining traces of notches on the specimen accelerated the fatigue rupture. The surface roughness of the reduced section should not be rougher than 3 micrometres in order not to induce fatigue cracks (AWS B4.0, 2016). The surface roughness of 3 micrometres can be achieved by milling the reduced section of the welded specimen. The influence of the surface roughness of the cut material on the fatigue strength was examined by the international institute of welding (IIW) fatigue recommendations specification. The guidelines of the IIW fatigue recommendations specification give the fatigue classes (FAT) for the machined edges by machined gas cut and machined thermally cut.

The welded plate surface defects should be examined by visual inspection prior to welding, during welding, and after completion of the weld. ISO 5817 (2014) describes the surface imperfections that are visually inspected such as crack, undercut, crater crack, slag inclusion, blowhole, porosity, lack of root penetration, etc. Magnetic particle testing (MT) will be used for flaw detection in this study. The welded plates that are fit for purpose should be defective-free or exhibit defect sizes smaller than class B when visual inspection and subsurface inspection are performed (ISO 5817, 2014).

1.3.10. Fracture behaviour of welded joints

Fracture mechanics is the methodology that could be utilised to determine the fatigue life of a welded joint by taking into consideration the flaws (i.e. cracks, inclusions, pores, cavities, etc.) in the material. Failure of the welded joint is depending on the mode of loading. There are three modes of loading which involve different crack surface displacements based on concepts of elastic theory (Dowling, 2005). The

typically three modes of loading are shown in Figure 4 such as Mode I – Opening mode (Tensile), Mode II – Sliding mode (in-plane shear), and Mode III – Tearing mode (out-of-plane shear). This study focuses on Mode I which is the most regular mode of loading.

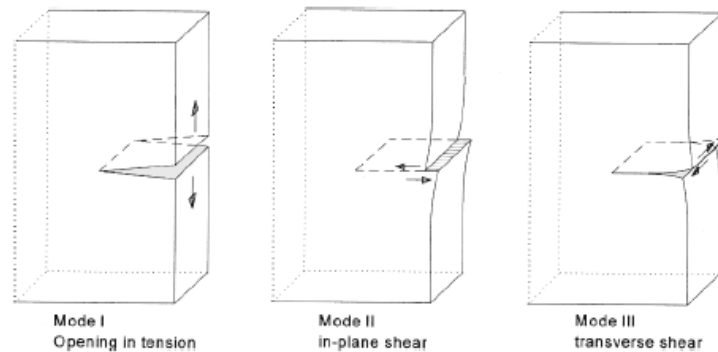


Figure 4: Three modes of crack surface displacements (Schijve, 2008)

The most common mode of failure for unwelded and welded steel structures under tension is ductile fracture. The material undergoes extensive plastic deformation before it fractures. The uniaxial-tension-loaded specimens usually have failure modes that have the characteristic appearance of the cup and cone fracture (Callister, 2017). Kazasidis and Pantelis (2017) observed different fracture modes on the ruptured specimens of the various HI levels. It was shown that the structure becomes weaker because of the high HI, which also causes slower cooling rates. Three types of fracture modes depicted in Figure 5 were observed:

- Double cup fracture mode at 0.5 kJ/mm HI
- Cup and cone fracture mode at 1 kJ/mm HI
- Shear mode of fracture at 1.5, 2 and 2.5 kJ/mm HI

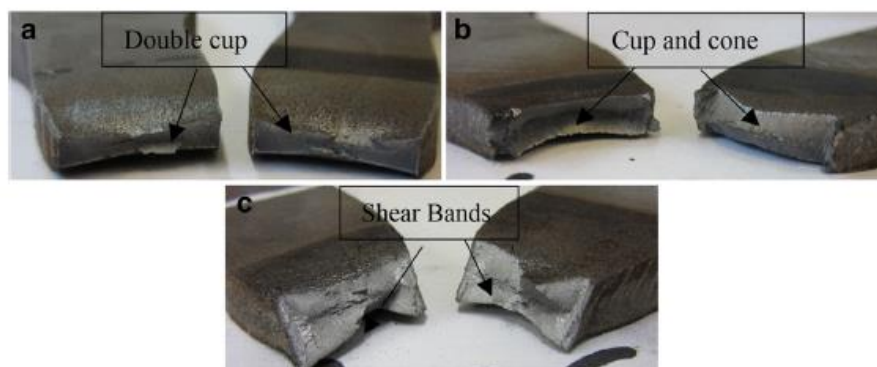


Figure 5: Ductile fracture modes of the welded joint (Kzasidis and Pantelis, 2017)

Kzasidis and Pantelis (2017) observed that the double cup fracture mode is the cleavage fracture when examining the ductile-fracture surface of a tensile specimen using the MZ6 Leica stereoscope. A mixed mode of fracture that has elongated dimples and cleavage shape has been identified as a cup and cone mode. The mixed mode of fracture is the optimum tensile fracture. The shear mode of fracture is due to voids nucleated from different spheroidal inclusions. Wang *et al.* (2018) used experimental tests and numerical simulation using various pitting parameters to study the impact of fracture position, mode of fracture failure and ductile failure initiation of steel butt welded joints. The three-fracture morphology

variation which are ductile fracture, mixed tear mode and shear fracture mode of corroded butt-welded joints were observed. Kang, Ge and Kato (2015) examined the ductile fracture behaviours of the welded joints through experimental tests under monotonic loading. Developed the ductile fracture model using finite element analysis to accurately predict ductile fracture behaviour across the specimen geometries.

Understanding the general behaviour and ductile fracture requires knowledge of the particular location where failure first occurs in welded joint material (Lee et al., 2014). The impact of three welding techniques, laser welding, GTAW, and MAG welding on the tensile characteristics and low-cycle fatigue (LCF) properties of dual-phase steel was examined by Lee et al. (2014). It was found that the cause of failure in the MAG welded joint material varied between tensile and LCF testing, and all three techniques fail in distinct areas (such as WM and HAZ). The surface condition (i.e. crack size, crack geometry, and stress levels) has a more significant effect on the fatigue properties than does the composition of the inner material (i.e. grain size). Kim et al. (2004) studied the effect of microstructural factors such as grain size to predict the LCF life. It was observed that the tensile specimen with a lower average grain size has higher tensile strength.

Tong et al. (2021) experimentally investigated the mechanical properties such as tensile test, bending test, Charpy V-notch impact test, hardness tests and fatigue behaviour of a butt-welded steel plate made of four types of high-strength steel grades of 460, 550, 690 and 960 MPa. The Q460 specimens' ultimate tensile fracture positions were found to be closer to the PM region than the Q550, Q690, and Q960D specimens, which all fractured in the WM or HAZ. Additionally, it was found that the HSS parent material's hardness value increases when steel grade increases from 460 to 960 MPa. It was confirmed that there is a limited influence of the weld strength of the studied grades of the steel on the fatigue properties. In contrast to tensile fracture locations, it was discovered that all fatigue fractures are situated near the weld or HAZ area.

The microstructure and mechanical characteristics of laser-welded S960 HSS were investigated by Guo et al. (2015). It was observed that the WM was resistant to tensile failure but the PM is susceptible to tensile failure of welded specimens. Guo et al. (2015) speculated that the cause of this failure of the welded specimens is due to the specific rolling direction and manufacturing method, which might be caused by variance in the chemical composition in the through-thickness direction. Guo et al. (2015) observed that the hardness of the PM is lower than that of the WM and HAZ. In steels, strength and hardness have comparable relationship, with the harder material often having more strength, however this not always the case (Guo *et al.*, 2015). The laser-welded specimens failed in the PM which has less hardness as compared to WM and HAZ. The weldability and mechanical behaviour of laser-welded TRIP 750 steel sheets were investigated (Gonçalves *et al.*, 2020). It was also observed that all the specimens fractured in the PM far from the weld line. The hardness level in the WM and HAZ are high compared to the PM.

The fatigue strength of the welded joint is mostly influenced by the geometry of the weld and the surface finish of the welded plate. Fatigue life is improved by grinding the weld flush with the plate, due to the minimisation of the geometric notch effect (Schijve, 2008; Stoschka *et al.*, 2013). The impact of weld bead geometry and microstructure on the fatigue properties of HSS butt welds was investigated (Ahiale and Oh, 2014). It was shown that specimens with welded beads have lower elongation but better tensile strength than specimens without beads. The lowest hardness points on specimens with and without weld beads experienced fatigue failure. As a result of the high stress concentration brought on by the geometric discontinuity of the bead shape, fatigue crack initiation of the welded structure occurred near the weld toe area (Stoschka *et al.*, 2013; Ahiale and Oh, 2014). The strength level at the lowest strength

level in the microstructure, such as the microstructural notch, was a determining factor in the fatigue failure of the welded joint without a weld bead (Ahiale and Oh, 2014).

According to Stoschka *et al.* (2013), the stress concentration at the edge of the base plate has no effect on crack initiation in the weld toe area of specimens with a welded bead and the root surface ground flat to the base plate. Despite flush grinding the weld bead and root surface of the welded connection, fracture initiation still happens at weld flaws in poor quality welds (Schijve, 2008). Amraei *et al.* (2019) observed that weld defects like porosity have little or no impact on the UTS of the welded joint material. However, it has a greater effect on the fatigue life of the weldment.

Precise prediction of the fatigue life of the welded joint structure is very difficult because the specimen fabrication and test condition can significantly affect its fatigue behaviour. It is quite challenging to create specimens that are geometrically identical, have the same metallurgical structure at the prescribed welding conditions, and have the similar residual stress distribution over the cross-section (Brooke and Miller, 1990). It is proven by many researchers that the fatigue life of the welded joint is influenced by geometric aspects like the stress concentration produced by the weld toe, microstructural features, residual stresses, and welding defects (Ahiale and Oh, 2014; Svoboda and Nadale, 2015). The evaluation of fatigue life of the welded joints is greatly influenced by these factors.

Test types of test specimens play major role in determining a reliable fatigue life. The rectangular welded plate and round welded bar experimental results are not always comparable due to the difficulty in obtaining an adequate surface finish and the fatigue cracks initiate preferably at the corners of the rectangle welded plate specimens (ISO 1099, 2006).

1.4. Scope of research

A need exists for improving the consistency of the UTS and fatigue properties of S355J2+N for welded joints produced by the MIG process. The mechanical properties of welded joints are influenced by the effects of welding parameters such as WFS, voltage and travel speed. Variations of welding parameters produce welding defects and affect the structural integrity of the welded joint (Basim *et al.*, 2017; Madyira, Kumba and Kaymakci, 2017). There is a need to optimise the welding parameters to produce welded joints with improved mechanical properties.

The purpose of this study is to conduct an experimental investigation into the impact of welding parameters namely WFS, voltage and travel speed on the UTS and fatigue life of structural steel S355J2+N welded joint using a robot. The goals of this study include examining prior research on related topics, developing an experimental methodology, compiling an experimental on UTS and fatigue database, evaluating the database, and interpreting the results. Design of experiments (DOE) was used to study the welding parameters by determining the relationship between controlled welding parameters factors (i.e. WFS, voltage and travel speed) affecting a process and the output of the process. In total 27 experiments were conducted using the orthogonal experimental design. The accuracy of the experimental data was evaluated by employing non-destructive testing (NDT) such as MT to test the welded joint plate before tensile and fatigue tests are conducted. A minimum number of three specimens for each number of experiments were tested for tensile and two specimens for each number of experiments were tested for fatigue to ensure the reliability of the experimental results. LCF testing was conducted to determine the number of cycles required to cause failure due to high-cycle fatigue (HCF) testing being expensive and the number of experiments tested in this study are many.

The compiled experimental tensile and fatigue data were used to evaluate the relationship between the tensile strength and fatigue life of the welded joint on the effect of the welding parameters. The data analysis of the experimental test results was performed by the ANOVA method. The ANOVA statistical tool was used for validation of the experimental results by:

- Determining whether welding parameters are statistically significant from each other with respect to levels being studied and the occurrence of the UTS and fatigue life of the welded joint.
- Determining the effect of the welding parameters on the UTS and fatigue life of the welded joint.
- Determining the level of contribution of each welding parameter to the overall improvement of the UTS and fatigue life of the welded joint.
- Determining the interaction effect of welding parameters at each level of welding parameters.

This study focuses on understanding the effects of welding parameters of the material S355J2+N, under static and fatigue loading of the welded joints. The statistical analysis method used takes into consideration the interactions between the welding parameters studied. All possible variable combinations produced by the design of experiments were tested. Undesirable welding defects that affect the welding structural integrity of the welded joint can be minimised by developing an optimum selection of welding parameters. Instead of merely planning for static failure, the thorough information that has been obtained may be applied in practice to design against static and fatigue failure.

1.5. Chapter outline

There are five chapters in this dissertation. The first chapter gives the introductory overview of the project and the reasoning behind undertaking the research. The literature study discusses the technical and theoretical background primarily consisting of the past studies that are conducted on the topic by other scholars and identify what has not been reported. The factors affecting the UTS, and fatigue life of the welded joint are covered. The effect of welding parameters, HI welding geometry, welding defects and fracture of the welded joints are discussed in detail in this chapter.

Chapter 2 covers the main theoretical aspects required for this research. The basic theories of static and fatigue loading of material are covered. The testing methods and standards used for specimen fabrication and testing are discussed in detail. Statistical variation in material properties and statistical method used for experimental analysis are covered.

An experimental plan, material preparation, and experimental methodologies is presented in Chapter 3. Tensile and fatigue testing of material are examined through a series of experimental tests to determine the optimum welding parameters.

The outcomes of the experiments are discussed in chapter 4. The effect of welding parameters on the UTS and fatigue life of the welded joint was investigated and validated by ANOVA. The influence of welding parameters on the welding defects are discussed.

Chapter 5 concludes the research work and gives recommendations for future work on the impacts of welding parameters on mechanical properties. The contributions and limitations of this project are outlined as well.

2. Basic Theory

This chapter introduces and explores the theoretical aspects that are applied throughout this dissertation. The basic theories of static and fatigue loading of material, mean stress effect, and the effect of the tensile strength on fatigue strength are explained in section 2.1. The test methods and standards that were considered to determine the weld joint geometry, the measurement methods that determine the precision of experimental results such as the use of robot welding, conducting non-destructive testing (NDT), validating and verifying the experimental results using analysis of variance (ANOVA) are deliberated in section 2.2.

2.1. Static and fatigue loading of welded joints

This study evaluates tensile and fatigue failure of various welded joints under uniaxial loading conditions and determines its response to UTS and fatigue life. The UTS of the welded joint will be evaluated by using a tensile test machine. The welded joints would be subjected to fracture under static loading. In a static test, a specimen is subjected to a gradually controlled tension till it breaks (fracture), and the loading does not vary with time. The tensile load is applied just once because the welded joint specimen is tested to the point of destruction. The material's ductility and UTS are revealed by the tensile test results. The UTS is the maximum tensile stress carried by a welded joint. The ductility of material is shown by two characteristics: elongation, which is defined as strain either before or after the location of fracture and a reduction in area following the fracture of the welded joints. The tensile test is performed according to the American Society for Testing and Material (ASTM) tensile test methods.

In a fatigue test, specimens are frequently subjected to repeated loading and unloading. The amplitude of cyclic loading applied to the specimens may be constant or variable. Fatigue failure involves crack formation, growth, and final fracture. The material does not have a definite fatigue limit. Stresses below the YS or UTS of the material can cause fatigue failure. Fatigue failure is affected by alternating stresses, mean stresses, surface finish, environmental conditions, and the presence of notches and flaws. Most small-scale laboratory fatigue tests performed in the literature reviewed were conducted under the condition of constant frequency, constant amplitude, and stress ratio between the maximum and minimum stresses.

2.1.1. Mean and amplitude stress effect

The fatigue stress of the structural welded joint is influenced by the mean stress. The average of maximum and minimum stresses experienced during a fatigue load cycle is the mean stress. The design standards $S-N$ (stress-life) curves are based on fatigue tests conducted under a fatigue load with zero-to-tension loading ($R = 0$) (Maddox, 2000). The zero-to-tension loading means that the minimum stress experienced during a cycle is zero (σ_{min}) which results in tensile mean stress.

It has been observed that many scholars typically conduct fatigue tests under zero-to-tension loading ($R = 0$), or tension-to-tension loading with a low R -value of $R = 0.1$. Fatigue life is significantly influenced by the impact of mean stress. Sakai *et al.* (2006) investigated how stress ratio affected the fatigue life of bearing steel when subjected to axial loads. The sloping region of each $S-N$ curve at $R = -1$ and $R = 0$ was seen to appear at nearly similar location in both situations, and the fatigue strengths are comparable. Therefore, this shows that the fatigue life of bearing steel is unaffected by compressive

stress. Subsequently, the determination of fatigue life using tensile mean stress ($R > 0$) is the most effective way to conduct experimental tests (Sakai *et al.*, 2006). The generally accepted observation is that an increase in the tensile mean stress decreases fatigue strength (Kihl and Sarkani, 1999). The constant amplitude loading for zero minimum stress (where $R = 0$) and tensile mean stress (where $R > 0$) are illustrated in Figure 6 respectively by points (a) and (b):

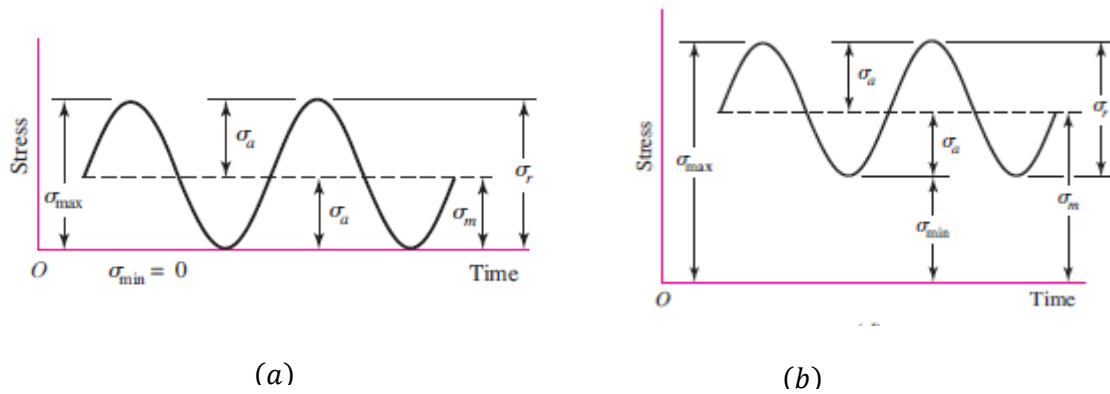


Figure 6: Constant amplitude alternating stress curve (Budynas–Nisbett, 1997)

The fatigue strength of the welded joint will be determined using the following equations below:

The stress range is calculated using the following equation:

$$\Delta\sigma = \sigma_{max} - \sigma_{min} \quad (2.1)$$

The stress amplitude is determined using the following equation:

$$\sigma_a = \frac{\Delta\sigma}{2} = \frac{\sigma_{max} - \sigma_{min}}{2} \quad (2.2)$$

The mean stress is determined using the following equation:

$$\sigma_m = \frac{\sigma_{max} + \sigma_{min}}{2} \quad (2.3)$$

The stress ratio is:

$$R = \frac{\sigma_{min}}{\sigma_{max}} \quad (2.4)$$

where σ_{max} is the maximum stress and σ_{min} is the minimum stress.

In order to determine the constant amplitude alternating stress curve variables, the suitable $S-N$ fatigue strength curve for the probabilistic design of the weld detail category must be selected. Figure 7 shows $S-N$ fatigue strength curves of the weld detail classifications which depend on the joint type, geometry and direction of loading, and mode of fatigue cracking. The weld detail classification links the description of the weld details with the suitable design $S-N$ fatigue strength curves. The weld detail classification is not based on the weld quality (Schijve, 2008).

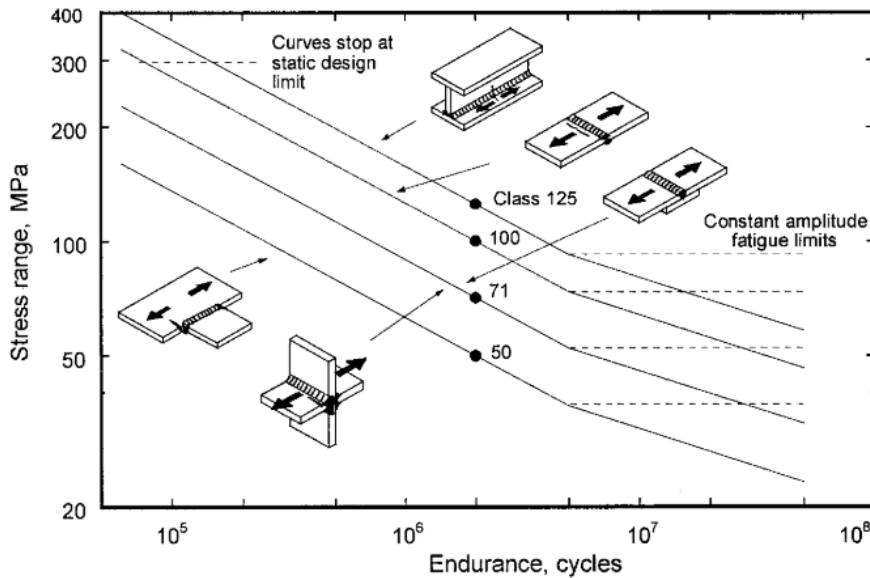


Figure 7: Fatigue strength curve for constant amplitude stress ranges (Maddox, 2000)

The fatigue strength curves are designed for a 75% confidence level of 95% probability of survival for a number of cycles by taking into consideration standard deviation, specimen size, and residual stress effects. The design value of the stress range that is used for the fatigue assessment corresponds to 2×10^6 number of cycles. If the constant amplitude stress range is less than the constant amplitude fatigue limit (i.e. 2×10^6 number of cycles), the welded joint will have infinite fatigue life. The specimen size influences the fatigue strength. It was experimentally proven that similar welded joint specimens with thicker plates have lower fatigue strength (Maddox, 2000).

The highest stress that a specimen can withstand for a given number of cycles without fracture is fatigue strength. The failure of a good welded joint should be between 10^6 cycles and 10^7 cycles in accordance with the international institute of welding (IIW) fatigue recommendations specification and fracture mechanics (Hobbacher, 2008). The S-N curves can be generated by testing each specimen from a higher stress amplitude of $0.9f_{ut}$ to a low-stress amplitude of $0.5f_{ut}$ at different stress levels. The S-N curve comprises two regions which are finite life and infinite life respectively, represented by $10^1 < N < 10^{6-7}$ and $N > 10^{6-7}$. Finite life is divided into two sub-regions which are LCF (i.e. $10^0 < N < 10^3$), and HCF (i.e., $N > 10^3$). LCF occurs when the stresses are held above the elastic limit and HCF occurs when the peak stress in the material is held within the elastic limit range. In this study, the fatigue life of the welded joint specimens will be evaluated by using the stress amplitude which is equal to the constant amplitude fatigue limits of the suitably selected fatigue strength curve.

2.1.2. The relationship between ultimate tensile strength and fatigue strength

There has been extensive research conducted on the effect of the UTS and fatigue life on various types of steel based on notched and unwelded material (Cerón-Bretón *et al.*, 2011). It has long been recognised that the fatigue design curves for welded joints are independent of the tensile strength of the material. Based on a statistical analysis of the test data on the unwelded, notched, and welded specimens, Figure 8 below shows the relationship between fatigue strength and static strength properties.

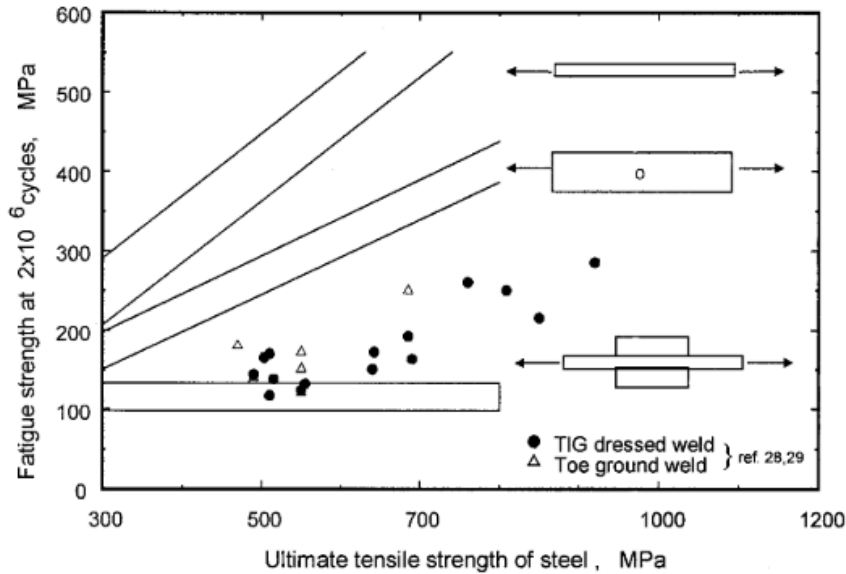


Figure 8: Fatigue strength vs ultimate tensile strength (Maddox, 2000)

Figure 8 illustrates that the fatigue strength of an unwelded material increases with the UTS. The fatigue strength of the notched material also increases with UTS, and its crack initiation is depending on the PM properties. The relation between the UTS and fatigue strength of the notched material and unwelded material is relatively similar. It has been proven by many scholars that welding influences the material characteristics of the PM (Flores *et al.*, 2016). The fatigue strength of the welded material is constant with the UTS of the material. It does not increase in proportion to UTS. The fatigue strength of the welded material contrast with unwelded material and notched material.

2.2. Testing standards and data validation method

The general design of the welded specimen was performed according to the specified design standards discussed (BS EN ISO 4136, 2012; AWS B4.0, 2016). These standards discuss the significance of mechanical tests, test apparatus, specimen preparation and the test procedure. Repeatability and reproducibility of the specimens, non-destructive testing, data analysis of the experimental results, and the effect of load frequency on the fatigue life of the specimen are also introduced in this section.

2.2.1. Welded joint geometry

AWS B4.0 (“Standard Methods for Mechanical Testing of Welds”) and BS EN ISO 4136 (“Destructive Tests on Welds in Metallic Materials – Transverse Tensile Test”) standards, specify the requirements for tensile testing of metallic material to ensure precise assessment of welds. These standards conjointly specify the geometry, specimen shape, and material preparation to obtain trustworthy data. Two distinctive ways for testing the welded butt joints like transverse rectangular tension test specimens and longitudinal tension test specimens are covered in the AWS B4.0 specification. This specification states that a transverse weld tension test is inappropriate for determining YS and elongation, because the gauge length experience uneven strain during yielding (AWS B4.0, 2016). However, it is exclusively suitable to determine the WM UTS of the welded joint specimen taken transverse to the longitudinal axis of the weld. The specimen configurations are shown in Figure 9 and Figure 10 below.

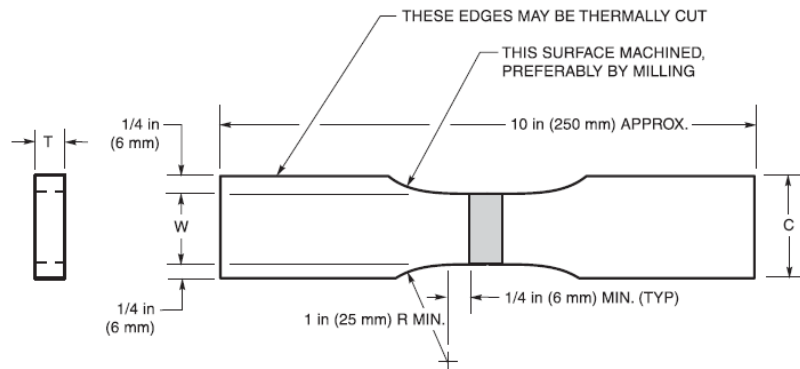


Figure 9: Specimens for transverse tensile test (AWS B4.0, 2016)

In Figure 9 T and W are as shown in the table:

T (Thickness)	W (Width)
$< 25 \text{ mm}$	$38 \text{ mm} \pm 0.25 \text{ mm}$
$\geq 25 \text{ mm}$	$25 \text{ mm} \pm 0.25 \text{ mm}$

The purpose of the research and capabilities of the test equipment available will determine the design and type of specimen utilised. The test specimen has three sections: a test section and two clamping ends. The clamp ends are created with the purpose of transferring load from the test machine to the test section (Brooke and Miller, 1990).

The transverse rectangular tensile test plate tends to tear and fracture close to the shoulder of the transition from the clamping ends to the test section, due to stress concentrations in the transition. In this situation, dimension C must not be greater than $1 \frac{1}{3}$ times the width of the testing section (W) (AWS B4.0, 2016). If the backing bar or any weld reinforcement is used it should be removed and the weld should be flush with the surface of the specimens. The large cross-sectional area of the weldment (W) can be tested based on the capabilities of available test equipment. The width of specimen (C) should be equal to the width of the reduced section (W) plus a 6 mm minimum on both sides. Within the reduced section, no surface should be no rougher than 3 micrometres (Ra). This can be achieved preferably by using a milling machine to machine surfaces within the reduced section. The rectangular welded test specimen without the reduced section can be used when necessary and when the material being tested permits. The PM's thickness close to the welded joint must be the same as the test specimen's thickness.

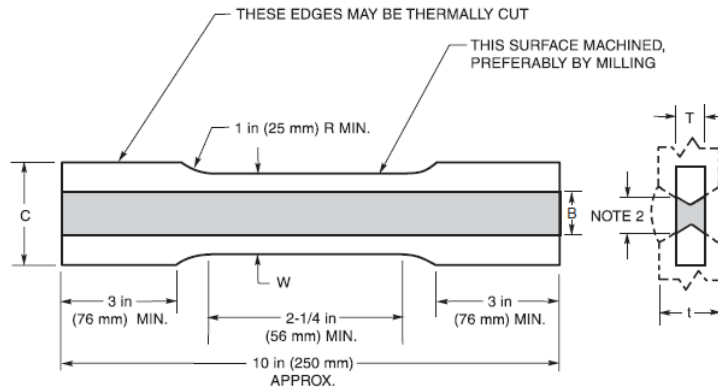


Figure 10: Specimens for longitudinal tension test (AWS B4.0, 2016)

In Figure 10 the dimensions W , B and C are as in the table:

Dimensions (mm)		
	Specimen 1	Specimen 2
W = Width	25 ± 1.25	38 ± 3
B = Width of weld	13	19
Nominal C = Width of grip section	38	50

AWS B4.0 (2016) specification recommends that longitudinal tensile test specimen weld should be flush with the surface of the specimens. The width of the weld (B) can be varied to approximately $1/2 W$ of the reduced section by selecting an applicable thickness (T). The gripping sections of the specimen should be symmetrical with the centre line of the reduced section within $3 mm$. Within the reduced section, no surface should be no rougher than 3 micrometres (Ra). This can be achieved preferably by using a milling machine to machine surfaces within the reduced section. The rectangular welded test specimen without the reduced section can be used when necessary and when the material being tested permits. The PM's thickness close to the welded joint must be the same as the test specimen's thickness.

The BS EN ISO 4136 standard covers the sizes of the specimens to be tested and the procedure for performing transverse tensile testing with the objective to determine the tensile strength and the precise location of a welded butt joint's fracture (BS EN ISO 4136, 2012). Figure 11 below shows the geometry of the transverse welded specimen.

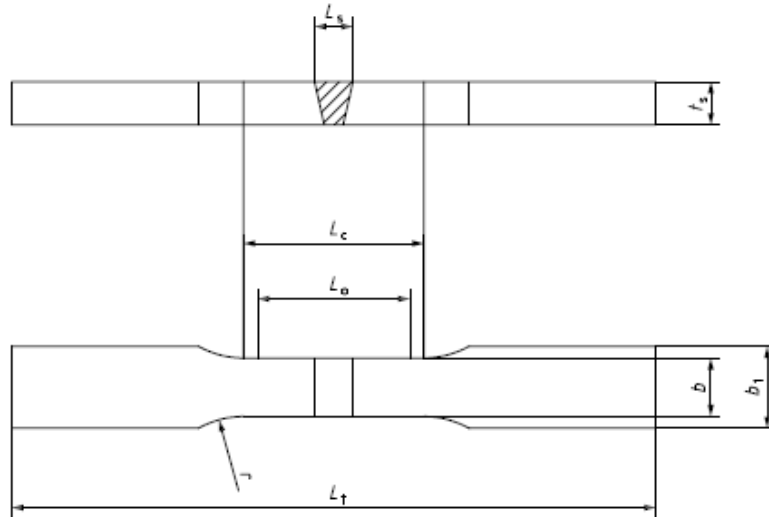


Figure 11: Test specimen for plates (BS EN ISO 4136, 2012)

In Figure 11 the dimensions L_t , b_1 , b and L_c are as in the table:

Dimensions (mm)	
L_t = The test specimen's overall length	Suitable for a specific testing machine
b_1 = The shoulder's width	$b + 12$
b = The parallel length's width	12 for $t_s \leq 2$ 25 for $t_s > 2$
L_c = Parallel length	$\geq L_g + 60$

The specimens should conform to one of the above alternative types of specimen configurations to accurately determine the effect of the welded joint. In this dissertation, the influence of welding variables is examined using a transverse weld tension test configuration.

2.2.2. Test methods

Tensile tests of the welded joint specimens should be conducted according to ASTM E8 ("Standard Methods for Tension Testing of Metallic Material"). These test procedures include those for determining of YS, yield point elongation, UTS, elongation and reduction of area of metallic materials under tension at room temperature. The machine used for tension testing should adhere to the specifications of ASTM E4-03 ("Standard Practices for Load Verification of Testing Machines"). The tensile force applied should be within the range of the testing machine. The design of the specimens should have proper gripping to ensure uniaxial tensile stresses are within the test section.

In the literature reviewed, the fatigue test machines mostly used to perform the uniaxial load fatigue test are electromechanical testing machines. The cyclic fatigue tests were carried out in the uniaxial total stress amplitude control mode with the fatigue type being fully reversed or positive tension. However, there is limited information regarding the fatigue test machine factors affecting the fatigue properties like test control parameters, resonant frequency, deflection of the test specimens and the effect of grip failure. To determine the fatigue strength of the specimens, uniaxial force-controlled fatigue tests must be performed in accordance with detailed instructions of ASTM E466-15 ("Standard Practice for Conducting Force Controlled Constant Amplitude Axial Fatigue Tests of Metallic

Materials”). The axial force fatigue test is used to assess the variances in the material, geometry, surface condition and stress, and other factors affect the fatigue resistance of metallic materials that have been subjected to direct stress for a significant number of cycles (ASTM E466-15, 2015).

A fatigue test of the welded joint specimens should be conducted in accordance with ASTM E466-15 (2015). The specimen should be designed so that failure happens in the area tested (i.e. reduced area of the specimen). The findings of the test can be significantly impacted by improper specimen preparation techniques. Proper specimen preparation needs to be established to minimise the variability of factors that might need to be kept constant. All specimens must undergo visual examination, and any evident irregularities, including fractures, machining marks, gouges, and undercuts, must not be tolerated (ASTM E466-15, 2015).

To minimise unneeded bending stress throughout the testing process, the specimen fixtures should be regularly positioned so that the primary axis of the specimens roughly corresponds with the load axis throughout each cycle.

2.2.3. Precision of test results

The exactness of measured outcomes is defined as trueness and precision in the standard of ISO 5725 (“Accuracy (Trueness and Precision) of Measuring Techniques and Results”). The term “trueness” is used to refer to how closely test findings’ arithmetic means correspond with the true or acceptable reference value. Therefore, it is only possible to verify whether measured data is accurate when a valid reference value is available. The degree of agreement between test findings from experimental studies is known as precision. Because tests conducted on the same material and using the same manufacturing process do not provide similar results, “precision” must be taken into account. This is linked to intrinsic random mistakes that cannot all be entirely controlled in measurements and are hence unavoidable. Dowling (2005) concurs that random errors are present in laboratory measurements of material properties due to factors such noise in electronic components, incorrect test specimen geometry, improper test machine alignment, and small calibration errors. Through experimental validation of the repeatability and reproducibility conditions, as stated in Table 2 below, the precision of the test procedure is determined.

Table 2: Precision condition

Factor	Repeatability conditions	Reproducibility conditions
Time	Measurement taken at the same times	Measurement taken at the different times
Calibration	No calibration between measurement	Calibration performed between measurements
Method	Same method	Different method
Operator	Same operator	Different operators
Material	Same material	Same material
Equipment	Same equipment	Different equipment

The variation in measurements made with the same material and the same method under the same conditions (such as the same times, the same operator, and the same equipment) is known as repeatability. Reproducibility measures the agreement between the results of experiments conducted by different operators, at different laboratories with different equipment.

The welded joint specimen must adhere to the requirements outlined in the ISO 5725 standard. The specimens should undergo the same reproducibility and repeatability steps. To ensure weld quality and reliability of the welded specimen the weld feature such as weld bead and slight welded plate misalignment will be ground flat to base plate thickness, to reduce the differences of the welded plates. Visual inspection and magnetic particle inspection will be used for decision-making on the acceptability or unacceptability of the defects of the welded specimen. The acceptance criteria specified by ISO 5817 will be used to assess different types of imperfections that occurred on the welded joints.

Welded joint specimens that have similar geometric characteristics, metallurgical structure, and residual stress distribution are difficult to achieve. At least a few specimens should be evaluated for each set of experiments in order to guarantee the validity of the results. The minimum number of specimens required for tension testing according to ASTM E8 is not specified. Lee *et al.* (2014); Kazasidis and Pantelis (2017) performed three tensile test trials per each set of welding parameter to guarantee the repeatability and reliability of the measurements. To ensure the correct evaluation of welds the manufacturing of transverse tensile tests must be performed in accordance with BS EN ISO 4136 and AWS B4.0 standards. Tensile and fatigue tests must be performed in accordance with ASTM E8 and ASTM E466-15 respectively.

The statistical variation in material properties must be evaluated using distinguishable statistical analysis methods to ensure the repeatability of the experimental results. Reddy Vempati, Brahma Raju and Venkata Subbaiah (2018) used Taguchi's Signal-to-Noise (S/N) ratio and ANOVA for data analysis of the experimental study. Taguchi's (S/N) ratio and ANOVA techniques are employed to evaluate the weld joint integrity of the material by identifying which welding parameters are significantly affecting the welded joint. These methods analyse the results by analysing the variance of the measured response.

2.2.4. Significance of robotic welding in minimising experimental variability

The quality of manual welding is dependent on the welder's skill and automated welding minimises the human factor and results in more homogeneous weld quality (Schijve, 2008). To guarantee the repeatability and reproducibility of the welded joint specimen, automated welding is required to execute the weld in the same wire electrode extension, torch position, and consistent welding parameters, repeatedly for all the welded joint specimens. A proper fixture of the welded joint part is also critical to achieving repeatability and avoiding misalignment. The welded joint part can be easily welded incorrectly if not fixed in an exact position during welding. All the prepared welded joint parts must have an exact geometrical dimension and an exact welding position. The incline angle between the tacked plates and the root gap specified must be consistent throughout the length of the weld. The inconsistency of the root gap may result in a cavity in the weld root run and variation in the depth of penetration.

The robot welding system does not have a vision system; it follows the specified weld path by the welding operator. It does not adjust the weld path automatically in real-time during welding to accommodate the discrepancies such as inconsistency of the root gap, root face and alignment. The repeatability and reproductivity depend on the competence of the robotic welding operator. A skilled welding operator understands the best practices and preventive maintenance of the robotic welding system such as cleaning the front end of the welding gun nozzle to remove spatter, cleaning the welding gun nozzle to improve the robotic welding system functionality and thereafter improve weld quality, repeatability and reproducibility.

The preparation of the groove on the welded joint component is essential to the weld quality. Prior to welding, all surfaces should be wire brushed to eradicate any cracks or flaws that might negatively impact the weld's quality. To ensure that the welded plates do not suffer incomplete fusion and crater cracks the run-on and run-off tabs should be added or included in the welded plates joint configuration (AWS D1.1/D1.1M, 2015). The run-on and run-off tabs must be removed upon completion and cooling of welding. If the weld tabs are not included in the welded plates, then discard 25 mm from the ends of the plate. In multi-pass welds, the weld bead should be wire brushed between passes. Thereafter, the filling passes all slag, and the weld spatter should be removed by grinding and polishing to a smooth surface.

2.2.5. Non-destructive testing

NDT needs to be performed to detect the welding defects that might affect the material properties, to ensure good quality weld and structural integrity. MT is the chosen NDT technique for this project since the tested plate thicknesses are 6 mm and it is a quick procedure. The ultrasonic testing (UT) technique is used to test ferritic steel weld plates with a minimum thickness of 8 mm (ISO 17640, 2010). In this project, the UT technique cannot be used due to plate thickness limitations. The reason that the UT technique cannot be performed on the 6 mm thick plate is that the scanning probe exit point and half-skip distance are near the WM. The root run of the weld cannot be scanned if there is no scanning distance. The exit point of the probe is 13 mm from the starting point of the weld. The refracted angle and material thickness are used to compute the sound beam's half skip distance as follows:

$$\text{Half skip distance} = t \cdot \tan \theta_R + \frac{1}{2} \cdot \text{Root Gap} \quad (2.5)$$

where t is thickness and θ_R is the refracted angle.

$$\text{Half skip distance} = 6 \text{ mm} \cdot \tan 70^\circ + \frac{1}{2} \cdot 1 \text{ mm} = 16.98 \text{ mm}$$

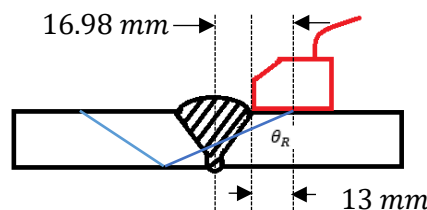


Figure 12: Half skip distance for calibration of angle-beam probe

Figure 12 depicts the available scanning distance using a maximum angle-beam transducer with a refraction angle of 70° and $8 \text{ mm} \times 9 \text{ mm}$ dimensions single crystal pulse-receive flat transducer of 4 MHz. The same bottlenecks were found using lower angle-beam transducers such as 45° and 60° . The UT technique cannot be used on a plate less than 8 mm thick, since it might result in missing defects and obtaining incorrect test results.

MT is the technique that is used to detect the surface and subsurface of the ferromagnetic material. MT uses a white contrast paint as a background, a black magnetic ink made of iron powder particles in a liquid form, and a hand-held electromagnetic yoke magnet for magnetising the welded plate to detect defects. The defects in the welded plate such as lack of penetration, lack of sidewall fusion, porosity, and crack generally attract and group the iron particles at the flux leakage fields when magnetised. This technique provides a visual indication of defects on the surface of the welded plate as depicted in Figure 13.

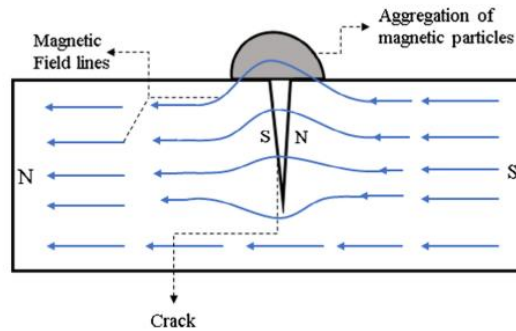


Figure 13: Principle of magnetic particle testing (Zolfaghari, Zolfaghari and Kolahan, 2018)

When performing a MT, it is very important to test the welded plate in the transverse direction and longitudinal direction of the weld to ensure that no defects are missed. It is essential that both NDT and destructive testing are conducted in accordance with the requirements outlined in BS EN ISO 15614-1 (“Specification and qualification of welding procedures for metallic materials - Welding procedure test – Part: Arc and gas welding of steels and arc welding of nickel and nickel alloys”).

In this research project, two types of examination and testing of the butt joint with full penetration will be conducted. The first test that will be conducted is a visual examination of all-welded joint plates as specified by EN ISO 17637 (“Non-destructive testing of welds – Visual testing of fusion-welded joints”). The visual testing will be conducted prior to, during and after welding. Visual testing prior to welding the joint preparation shape and dimensions will be checked. During welding, the root run will be checked for visible flaws (i.e. cavities or cracks). The final visual testing will be conducted for a complete welded joint.

The second test that will be conducted to examine the welded joint plates is MT. Magnetic particle testing must be conducted as specified by BS EN ISO 17638 (“Non-destructive testing of welds – Magnetic particle testing”) and adhere to acceptance criteria specified by BS EN 1291 (“Non-destructive testing of welds – Magnetic particle testing of welds – Acceptance levels”). The tested welded joint plate’s surface must be free of scale, grease, oil, weld spatter, machining marks, dirt, and any other foreign objects that might compromise the test method’s sensitivity.

The welds must be magnetised in two directions that are perpendicular and parallel to the weld joint in the direction of the rolling direction to ensure the detection of defects in all orientations. The acceptance criteria specified by ISO 5817 (“Quality levels for imperfection of welded joints in steel, nickel, titanium, and their alloys”) will be also used to evaluate the completeness of the root fusion with acceptable penetration (ISO 5817, 2014). Each welded joint plate is subjected to the same test requirements.

2.2.6. Analysis of variance (ANOVA)

In this study, the data analysis of the experimental results will be conducted by the ANOVA method described in applied statistics for engineers and scientists (Devore, Farnum, 2001). This technique is used to test hypotheses concerning the means of the experimental results. There are more than five types of ANOVA methods including single factor, two-factor with replication, two-factor without replication, three-factor with replication and three-factor without replication. The type of ANOVA test used depends mainly on the number of control factors. The ANOVA test design that has the same number of specimens for each factor-level combination is called a balanced design.

To study the effect of welding parameters such as WFS, voltage and travel speed on the tensile strength and fatigue life, three control factors (i.e. WFS (*A*), voltage (*B*) and travel speed (*C*)) with the three levels of the welding parameters are selected. It is evident that single-factor and two-factor with and without replication are not suitable for this study. This study deals with a three-factor ANOVA that will be used to test a variety of hypotheses of equality of means. The hypotheses test will be conducted by examining the variance between and within level means of the experimental results using the null hypothesis (H_0) and alternative hypothesis (H_a). The null hypothesis (H_0) tests that the effect does not exist, and the alternative hypothesis (H_a) tests that the effect is present. The null hypothesis is initially assumed to be true until the experimental results evidence suggests that the null hypothesis is false. If the experimental results do not strongly contradict the null hypothesis, the assertion will continue to be true. There are two possible conclusions from hypothesis testing analysis to reject H_0 or fail to reject H_0 (Devore, Farnum, 2001). Three-way ANOVA test, tests for the presence of each main effect and the interaction effect between factors.

The possible null hypotheses for comparing means of three factors (i.e., *A*, *B* and *C*) are:

- There is no difference in the means of factors.
- There is no interaction between factors.

$$H_{0A}: \text{Means are all equal} \quad (2.6)$$

$$H_{0B}: \text{Means are all equal} \quad (2.7)$$

$$H_{0C}: \text{Means are all equal} \quad (2.8)$$

$$H_{0AB}: \text{Means are all equal} \quad (2.9)$$

$$H_{0AC}: \text{Means are all equal} \quad (2.10)$$

$$H_{0BC}: \text{Means are all equal} \quad (2.11)$$

$$H_{0ABC}: \text{Means are all equal} \quad (2.12)$$

The possible alternative hypotheses for comparing means of three factors (i.e., *A*, *B* and *C*) are:

- At least one mean is different from other factors.
- There is an interaction between factors.

$$H_{aA}: \text{Means are not all equal} \quad (2.13)$$

$$H_{aB}: \text{Means are not all equal} \quad (2.14)$$

$$H_{aC}: \text{Means are not all equal} \quad (2.15)$$

$$H_{aAB}: \text{Means are not all equal} \quad (2.16)$$

$$H_{aAC}: \text{Means are not all equal} \quad (2.17)$$

$$H_{aBC}: \text{Means are not all equal} \quad (2.18)$$

$$H_{aABC}: \text{Means are not all equal} \quad (2.19)$$

Sums of squares formulas for Three-Way ANOVA with replication are defined by separating sum of squares for each source of variation as follows:

Sums of squares for each source of variation is given by:

$$SSA = bcr \sum_{i=1}^a (\bar{A}_i - \bar{X})^2 \quad (2.20)$$

$$SSB = acr \sum_{j=1}^b (\bar{B}_j - \bar{X})^2 \quad (2.21)$$

$$SSC = abr \sum_{k=1}^c (\bar{C}_k - \bar{X})^2 \quad (2.22)$$

Sum of squared deviations of all individual response values X_{ijkl} from the grand mean average of the data, \bar{X} :

$$SST = \sum_{i=1}^a \sum_{j=1}^b \sum_{k=1}^c (X_{ijkl} - \bar{X})^2 \quad (2.23)$$

Sum of squared deviations of response values X_{ijkl} from the corresponding cell means, \bar{X}_{ijk} :

$$SSE = \sum_{i=1}^a \sum_{j=1}^b \sum_{k=1}^c (X_{ijkl} - \bar{X}_{ijk})^2 \quad (2.24)$$

$$SS(AB) = cr \sum_{i=1}^a \sum_{j=1}^b (\bar{AB}_{ij} - \bar{X})^2 - SSA - SSB \quad (2.25)$$

$$SS(AC) = br \sum_{i=1}^a \sum_{k=1}^c (\overline{AC}_{ik} - \bar{X})^2 - SSA - SSC \quad (2.26)$$

$$SS(BC) = ar \sum_{j=1}^b \sum_{k=1}^c (\overline{BC}_{jk} - \bar{X})^2 - SSB - SSC \quad (2.27)$$

$$SS(ABC) = SST - SSA - SSB - SSC - SS(AB) - SS(AC) - SS(BC) - SSE \quad (2.28)$$

where

X_{ijkl} is l^{th} observation when A is level i , B is level j and C is level k

a is number of levels of factor A

b is number of levels of factor B

c is number of levels of factor C

r is number of replications per cell

\bar{A}_i is an average of all response values associated with i^{th} level of factor A

\bar{B}_j is an average of all response values associated with j^{th} level of factor B

\bar{C}_k is an average of all response values associated with k^{th} level of factor C

\overline{AB}_{ij} is an average of all response values associated with i^{th} level of factor A and j^{th} level of factor B

\overline{AC}_{ik} is an average of all response values associated with i^{th} level of factor A and k^{th} level of factor C

\overline{BC}_{jk} is an average of all response values associated with j^{th} level of factor B and k^{th} level of factor C

Mean of squares is given by dividing each sum of squares by its degrees of freedom (df):

$$MSA = \frac{SSA}{a - 1} \quad (2.29)$$

$$MSB = \frac{SSB}{b - 1} \quad (2.30)$$

$$MSC = \frac{SSC}{c - 1} \quad (2.31)$$

$$MS(AB) = \frac{SS(AB)}{(a - 1)(b - 1)} \quad (2.32)$$

$$MS(AC) = \frac{SS(AC)}{(a - 1)(c - 1)} \quad (2.33)$$

$$MS(BC) = \frac{SS(BC)}{(b - 1)(c - 1)} \quad (2.34)$$

$$MS(ABC) = \frac{SS(ABC)}{(a - 1)(b - 1)(c - 1)} \quad (2.35)$$

$$MSE = \frac{SSE}{abc(r - 1)} \quad (2.36)$$

where $ab(r - 1)$ is error degrees of freedom.

These hypotheses are tested based on the significance Level α :

H_{0A} : There is no main effect for A , F statistics (F -ratio) is given by:

$$F = \frac{MSA}{MSE} \quad (2.37)$$

where degrees of freedom for P -value determination are $a - 1$, $abc(r - 1)$.

H_{0B} : There is no main effect for B , F statistics (F -ratio) is given by:

$$F = \frac{MSB}{MSE} \quad (2.38)$$

where degrees of freedom (df) for P -value determination are $b - 1$, $abc(r - 1)$.

H_{0C} : There is no main effect for C , F statistics (F -ratio) is given by:

$$F = \frac{MSC}{MSE} \quad (2.39)$$

where degrees of freedom (df) for P -value determination are $c - 1$, $abc(r - 1)$.

H_{0AB} : There is no effect for AB interaction effect, F statistics (F -ratio) is given by:

$$F = \frac{MS(AB)}{MSE} \quad (2.40)$$

where degrees of freedom for P -value determination are $(a - 1)(b - 1)$, $abc(r - 1)$.

H_{0AC} : There is no effect for AC interaction effect, F statistics (F -ratio) is given by:

$$F = \frac{MS(AC)}{MSE} \quad (2.41)$$

where degrees of freedom for P -value determination are $(a - 1)(c - 1)$, $abc(r - 1)$.

H_{0BC} : There is no effect for BC interaction effect, F statistics (F -ratio) is given by:

$$F = \frac{MS(BC)}{MSE} \quad (2.42)$$

where degrees of freedom for P -value determination are $(b - 1)(c - 1)$, $abc(r - 1)$.

H_{0ABC} : There is no effect for ABC interaction effect, F statistics (F -ratio) is given by:

$$F = \frac{MS(ABC)}{MSE} \quad (2.43)$$

where degrees of freedom for P -value determination are $(a - 1)(b - 1)(c - 1)$, $abc(r - 1)$.

The F statistics determine the ratio of two mean square values (i.e. between means of squares and within means of the square). The F -test is used to statistically test the equality of variances using F -distribution to determine whether the variance is statistically significant by testing errors in hypothesis testing. The F -distribution assumes that the variance of means is equal between levels (i.e. assuming that H_0 is true). To compute the F -test, the critical F value needs to be calculated using the chosen significant level (α) and degrees of freedom values (i.e. $(a - 1)(b - 1)$, $(a - 1)(c - 1)$, $(b - 1)(c - 1)$, $(a - 1)(b - 1)(c - 1)$; error degrees of freedom $abc(r - 1)$). Then the critical F value is selected in the table of probabilities for the F -distribution. The null hypothesis is rejected in favour of the alternative hypothesis if the estimated F statistics value is greater than the chosen critical F value.

The P -value is determined from the F statistic and degrees of freedom values (i.e. $(a - 1)(b - 1)$, $(a - 1)(c - 1)$, $(b - 1)(c - 1)$, $(a - 1)(b - 1)(c - 1)$; error degrees of freedom $abc(r - 1)$). The P -value tests the null hypothesis that data from all the levels drawn from experimental results with the same mean. If the calculated P -value is less than (or equal to) the chosen significance level (α), then the null hypothesis is rejected in favour of the alternative hypothesis. This indicates that the experimental results are statistically significant (Devore, Farnum and Doi, 2001; Reddy Vempati, Brahma Raju and Venkata Subbaiah, 2018). If the calculated P -value is greater than the chosen significance level (α), then the null hypothesis is not rejected.

ASTM E739-91 (“Standard Practice for Statistical Analysis of Linearized Stress-Life ($S-N$) and Strain-life ($\epsilon-N$) Fatigue Data”) statistical analysis method uses similar fundamental principles such as hypotheses testing and statistical significance like ANOVA method for fatigue test (ASTM E739-91, 2009). The significance level of 0.05 is used to determine the statistical significance of the experimental results (Reddy Vempati, Brahma Raju and Venkata Subbaiah, 2018).

2.3. Conclusion

To ensure weld quality and reliability of the experimental results the manufacturing and testing of the welded joints should be conducted in accordance with specified standards highlighted in chapter 2. The welded joints should be ground flush to the thickness of the PM to minimise the geometric notch effect. At least more than one specimen for each set of welding parameters should be tested to ensure the correct evaluation of welds. The specimens should undergo the same reproducibility and repeatability steps.

The experimental design method used should test all the possible variable combinations to produce reliable experimental results. The Taguchi method does not test all variable combinations which results in the inconclusive interpretation of the experimental results. The experimental results obtained are only relative and do not precisely demonstrate what parameters have the highest effect on the performance output of the welded joint, and the interactions between welding parameters are not considered. The next chapter discusses the experimental methodology implemented for this study.

3. Research methods and material

The performance of the welded joint by variation of welded parameters like WFS, voltage and travel speed of the MIG welding process needs to be tested to determine its effects on the weld strength and fatigue life. The experimental methods used for this investigation is described in this chapter. A minimum number of five specimens for each set of welding parameters were fabricated using the guideline outlined in section 2.2. The specimens were tested using two different machines: MTS Criterion Model 45 Universal Testing Machine for tensile testing and 100kN Hydropuls universal testing machine for fatigue testing. The experimental tests were conducted in controlled laboratory conditions at an atmospheric temperature.

The selection of the PM, the input welding parameters, and the welding parameters that were kept constant are discussed in section 3.1. Section 3.2 discusses the geometry and fabrication of the welded joint specimen. The experimental setup and testing procedure for tensile and fatigue testing of the welded joints are discussed in section 3.3.

3.1. Material and welding parameters selection

The robotic MIG welding process was used to study the effect of welding parameters such as WFS, voltage, and travel speed on the UTS and fatigue life of the structural welded joints S355J2 normalised steel plates. In the robotic MIG welding process, the current is not directly set as input, but it is directly related to WFS which can be set directly as input. In this study, the wire-feed speed was used as input to control the current.

There are various types of welding joints that are commonly used in the industries like rolling stock, automotive, construction, manufacturing, mining, etc. However, a butt joint is the most common type of joint used in the manufacture of steel structures. A butt joint type was used for this investigation of this study. The manual welding procedure specification (WPS) qualified by Transnet Engineering was used as a benchmark and altered by experimentation to suit the automated welding procedure. The welding procedure of the single-V butt joint was established by executing several case studies to determine which welding parameters range produces a sound weld joint in robotic welding. It was observed that the sound of the welding and spatters generated during welding indicate the arc stability. The best weld should have a smooth weld bead and few spatters. It was additionally observed that the use of a ceramic backing bar improves weld root penetration, and it minimises the risk of lack of fusion. The removable ceramic backing bar was used in this study since is a convenient method to avoid unnecessary weld defects.

The optimum current value was found to be about 140 amps for the root run and 230 amps for the capping run; anything much higher or lower produced welding defects. When the current was too low it produced unstable arc resulting in excessive spatter and porosity, and when the current was higher it produced undercut and high narrow weld bead. The suitable voltage and travel speed were attained to reduce unnecessary welding defects such as burn-through of the welded joints caused by slow wire feed speed.

DOE was used to study the effect of WFS, voltage and travel speed on the mechanical properties of the welded joint to find out the optimal level combination. The DOE method utilised for the experiments is orthogonal design. Three level welding parameters that is WFS, voltage and travel speed were

selected based on the pilot experiments performed. The controllable input parameters were arranged in three levels in the order of minimum (level 1), average (level 2), and maximum (level 3) as shown in Table 3.

Table 3: Input welding parameter

Run	Variables	Level 1	Level 2	Level 3	Units
1 (Root run) Input Parameters	Wire feed speed (<i>WFS</i>)	3.5	3.7	3.8	<i>m/min</i>
	Voltage (<i>V</i>)	16	17	18	<i>volts</i>
	Travel Speed (<i>S</i>)	15	16	17	<i>cm/min</i>
	Current (<i>I</i>)	142	145	148	<i>Amps</i>
2 (Capping run) Input Parameters	Wire feed speed (<i>WFS</i>)	9.2	9.6	10.0	<i>m/min</i>
	Voltage (<i>V</i>)	25	27	29	<i>volts</i>
	Travel Speed (<i>S</i>)	36	40	44	<i>cm/min</i>
	Current (<i>I</i>)	232	236	240	<i>Amps</i>

The welding parameters that were kept constant during welding process are as follows:

- Electrode size and brand: 1.2 *mm*
- Gas flow rate: 15-18 *L/min*
- Shielding gas composition: 2% O_2 12% CO_2 in Argon
- Welding position and direction: Horizontal travel position (*PA*)
- Torch angle: 90-degree
- Nozzle distance: 20 *mm*
- Concave ceramic weld backing: Length (350 (25x25)); sizes (6 *mm*)

The two distinctive metal transfer techniques which are short-circuiting, commonly known as short arc, and spray arc were used for welding. Short arc metal transfer was used to weld the root run of the specimen at low current and voltage to minimise distortion of the welded joint specimen. Spray metal transfer was used for the filling run to produce good arc stability at the raised current and voltage.

The PM designation, filler material, and shielding gas used, comply respectively with BS EN 10025-2, EN ISO 14341-A-G-42 4 G3Si1 (“Welding consumables — Wire electrodes and weld deposits for gas shielded metal arc welding of non-alloy and fine grain steels”) and ISO 14175-M24 (“Welding consumables - Gases and gas mixtures for fusion welding and allied processes”). The mechanical properties of steel plate and WM based on filler metal specification and classification are given respectively in Table 4.

Table 4: Nominal mechanical properties of S355J2+N base plates and welding material

Material type	Yield strength (<i>MPa</i>)	Tensile strength (<i>MPa</i>)	Elongation (%)
Base plates	355	470 – 630	20
Weld metal	420	500 – 640	20

3.2. Welded joint specimen geometry

The general design of the specimen geometries for the butt was carried out following the transverse welded joint configuration and dimensions specified by BS EN ISO 4136 and AWS B4.0. The specimen

design also complies with ASTM E8 and ASTM E466-15. The specimen is designed so that failure does not occur in the clamp section but rather in the test section (i.e. reduced area). Figure 14 shows the required dimension of the butt joint. A 6 mm thick plate was bevelled to create a single V angle (32 degrees) with zero mm root faces to make a total of 64-degrees inclined angle between two plates. Deposited WM width is slightly greater than the 6 mm thickness of the plate. The ISO 9692-1 (“Welding and allied processes – Types of joint preparation – Part 1”) standard was followed in the weld preparation process.

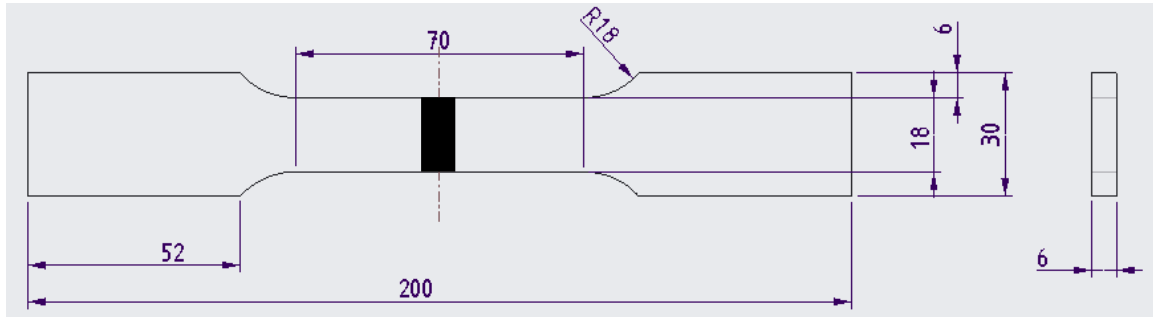


Figure 14: Geometry of welded joint

The specimen cross-sectional area was adjusted to be evaluated using the capabilities of the testing machinery available (AWS B4.0, 2016). The selected welding parameters and joint configuration are based on a specified range of parent materials and welding consumables outlined in ISO 15609-1 (“Specification and qualification of welding procedure for materials – Welding procedure specification – Part 1: Arc welding”). This standard specifies all the variables influencing the quality of the welded joint.

3.3. Experimental welding procedure

3.3.1. Welding procedure

To obtain a good quality weld, a proper selection of welding parameters is required. Three sets of values of input parameters shown in Table 3 were used to examine the effect of welding parameters on the mechanical properties of the MIG welded joint. The orthogonal design method was used to study the effect of welding parameters by determining the relationship between controlled parameter factors affecting a welding process and the output response like UTS and fatigue life. The experimental design used for the parameters is $L_{27}(3^3)$ orthogonal array shown in Table 5. The notation 3^3 implies that there are three factors, each at three levels that are investigated using an orthogonal array. This method requires 27 experiments ($3^3 = 27$ experiments) to be conducted.

Fabrication of the specimens was done by cutting the steel plates with dimensions $350\text{ mm} \times 125\text{ mm} \times 6\text{ mm}$ and bevelled into the required dimensions (i.e. root face of 0 mm and bevel angle of 32°) in the rolling direction. Then the edges of the plates with a single V configuration were tacked together to maintain the root gap of 2.4 mm. Then the steel plates were first adjusted in the proper position before welding. The welding process was conducted with a six-axis automatic Yaskawa Motoman XRC robotic arm using the SKS Q80 welding system and the six-axis robotic arm is servo-driven. The robot was programmed with a pendant and touch screen SKS Q80 controller. The pendant was used to control the robot’s step-by-step welding procedure while each point was recorded.

Thereafter the robot moved from one point to the next automatically. Figure 15 depicts the arc welding robot MIG.

Table 5: Welding parameters design of experiment

No. of Exp.	Root Run (1) Input Parameters				Capping Run (2) Input Parameters			
	Current (Amps)	Wire-feed Speed (m/min)	Voltage (volt)	Travel Speed (cm/min)	Current (Amps)	Wire-feed Speed (m/min)	Voltage (volt)	Travel Speed (cm/min)
1	142	3.5	16	15	232	9.2	25	36
2	142	3.5	16	16	232	9.2	25	40
3	142	3.5	16	17	232	9.2	25	44
4	142	3.5	17	15	232	9.2	27	36
5	142	3.5	17	16	232	9.2	27	40
6	142	3.5	17	17	232	9.2	27	44
7	142	3.5	18	15	232	9.2	29	36
8	142	3.5	18	16	232	9.2	29	40
9	142	3.5	18	17	232	9.2	29	44
10	145	3.7	16	15	236	9.6	25	36
11	145	3.7	16	16	236	9.6	25	40
12	145	3.7	16	17	236	9.6	25	44
13	145	3.7	17	15	236	9.6	27	36
14	145	3.7	17	16	236	9.6	27	40
15	145	3.7	17	17	236	9.6	27	44
16	145	3.7	18	15	236	9.6	29	36
17	145	3.7	18	16	236	9.6	29	40
18	145	3.7	18	17	236	9.6	29	44
19	148	3.8	16	15	240	10.0	25	36
20	148	3.8	16	16	240	10.0	25	40
21	148	3.8	16	17	240	10.0	25	44
22	148	3.8	17	15	240	10.0	27	36
23	148	3.8	17	16	240	10.0	27	40
24	148	3.8	17	17	240	10.0	27	44
25	148	3.8	18	15	240	10.0	29	36
26	148	3.8	18	16	240	10.0	29	40
27	148	3.8	18	17	240	10.0	29	44

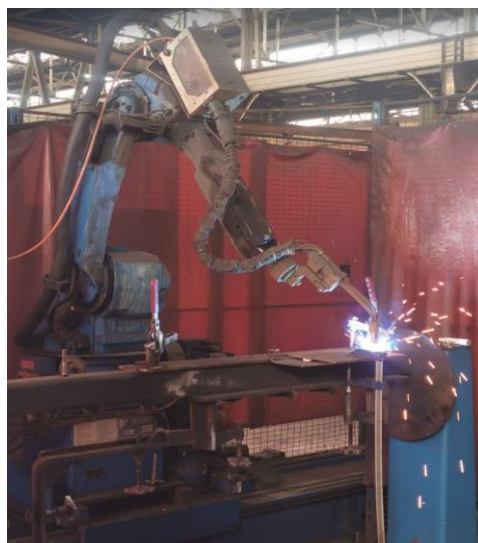


Figure 15: Yaskawa Motoman XRC robot

The parameters on the robot process controller were programmed to the first experimental input parameters such as root run and capping run welding parameters. The MIG welding process was performed with mild steel wire of 1.2 mm diameter filler and Argon/CO₂ welding mix grade gas. The steel plates were welded in the direction of the rolling direction of the plates. The specimens were not subjected to a preheat or post-heat treatment. During welding, the welded joints were visually inspected to ensure that visible defects like surface porosity, lack of penetration, underfill and blowholes were not missed if there were generated, to ensure good welding quality. This procedure was repeated for the selected 27 number of experiments for a butt joint. All the welding parameters were properly recorded, including the welding time. The specimens were extracted symmetrically to the welding direction into the required dimensions from the welded plate as specified by BS EN ISO 15614-1. Then the welds were ground flush equal to the thickness of the PM. Each test specimen per experimental test was marked for identification. Figure 16 depicts the detailed procedure of butt-welded joint specimens extracted from the welded plate.

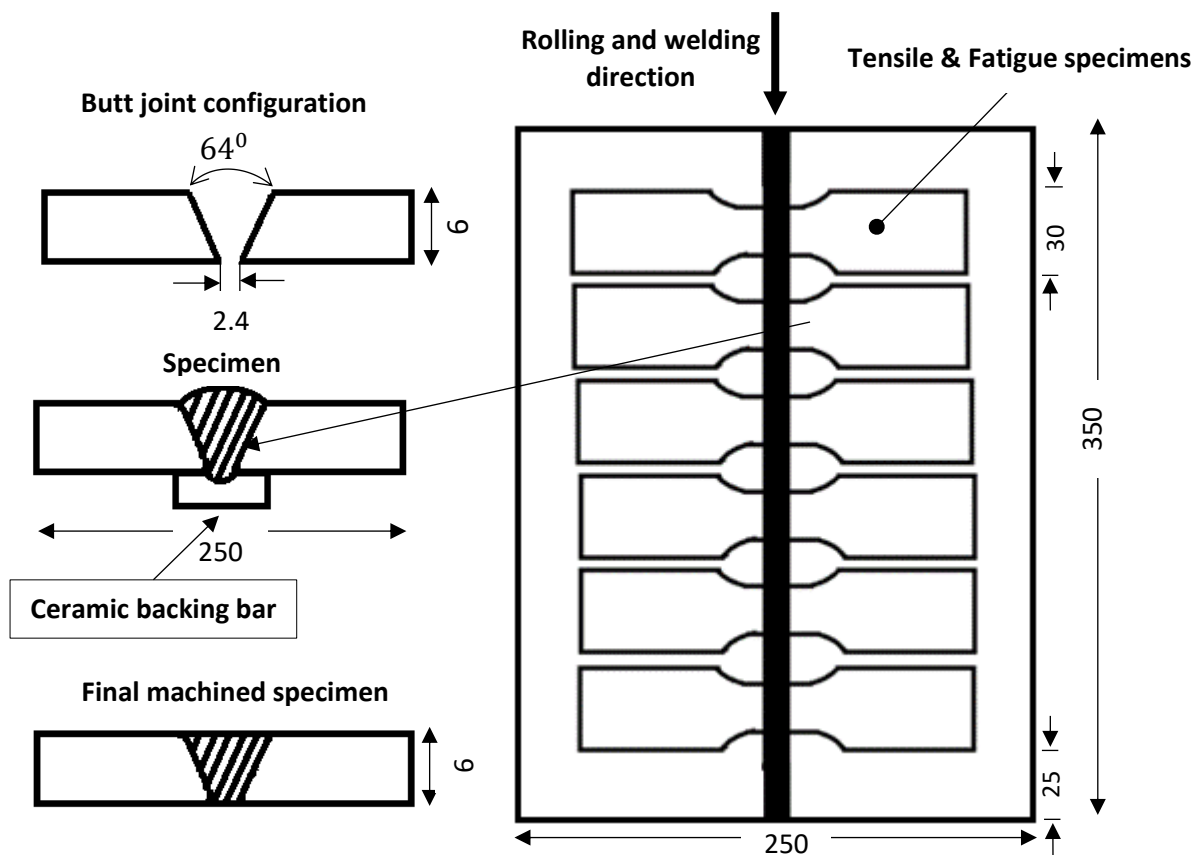


Figure 16: Details of butt-welded joint specimens extracted from the welded plate

To ensure the guarantee that the test specimens were of higher quality such that no bias of the results would occur, the specimen fabrication preparation was developed according to ISO 9692-1, BS EN ISO 4136, and ASTM E466-15. The welding procedure test specification was conducted in accordance with EN ISO 17637 and BS EN ISO 17638 standards. Visual inspection was conducted by looking for visual weld defects (i.e. undersized welds, undercuts, overlap, surface cracking, surface porosity, underfill, incomplete root penetration and excessive root penetration) and checking for the correctness of the weld geometry. The visual test included feeling the entire weld by hand. The surface roughness of the ground flush to the plate was maintained constant by using the same sanding flap disc and grinder. Magnetic

particle inspection testing was also conducted to identify the weld joint specimens with defects. Then the specimens were wire brushed prior to conducting destructive testing to remove any rust and oil films on the surface of the specimens. Detailed instructions regarding the fabrication of the welded joint specimen are given in Appendix A.

3.3.2. Tensile testing experimental setup

The MTS Criterion Model 45 Universal Testing Machine available at Transnet Engineering Research & Development Department was used to test the tensile strength of the welded joint specimens. The machine uses the servo-hydraulic testing system technology, and it has a 100 *kN* load frame. The machine is a computer-controlled testing machine that operates using MTS software which has various features such as MTS – Video extensometer, used for data collection. The machine has a wide variety of fixtures that can be used depending on the geometry and dimensions of the test specimen. The hydraulic wedge grips mounted on the MTS test frame are operated using MTS software or Handset. Figure 17 illustrates the tensile testing setup arrangement.

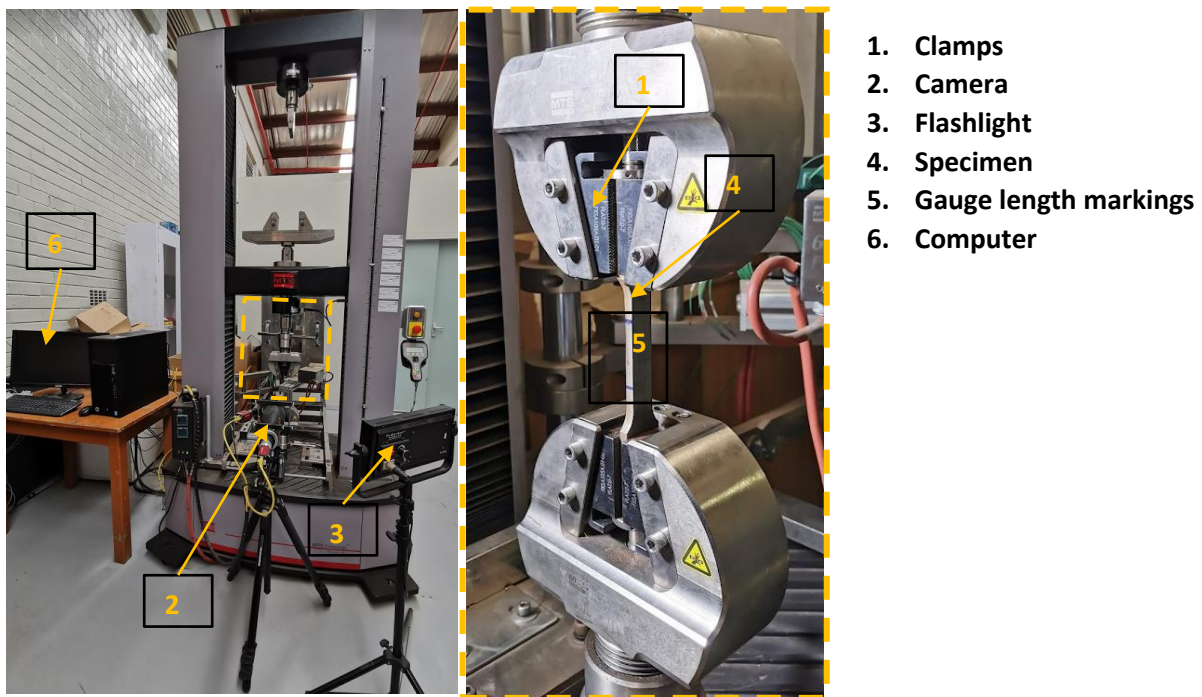


Figure 17: Experimental tensile testing

To apply the tensile load in the testing apparatus, the specimen needs to be gripped at both ends. The gripping should guarantee a uniform load distribution at the ends of the specimen. As shown in Figure 17, the specimen is clamped at both ends. It is important to ensure that the specimen is properly secured inside the clamps and axially coincides with the centreline of the clamps to ensure that no bending stresses are introduced during testing (Schijve, 2008). It is advised to examine each tested specimen alignment.

3.3.2.1. Tensile testing procedure

The standard procedure is developed within the MTS software program for tension testing. The program requires general inputs about the specimen's geometry and selected testing standards. The tensile testing machine is equipped with a video extensometer which is used to measure the elongation of the specimens during testing. At least three specimens per experiment were tested to determine the average UTS of the welded joints. A total of 81 tensile tests were conducted for the butt-welded joints. During these testing, the following procedures were followed:

- The specimen thickness, width and gauge length of 50 mm are measured before testing using a calibrated digital vernier, and the gauge length of each specimen is marked using a black permanent marker.
- The tensile testing machine is switched on and the flashlight for the camera is switched on depending on the light intensity in the laboratory.
- The lens caps from the big and small cameras are removed.
- The handset is unlocked and ready to be used to align and position the clamps according to the test specimen length.
- The specimen is inserted inside the clamping fixtures and proper alignment is achieved to minimise bending and then the clamp fixtures are tightened.
- The correct template is selected when the TW Elite software is launched from the desktop.
- The video extensometer big camera and a small camera are focused on a test specimen by checking them on the computer screen.
- The selected targets are positioned on the markings of the gauge length on the test specimen to measure the elongation of the specimen during testing.
- The necessary information required by TW Elite program is added before the specimen is uniaxially subjected to a gradually controlled tension until fracture.
- The MTS software automatically plots the load [kN] versus elongation [%] curve that shows the peak load which is the ultimate tensile load reached before fracture along with the elongation percentage during the test.
- After testing the gauge length, width, and thickness of each specimen are measured for completeness to calculate the elongation percentage.
- The MTS software calculates mechanical properties such as UTS, tensile stress at 0.2% offset YS, tensile strain at maximum load and young's modulus automatically.

The specimen fracture should occur within gauge length to satisfy the acceptance testing failure criteria. If the specimen does not meet the specified requirements, the specimen is noted.

3.3.3. Fatigue testing experimental setup

Fatigue testing was performed using the Servo-Hydraulic Universal-Axial Testing Machine PSA available at the University of Pretoria. This axial testing machine has a loading capability of 100kN. It is suitable for the investigation of specimens with a small cross-section under tension, compression, or reversal load. The experimental setup depicts the test frame and specimen secured in the lower clamps and the upper clamps as illustrated in Figure 18.



Figure 18: Experimental fatigue testing


To apply the fatigue load in the testing apparatus, the specimen needs to be gripped at both ends. The specimen must be properly secured inside the grips and the center axis of the specimen must coincide with the loading axis of the fatigue testing apparatus, to guarantee a uniform load distribution at the specimen ends.

3.3.3.1. Specifications for fatigue testing

The fatigue tests of the welded joints were evaluated under constant amplitude alternating stress and proportional loading. It was performed in the uniaxial stress amplitude control mode with a stress ratio of $R = \frac{\sigma_{min}}{\sigma_{max}} = 0.1$ that cycle between two positive tensile stresses and a test load frequency of 5 Hz.

The fatigue test was performed according to ASTM E466-15 fatigue test methods to investigate the impact of variation of welding parameters in welded joint material.

The international institute of welding (IIW) fatigue recommendations specification was used for the selection of the weld classes to determine fatigue testing machine inputs. The weld classes are defined as the fatigue strength or allowable stress at 2×10^6 cycles using a slope of $m = 3$ and a survival probability of 95%. The detail fatigue strength category for the transverse butt welds is $\Delta\sigma_c = 112 \text{ MPa}$ specified by the standard at 2×10^6 cycles. Figure 19 depicts the fatigue resistance value for transverse butt welded joint with its direction of loading. The S-N (stress-life) curve shows the relationship between the stress and the fatigue life of the specimen.

No.	Structural Detail	Description (St.= steel; AL.= aluminium)	FAT St.	FAT AL.	Requirements and Remarks
200	Butt welds, transverse loaded				
211		Transverse loaded butt weld (X-groove or V-groove) ground flush to plate, 100% NDT	112	45	All welds ground flush to surface, grinding parallel to direction of stress. Weld run-on and run-off pieces to be used and subsequently removed. Plate edges ground flush in direction of stress. Welded from both sides. Misalignment < 5% of plate thickness. Proved free from significant defects by appropriate NDT

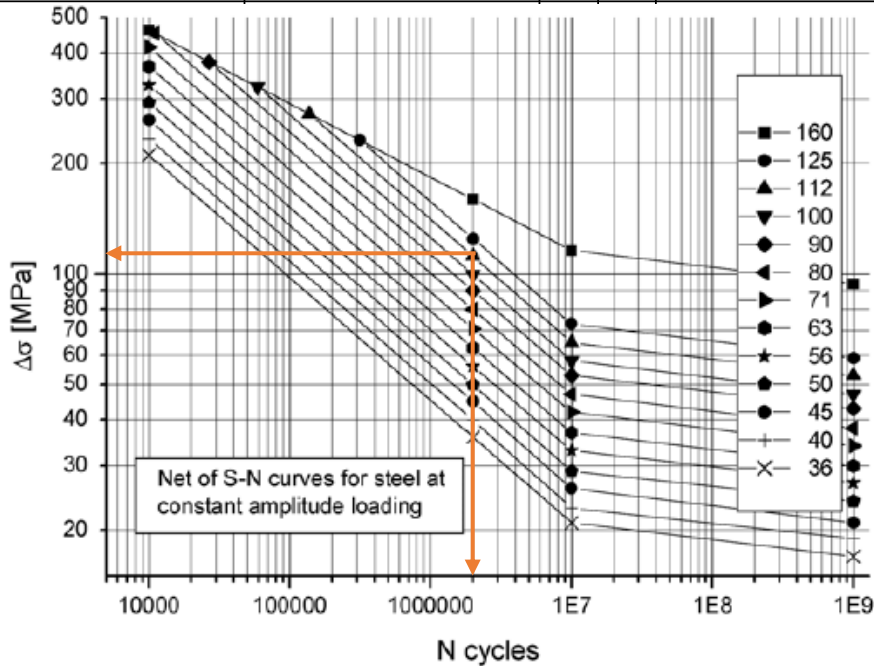


Figure 19: Fatigue strength curve for direct stress range (Hobbacher, 2008)

The specified fatigue class for 2×10^6 cycles was used to calculate the new fatigue class for 4×10^4 cycles with the slope of $m = 3$ as follows:

$$\Delta\sigma_{c,new} = \Delta\sigma_c \left(\frac{N_c}{N_{new}} \right)^{\frac{1}{m}} = 122 \times \left(\frac{2 \times 10^6}{4 \times 10^4} \right)^{\frac{1}{3}} = 412.61 \text{ MPa}$$

The general inputs of the fatigue testing machine were calculated as follows:

The stress range is calculated using the following equation:

$$\Delta\sigma_{c,new} = \sigma_{max} - \sigma_{min} = 412.61 \text{ MPa}$$

The stress ratio is:

$$R = \frac{\sigma_{min}}{\sigma_{max}} = 0.1$$

The calculated maximum stress and minimum stress are:

$$\sigma_{max} = 458.46 \text{ MPa and } \sigma_{min} = 45.85 \text{ MPa}$$

The stress amplitude is calculated using the following equation:

$$\sigma_a = \frac{\sigma_{max} - \sigma_{min}}{2} = 206.31 \text{ MPa}$$

The maximum and minimum static loads are calculated using the following equations:

$$F_{max} = A \times \sigma_{max} = (18 \text{ mm} \times 6 \text{ mm}) \times 458.46 \text{ MPa} = 49.51 \text{ kN}$$

$$F_{min} = A \times \sigma_{min} = (18 \text{ mm} \times 6 \text{ mm}) \times 45.85 \text{ MPa} = 4.95 \text{ kN}$$

where A is the cross-sectional area of the specimen.

The static load and dynamic loads imposed on the specimen are calculated using the following equations:

$$F_{static} = \frac{F_{max} + F_{min}}{2} = 27.23 \text{ kN}$$

$$F_{dynamic} = \frac{F_{max} - F_{min}}{2} = 22.28 \text{ kN}$$

The calculated static load and the dynamic load will be imposed on the test specimen until the fatigue test is complete. Figure 20 shows the amplitude of the sine wave representing the dynamic load and the sine wave average value representing the static load.

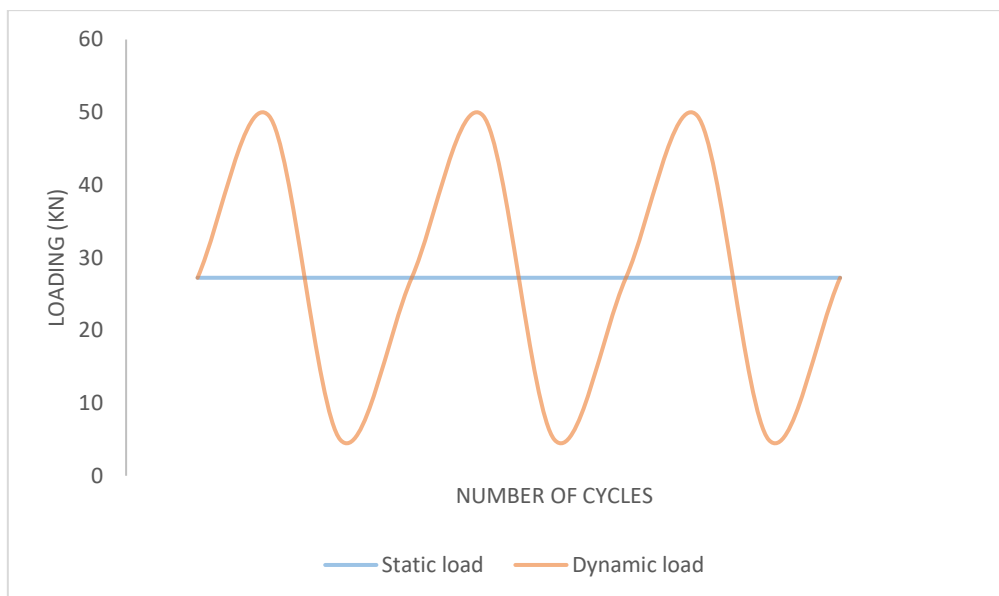


Figure 20: Fatigue loading diagram

3.3.3.2. Fatigue testing procedure

The flat grips were selected and inserted inside the jigs. Then the specimen was inserted inside the clamping fixtures and proper alignment was achieved to minimise bending and then the clamp fixtures were tightened. To run the test, the data logger software was activated, and testing parameters were inserted into the K7500 Servo-controller such as voltage data and the test loading frequency of 5 Hz. The maximum and minimum static loads of the tests were converted into volts since the fatigue testing machines use voltage data as loads in this case 1 V is equal to 10 kN. The safeguard protection was set for the maximum and minimum static loading. This assists the machine to stop automatically when the safeguard value is reached to avoid the risk of damaging the system when the specimen fractures. The data logger software measures and stores DC Voltage readings automatically. The voltage data input creates a sinusoidal graph that is consistent with the feedback response obtained from the sensors. Figure 21 depicts the data logger software measured Microsoft Excel sinusoidal graph. CH 0 represents channel 0 and time is the number of cycles measured. The specimen was subjected to cyclic load until fracture.

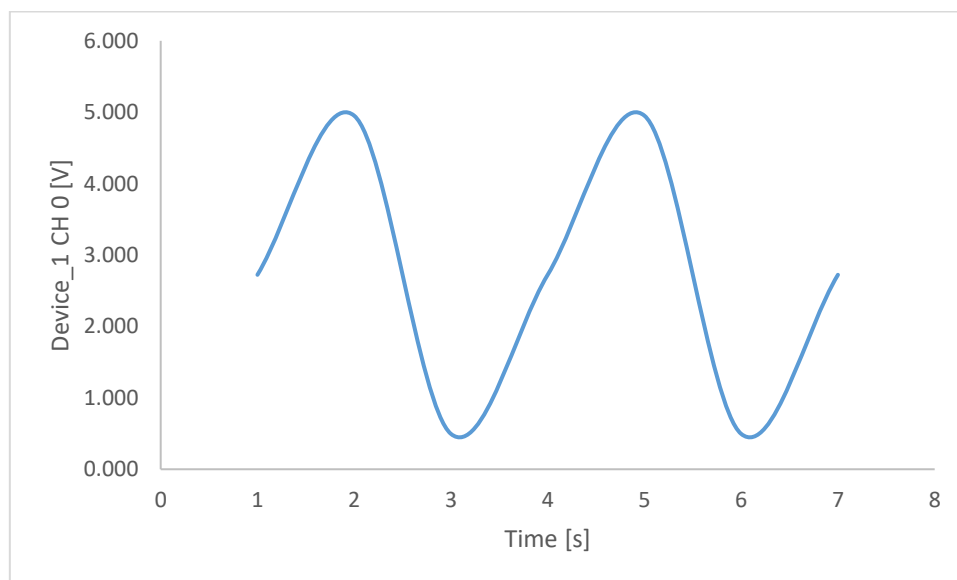


Figure 21: Data logger cyclic loading

The specimen fracture should occur within the reduced area or the radius of the fillet to satisfy the acceptance testing failure criteria. The run-out limit was set to 2×10^6 load cycles. If the specimens did not meet the specified requirements, the specimens were discarded.

3.3.4. Stereoscope and hardness measurement

The three experiments were selected that is 3, 11 and 27 to represent all 27 experiments to study the failure of the welded joint specimens. A large enough cross-section area perpendicular to the weld that permits measurement of weld fusion, HAZ, PM, and fracture at the necessary magnification was extracted from the specimens for macrostructural examination. Hardness traverse test specimens were cut transversely offset to the centreline of the weld to permit measurement of the half weld fusion, HAZ, and PM beyond the fracture point of all tested specimens. The extracted specimens were hot embedded with black bakelite resin. The specimen surface preparation for image analysis which includes mounting and polishing was performed according to the ASTM E3 – 11 (“Guide for Preparation of

Metallographic Specimens”). The specimens were ground and polished using 9 μm to 3 μm DiaDuo-2 a water-based diamond suspension made up of monocrystalline diamonds and a cooling lubricant. The hardness specimens were etched with 2% nitric acid. Figure 22 and Figure 23 show the mounted specimens for macrostructural examination and hardness test respectively.



Figure 22: Mounted specimens for macrostructural examination



Figure 23: Mounted specimens for hardness test

The measurements of the macrostructural examinations were performed using a microscope CCD camera and computer which has customized software to scan the specimen surface. The stereoscope tests of the specimens were conducted in accordance with the ASTM E1382 (“Standard Test Methods for Determining Average Grain Size Using Semiautomatic and Automatic Image Analysis”).

The Vickers hardness tests were conducted with a load of 0.5 *kgf* applied at 1 *mm* interval using an EMCO Test DuraScan to investigate the welded specimen failures. The same three experiments (i.e. 3, 11 and 27) which were selected for macrostructural examination were analysed. The hardness traverse profile was measured from the midpoint of the WM into the HAZ to the PM. The hardness measurements were carried out according to AWS B4.0 and ASTM E384 (“Standard Test Method for Micro-indentation Hardness of Material”).

3.4. Conclusion

The experimental methodology should be executed in accordance with the above-discussed methods and standards to ensure the reliability of the obtained experimental data. The literature study conducted in section 1.3 endorses fabrication, testing of the specimens and the experimental methodology executed in this study. The experimental results that were gathered while using these procedures are discussed in the next chapter. The evaluation and analysis of the data that was collected are also included in the subsequent chapter.

4. Results and discussion

The analysis and interpretation of the experimental data are introduced in this chapter. The experimental investigation was performed on the welded joints to evaluate the effect on UTS and fatigue life, the results are discussed in section 4.1. ANOVA was used to study and validate the impact of welding variables on the UTS and fatigue life of the welded joint. The findings are described and analysed in section 4.2. The failure mode of the welded joint is discussed in section 4.3. The results of the NDT are discussed in section 4.4. The impact of welding variables on UTS and fatigue life of the welded joint is discussed in section 4.5 and the chapter conclusions are discussed in section 4.6.

4.1. Effect of the welding parameters on ultimate tensile strength and fatigue life

Investigation was conducted into how welding parameters namely WFS, voltage and travel speed affected the UTS and fatigue life of the welding joint. There was a total of 27 experiments conducted with various WFS's, voltages and travel speeds. The DOE method was used to study the effect of welding parameters by determining the relationship between controlled parameters affecting the MIG welding process and the output response like UTS and fatigue life. Three specimens per experiment were tested under uniaxial tensile loading and two specimens per experiment were tested for fatigue loading to replicate the measured response of the UTS and the number of cycles to failure (N_f). The obtained experimental results for the UTS and the N_f are shown in Table 6. All the UTS experimental results of the specimens exceeded the specified minimum tensile strength requirements of the S355J2+N PM and WM according to the specified code respectively BS EN 10025-2 (2004) and BS EN ISO 14341 (2011). This ensured a satisfactory weld quality of the welded joint specimens. The fatigue experimental results were evaluated against its calculated fatigue strength of 412.6 MPa at 40000 cycles. Most fatigue experimental results of the specimens exceeded the specified N_f . The fatigue quality of the welded joint is measured by the N_f .

The optimal welding parameters are identified by the maximum UTS and the N_f of the test specimens. The tensile test experimental results show that experiment number 11 has a maximum UTS compared to other specimens followed by experiment numbers 10 and 9 respectively. Experiment number 11 has the best welding parameters combination which resulted in good welded joint structural integrity followed by experiment numbers 10 and 9 respectively. The fatigue test experimental results obtained show that experiment number 13 has a maximum N_f followed by experiment numbers 26 and 16. This indicates that experiment numbers 13, 26 and 16 have the best welding parameters combination.

The impact of welding variables on the UTS and the fatigue life of the welded joint was analysed by plotting its correlation between the UTS and the N_f . The effect of welding parameters was established by varying the WFS, voltage and keeping the travel speed constant. Then WFS was increased from lower to higher WFS while evaluating its effect on the UTS and the fatigue life as illustrated in following Figure 24 to Figure 26.

Table 6: Experimental results for UTS and fatigue life

Number of Experiments	Welding Heat Input			Ultimate Tensile Strength				Number of cycles to failure		
	Root run Heat Input (J/mm)	Capping run Heat Input (J/mm)	Total Heat Input (J/mm)	Test 1 (No. A) (MPa)	Test 2 (No. B) (MPa)	Test 3 (No. C) (MPa)	Average Tests (MPa)	Test 1 (No. A) (cycles)	Test 2 (No. B) (cycles)	Average Test (cycles)
1	727	773	1500	576.5	574.0	572.8	574	26408	55915	41161
2	682	696	1378	579.2	578.3	559.2	572	56638	26003	41321
3	642	633	1274	577.0	558.7	566.9	568	50698	38068	44383
4	772	835	1608	579.5	583.8	558.0	574	49020	43633	46326
5	724	752	1476	565.7	576.3	569.2	570	34215	42570	38393
6	682	683	1365	574.9	584.2	566.5	575	41174	43044	42109
7	818	897	1715	564.8	563.9	569.0	566	48591	49716	49153
8	767	807	1574	570.6	556.4	562.7	563	24803	47673	36238
9	722	734	1456	584.1	598.4	585.6	589	55475	42924	49199
10	742	787	1529	591.1	592.2	586.2	590	54847	56110	55479
11	696	708	1404	581.8	583.5	608.0	591	45822	47287	46555
12	655	644	1299	569.0	570.7	575.2	572	38718	44336	41527
13	789	850	1638	560.7	561.5	550.6	558	71240	61865	66552
14	740	765	1504	545.0	537.9	618.1	567	36585	37807	37196
15	696	695	1391	584.3	568.6	580.9	578	70251	50144	60198
16	835	913	1748	553.5	555.2	548.5	552	56569	64438	60503
17	783	821	1604	578.6	589.0	581.4	583	49004	50054	49529
18	737	747	1484	587.1	565.5	590.9	581	51379	45581	48480
19	758	800	1558	564.6	567.8	563.4	565	43444	35383	39413
20	710	720	1430	584.3	573.0	563.8	574	51755	65734	58744
21	669	655	1323	580.0	563.6	578.7	574	56596	58244	57420
22	805	864	1669	571.0	565.7	563.9	567	36237	63098	49667
23	755	778	1532	583.4	575.5	578.1	579	43937	56334	50135
24	710	707	1417	578.3	582.7	580.9	581	42800	55582	49191
25	852	928	1780	548.7	551.8	572.5	558	42681	66716	54699
26	799	835	1634	588.1	576.7	571.5	579	68336	57715	63026
27	752	759	1511	588.9	544.4	562.7	565	47075	30500	38787

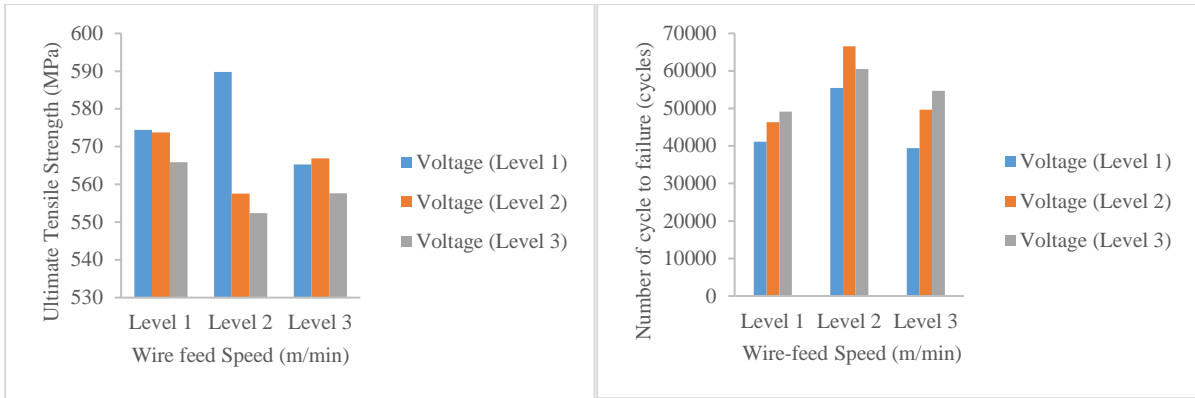


Figure 24: Ultimate tensile strength and fatigue life vs. wire-feed speed diagram for constant travel speed (Level 1)

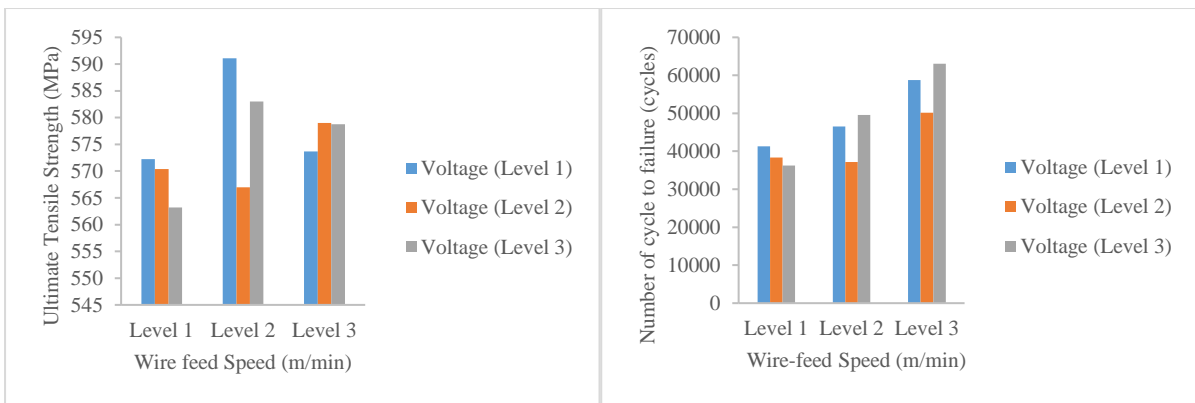


Figure 25: Ultimate tensile strength and fatigue life vs. wire-feed speed diagram for constant travel speed (Level 2)

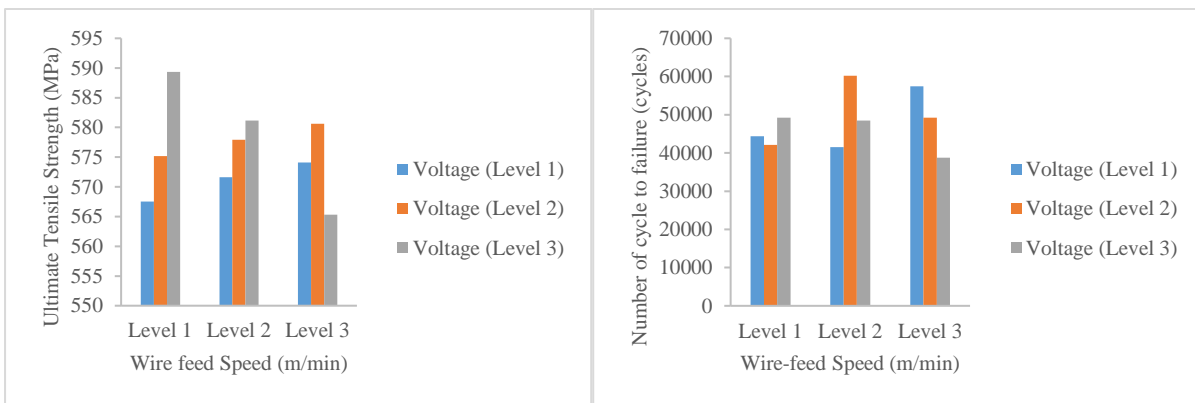


Figure 26: Ultimate tensile strength and fatigue life vs. wire-feed speed diagram for constant travel speed (Level 3)

The experimental tensile results show that increasing voltage from level 1 to level 3 and WFS from level 1 decreases the UTS of the welded joint by increasing the travel speed of level 1 and level 2. The travel speed of level 3 shows that increasing voltage from 1 to level 3 and WFS from level 1 increases the UTS. The UTS at level 1 WFS gradually decreases with increasing the travel speed from level 1 to level 3 respectively from 574 MPa, 572 MPa and 568 MPa. The tensile experimental results also show that increasing voltage from level 1 to level 3 and WFS from level 3 increases the UTS to level 2 voltage

and then decreases with increasing voltage. The UTS at level 3 WFS gradually increases with increasing the travel speed from level 1 to level 3 respectively from 567 MPa, 579 MPa and 581 MPa.

The experimental fatigue results show that increasing voltage from level 1 to level 3 and WFS from level 2 increases the N_f of the welded joint to level 2 of voltage and then decreases with increasing voltage by increasing the travel speed of level 1 and level 3. The travel speed of level 2 shows that increasing voltage from level 1 to level 3 and WFS from level 2 decreases the N_f of the welded joint to level 2 of voltage and then increases with increasing voltage. The maximum values for UTS and N_f that were obtained are 590 MPa; 66552 cycles, 591 MPa; 63026 cycles, and 589 MPa; 60198 cycles, respectively with travel speed from level 1 to level 3.

4.2. Analysis of variance results

The data analysis of the experimental test results was performed by the ANOVA method. The hypotheses test was conducted by examining the variance between and within level means of experimental test results to determine the statistical significance of the experimental results. Testing of the significance of the welding parameters and their interactions were conducted by comparing the means of square that is between means of squares (MSA , MSB , MSC , $MS(AB)$, $MS(AC)$, $MS(BC)$, and $MS(ABC)$) and within means of the square (MSE) against an approximation of experimental errors at the 95% confidence level. Then, the ANOVA was used to calculate the level of contribution of each welding parameter to the total improvement of the UTS and the N_f of the welded joint. The impact of welding parameters was ranked based on the total sum of squares delta values.

4.2.1. Effect of welding parameters on ultimate tensile strength of the welded joints

The three-way ANOVA test was conducted to determine which effects of three controlled factors such as WFS (A), voltage (B) and travel speed (C) are significant, and which are not. The interaction between factors such as two-factor interactions and three-factor interactions was also examined to determine if there is a significant difference in the means for one of the three controlled factors. The main effects (i.e. A , B and C) and interaction effects (i.e. AB , AC , BC and ABC) on the UTS were studied using a probability value of $p\text{-value} \leq 0.05$, assuming that the null hypothesis is true. Table 7 depicts the summarised results of the analysis of variance for UTS.

Table 7: Summary results of analysis of variance for ultimate tensile strength of the welded joints

Control Factors	Sum of Squares (SS)	DOF (df)	Mean Square (MS)	F -ratio	P -value	F critical	P -test	Rank	Contribution
A	158.94	2	79.47	0.5	0.599	3.2	Insignificant	3	4%
B	327.89	2	163.95	1.1	0.351	3.2	Insignificant	2	7%
C	1316.52	2	658.26	4.3	0.019	3.2	Significant	1	29%
AB	1326.34	4	331.58	2.2	0.086	2.5	Insignificant		15%
AC	887.88	4	221.97	1.4	0.232	2.5	Insignificant		10%
BC	1644.15	4	411.04	2.7	0.041	2.5	Significant		18%
ABC	1774.59	8	221.82	1.4	0.200	2.1	Insignificant		10%
SSE	8292.33	54	153.56						7%
SST	15728.65	80							

The presence of any interaction was tested at a significance level of $\alpha = 0.05$. It appears that there is an interaction between two factors like the voltage (B) and travel speed (C) with respect to levels being

studied and the occurrence of the UTS. If the p-value is less than 0.05, H_{0BC} is rejected. There is no interaction between factors for AB (WFS and voltage) and AC (WFS and travel speed) and ABC (WFS, voltage and travel speed). If the p-value is greater than 0.05 then H_{0AB} , H_{0AC} and H_{0ABC} are not rejected. There is no dependence of one welding parameter on the value of another welding parameter for AB , AC and ABC .

The p-value is acceptably higher than the chosen significant level of $\alpha = 0.05$ for WFS (A) and voltage (B) with respect to UTS, which indicates that there is no statistically significant difference between WFS (A) and voltage (B) with respect to levels being studied and the occurrence of the UTS. However, the p-value is less than 0.05 for travel speed (C) with respect to levels being studied and the occurrence of the UTS. This indicates that there is a statistically significant difference between travel speed (C) with respect to levels being studied and occurrence of the UTS. The computed F-statistic from the data corresponds with the p-value results. F-statistic for WFS (A), voltage (B) is less than selected critical F-values at a 95% confidence level, then the null hypothesis is not rejected. If the computed F-statistic of the travel speed (C) is greater than the selected critical F-values at 95% confidence level, then the null hypothesis is rejected in favour of the alternative hypothesis.

The acceptably high p-value indicates that there is less disagreement between UTS with respect to wire-feed speed data with the null hypothesis. We fail to reject the null hypothesis that the wire-feed speed has an effect on the UTS of the welded joint. There is no evidence that indicates the wire-feed speed influence the UTS of the welded joint, and there is no difference between the wire-feed speed with respect to levels being studied and the occurrence of the UTS.

The acceptably high p-value indicates that there is less disagreement between UTS with respect to voltage data with the null hypothesis. We fail to reject the null hypothesis that the voltage has an effect on the UTS of the welded joint. There is no evidence that indicates the voltage influence the UTS of the welded joint, and there is no difference between voltage with respect to levels being studied and the occurrence of the UTS.

The small p-value indicates that there is substantial disagreement between UTS with respect to travel speed data with the null hypothesis. We reject the null hypothesis that the travel speed does not have an effect on the UTS of the welded joint. There is evidence that indicates the travel speed influence the UTS of the welded joint, and there is some difference between travel speed with respect to levels being studied and the occurrence of the UTS.

The impact of welding parameters on the UTS was ranked from first to last and the percentage contribution of welding parameters on the UTS was calculated as shown in Table 7. The standard error of the mean contributed 7% which is mainly due to specimen fabrication variation and human error.

4.2.2. Main effects and interaction effects plots of ultimate tensile strength on welded joints

The experimental outcomes were interpreted by examining the main effects and interaction effects plots after conducting statistical tests. The effect plots do not take into consideration the statistical tests. All main effects of controlled factors, the two-factor and three-factor interaction effects of this experiment were graphically represented by plotting the average response of the welding parameters versus the

factor levels. When statistical analysis indicates an interaction effect is significant, the interaction plots, not the main effects plots, must be examined in order to assess the experiment's outcomes.

Firstly, the interaction between welding parameters like *AB* (WFS and voltage), *AC* (WFS and travel speed), *BC* (voltage and travel speed), and *ABC* (WFS, voltage and travel speed) was examined. No interaction effect of welding parameters is usually represented graphically by approximately parallel lines on the plot and interaction is represented by lines that converge or diverge or cross over each other on the plot. The interaction effect plot is a plot of the means of welding parameters (i.e. WFS, voltage and travel speed) at each level of welding parameters. The plot compares the mean magnitudes of UTS effects across welding parameters. Figure 27 to Figure 29 shows the two-factor interaction plots of the mean response of the UTS relative to welding parameters. Notice that levels of factors are denoted by *L1*, *L2* and *L3* in the graphs.

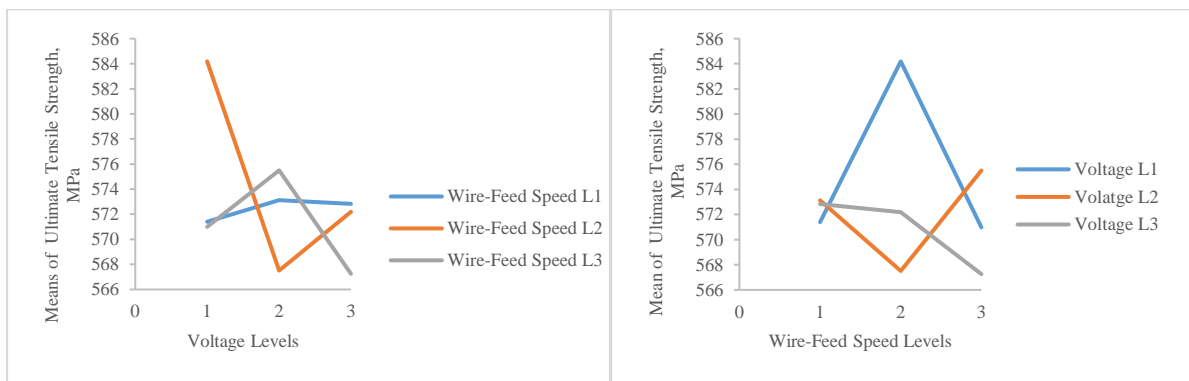


Figure 27: Interaction plots for wire-feed speed, voltage and vice versa for mean of UTS

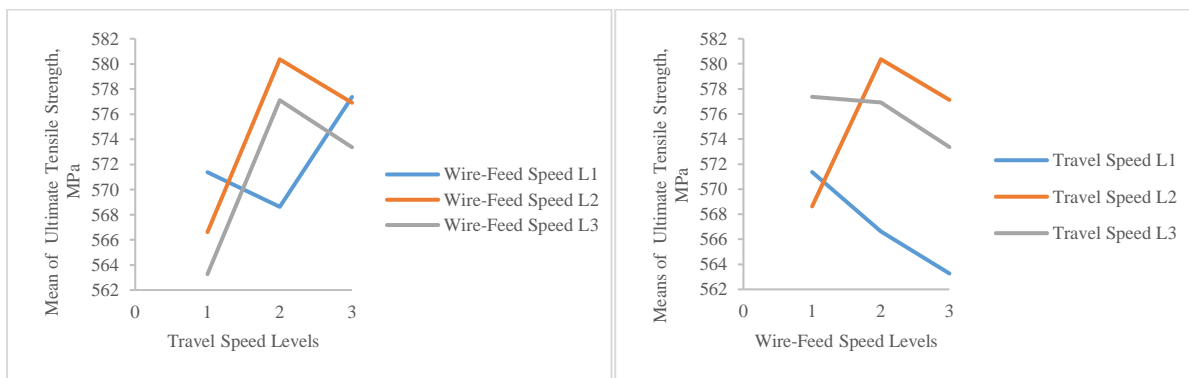


Figure 28: Interaction plots for wire-feed speed, travel speed and vice versa for mean of UTS

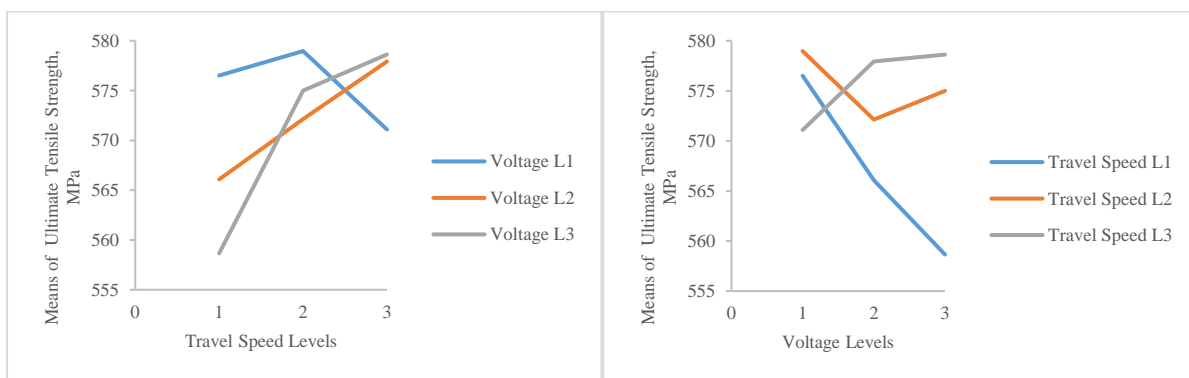


Figure 29: Interaction plots for voltage, travel speed and vice versa for mean of UTS

The interaction plots for AB and AC give a misleading graphical representation of the experimental results. The interaction plot for AB and AC are not statistically significant according to the statistical testing. The interaction plot for BC (voltage and travel speed) shows that one factor depends on the level of the other factor. There is a significant effect on the UTS of the two-way interaction BC, then experimental results must be interpreted by evaluating the interaction plots, not the main effects plot of travel speed (C). Increasing voltage from level 1 to level 3 increases the UTS at the higher range (level 3) of travel speed while decreasing the UTS in the lower and medium range (i.e. level 1 and level 2) of travel speed. Increasing travel speed from level 1 to level 3 increases the UTS at medium and higher ranges (i.e., level 2 and level 3) of voltage. WFS is not significant, choosing any level should give substantially the same UTS.

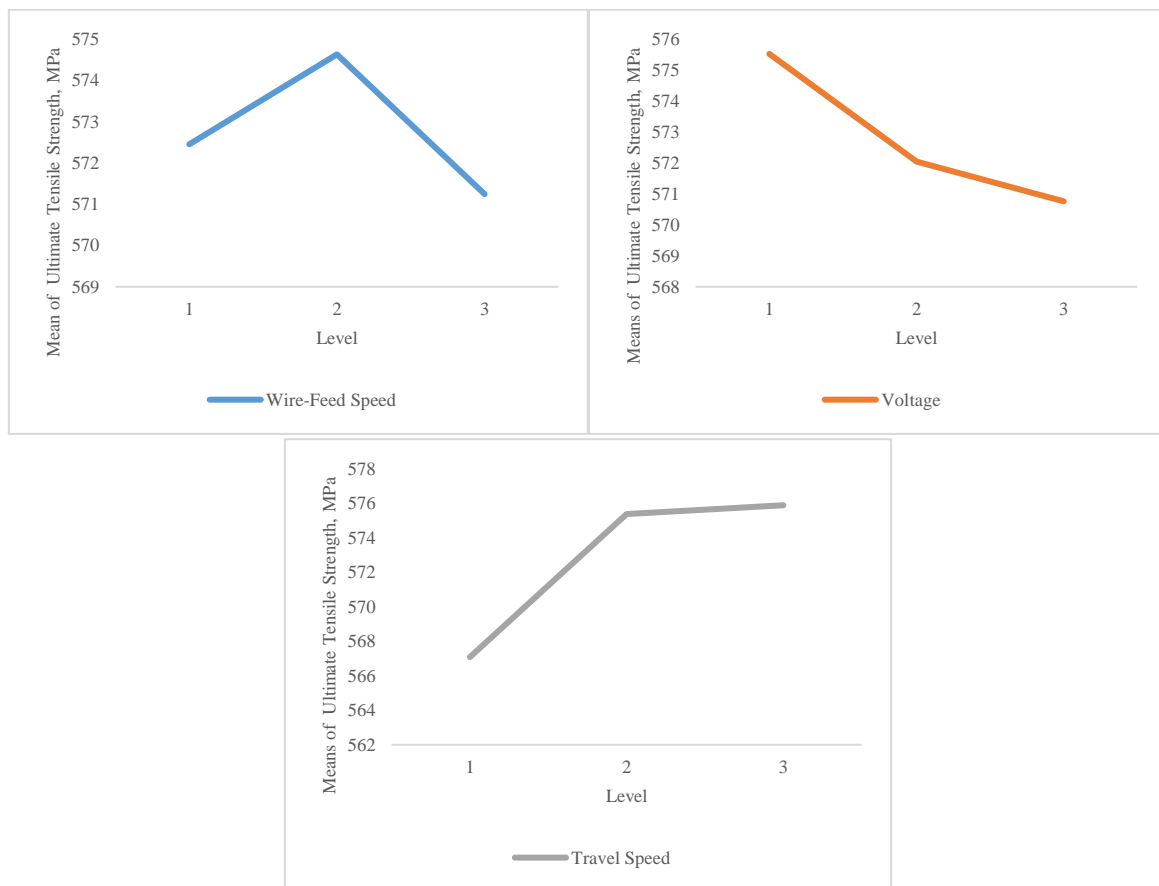


Figure 30: Effect of welding parameters on the mean of ultimate tensile strength on each level

The main effects plots such as WFS, voltage, and travel speed on the average UTS are illustrated in Figure 30. These plots illustrate the effect that changing the levels of the factors has on the UTS. It is observed that the average UTS of the welded joint increase as WFS changes from level 1 to level 2 and then decreases from level 2 to level 3, whereas changing voltage from level 1 to level 3 has the effect of decreasing the average UTS. It was also observed that the average UTS tends to increase as travel speed changes from level 1 to level 3. The optimum setting for WFS, voltage, and travel speed is level 2, level 1 and level 2 respectively. The main effects for WFS and voltage are not significant, and the interaction between WFS and voltage; and WFS and travel speed are not significant. The interaction effect plot for voltage and travel speed is used to examine the UTS experimental results not the main effect plot of the travel speed.

4.2.3. Effect of welding parameters on fatigue life of the welded joints

A three-way ANOVA test was conducted to determine which effects of three controlled factors such as WFS (A), voltage (B) and travel speed (C) are significant, and which are not. The interaction between factors such as two-factor interactions and three-factor interactions was also examined to determine if there is a significant difference in the means for one of the three controlled factors. The main effects (i.e. A , B and C) and interaction effects (i.e. AB , AC , BC and ABC) on the N_f were studied using a probability value at p -value ≤ 0.05 , assuming that the null hypothesis is true. Table 8 depicts the summarised results of the analysis of variance for the N_f .

Table 8: Summary results of analysis of variance for number of cycles to failure

Control Factor	Sum of Squares (SS)	DOF (df)	Mean Square (MS)	F -ratio	P -value	F critical	P -test	Rank	Contribution
A	8.42×10^8	2	4.21×10^8	8.1	0.001	3.168	Significant	1	36%
B	6.25×10^7	2	3.13×10^7	0.6	0.554	3.168	Insignificant	3	3%
C	2.11×10^8	2	1.06×10^8	2.0	0.142	3.168	Insignificant	2	9%
AB	1.35×10^8	4	3.38×10^7	0.6	0.632	2.543	Insignificant		3%
AC	1.14×10^9	4	2.85×10^8	5.4	0.001	2.543	Significant		24%
BC	5.64×10^8	4	1.41×10^8	2.7	0.040	2.543	Significant		12%
ABC	7.91×10^8	8	9.89×10^7	1.9	0.080	2.115	Insignificant		8%
SSE	2.82×10^9	54	5.23×10^7						4%
SST	6.57×10^9	80							

The presence of any interaction was tested at a significance level of $\alpha = 0.05$. It appears that there is an interaction between two factors like AC (WFS and travel speed), BC (voltage and travel speed) with respect to levels being studied and the occurrence of the N_f . If the p -value is greater than 0.05 then H_{0AB} and H_{0ABC} are not rejected. There is no dependence of one welding parameter on the value of another welding parameter for AB and ABC .

The p -value is less than 0.05 for WFS (A) with respect to levels being studied and the occurrence of the N_f which indicate that there is a statistically significant difference between WFS (A) with respect to levels being studied and the occurrence of the N_f . However, the p -value is acceptably higher than the chosen significant level of $\alpha = 0.05$ for voltage (B) and travel speed (C) with respect to the N_f . This indicates that there is no statistically significant difference between voltage (B) and travel speed (C) with respect to levels being studied and the occurrence of the number of cycles to fatigue failure. If the computed F -statistic of the WFS (A) is greater than selected critical F -values at a 95% confidence level, then the null hypothesis is rejected in favour of the alternative hypothesis. The computed F -statistic from the data corresponds with the p -value results. F -statistic for voltage (B) and travel speed (C) is less than selected critical F -values at a 95% confidence level, the null hypothesis is not rejected.

The small p -value indicates that there is substantial disagreement between the N_f with respect to wire-feed speed data with the null hypothesis. We reject the null hypothesis that the wire-feed speed does not have an effect on the N_f of the welded joint. There is evidence that indicates the wire-feed speed influence the N_f of the welded joint, and there is some difference between the wire-feed speed with respect to levels being studied and the occurrence of the N_f .

The acceptably high p-value indicates that there is less disagreement between the N_f with respect to voltage data with the null hypothesis. We fail to reject the null hypothesis that the voltage has an effect on the N_f of the welded joint. There is no evidence that indicates the voltage influence the N_f of the welded joint, and there is no difference between voltage with respect to levels being studied and the occurrence of the N_f .

The acceptably high p-value indicates that there is less disagreement between the N_f with respect to travel speed data with the null hypothesis. We fail to reject the null hypothesis that the travel speed has an effect on the N_f of the welded joint. There is no evidence that indicates the travel speed influence the N_f of the welded joint, and there is no difference between travel speed with respect to levels being studied and the occurrence of the N_f .

The effect of welding parameters on the N_f was ranked from first to last and the percentage contribution of welding parameters on the N_f was calculated as shown in Table 8. The standard error of the mean contributed 4% which is mainly due to specimen fabrication variation and human error.

4.2.4. Main effects and interaction effects plots of fatigue life on welded joints

The results of the experiments were interpreted by examining the main effects and interaction effects plots after conducting statistical tests. The effect plots do not take into consideration the statistical tests. All main effects of controlled factors, two-factor and three-factor interaction effects of this experiment were graphically represented by plotting the average response of the welding parameters versus the factor levels. When statistical testing indicates that an interaction effect is significant, the experiment's results must be evaluated using interaction plots rather than the main effects plots.

Firstly, the interaction between welding parameters like AB (WFS and voltage), AC (WFS and travel speed), BC (voltage and travel speed), and ABC (WFS, and voltage and travel speed) was examined. No interaction effect of welding parameters is usually represented graphically by approximately parallel lines on the plot and interaction is represented by lines that converge or diverge or cross over each other on the plot. The interaction effect plot is a plot of the means of welding parameters (i.e. WFS, voltage and travel speed) at each level of welding parameters. The plot compares the mean magnitudes of N_f effects across welding parameters. Figure 31 to Figure 33 shows the two-factor interaction plots of the mean response of the number of cycles to failure (N_f) relative to welding parameters. Notice that levels of factors are denoted by $L1$, $L2$, and $L3$ in the graphs.

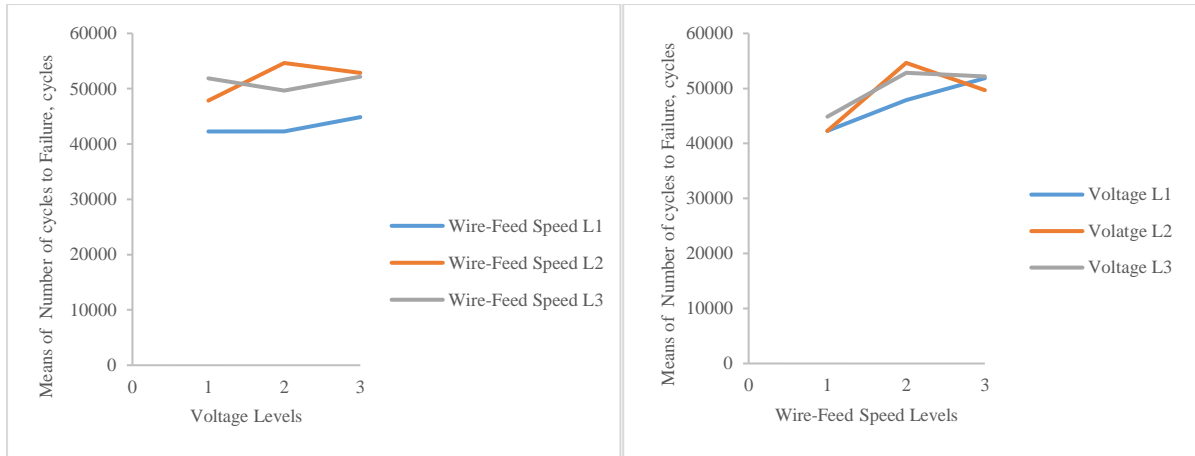


Figure 31: Interaction plots for wire-feed speed, voltage and vice versa for mean of N_f

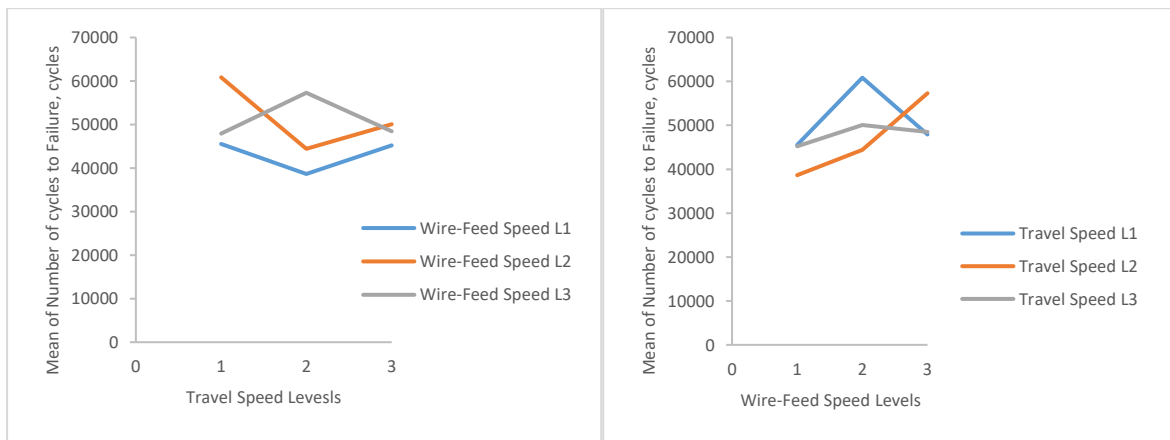


Figure 32: Interaction plots for wire-feed speed, travel speed and vice versa for mean of N_f

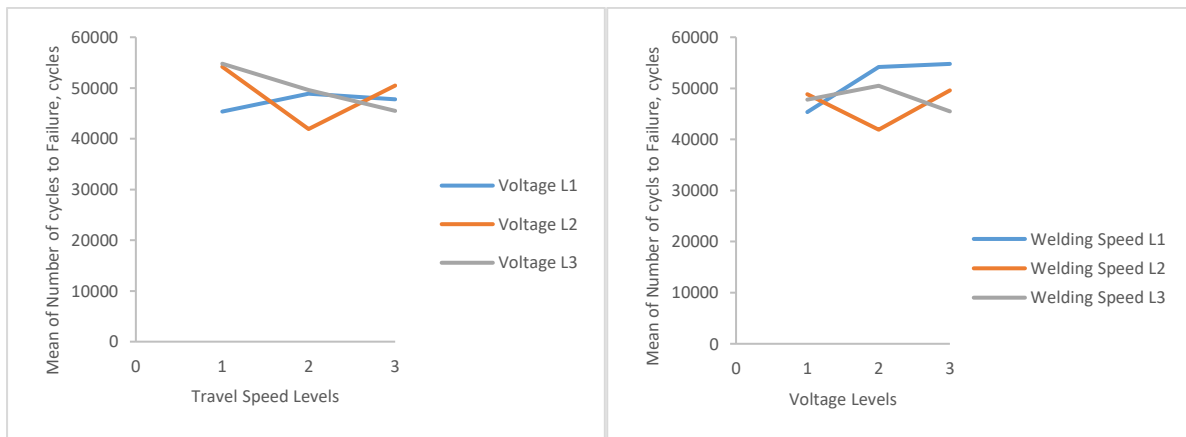


Figure 33: Interaction plots for voltage, travel speed and vice versa for mean of N_f

The interaction plot for AB (WFS and voltage) gives a misleading graphical representation of the experimental results. The interaction plot for AB is not statistically significant according to the statistical testing. The interaction plot for AC (WFS and travel speed) and BC (voltage and travel speed) shows that one factor depends on the level of the other factor. Because the two-way interaction between AC and BC has a significant impact on the N_f , it is necessary to interpret the experimental results by looking at the interaction plots rather than the main effects plots of WFS (A). Increasing WFS from level 1 to

level 3 increases the N_f at the medium range (level 2) of travel speed while increasing travel speed from level 1 to level 3 decreases the N_f in the lower and medium (i.e. level 1 and level 2) of WFS. Increasing travel speed from level 1 to level 3 decreases the N_f in the highest range (level 3) of voltage while increasing voltage from level 1 to level 3 increases the N_f in the lower range (level 1) of travel speed.

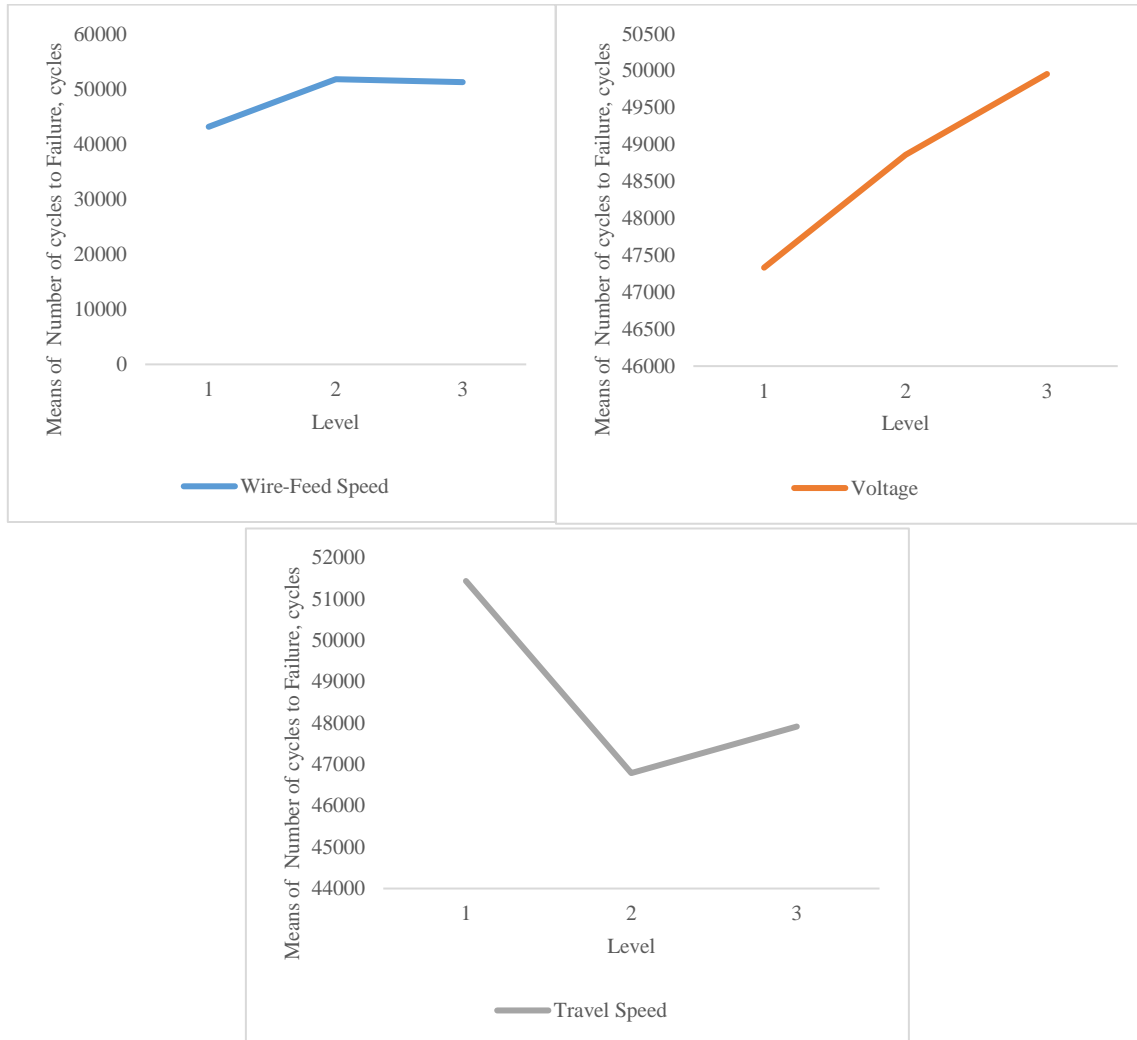


Figure 34: Effect of welding parameters on the mean of N_f on each level

The effect of main effects plots such as WFS, voltage and travel speed on the average N_f are illustrated in Figure 34. These plots illustrate the effect that changing the levels of the factors has on fatigue life. It is observed that the average N_f of the welded joint increase as WFS changes from level 1 to level 2 and then slightly decrease from level 2 to level 3, whereas changing voltage from level 1 to level 3 increases the average N_f . It was also observed that the average N_f tends to decrease as travel speed changes from level 1 to level 2 and increases from level 2 to level 3. The optimum setting for WFS, voltage and travel speed is level 2, level 2 and level 1 respectively. The main effects for voltage and travel speed are not significant and the interaction effect between WFS and voltage is not significant. The interaction effects plot for *AC* (WFS and travel speed) and *BC* (voltage and travel speed) are used to examine the experimental results not the main effect plot of WFS (*A*).

4.2.5. Discussion of ANOVA results

The tensile experimental result shows that there is an interaction between the voltage and travel speed that influence the UTS of the S355J2+N structural steel welded joints. The travel speed is the most significant welding parameter which influences the weld strength of the welded joints. Other welding parameters like WFS and voltage are not significant for UTS. The effect of travel speed is found to have most influence on the tensile strength of welded joints according to literature studies. The interaction between the welding parameters was not examined by many researchers in this field. There is a difference between the experimental findings because the different materials, filler material, shielding gas, plate thickness, and the number of passes per weld size were used by other researchers. The potential relationship between the welding parameters must be examined to be able to understand the strength of the relationship in relation to the UTS of the welded joint. Not including interaction effect in statistical design results in incomplete or misleading experimental results. The interaction between voltage and travel speed shows what happens to the UTS when the voltage or travel speed level is increased. As discussed by Dowling (2005), calibration errors, not perfect test specimen geometry, testing machine misalignment, and laboratory measurements that are not accurate all have an impact on laboratory measurements of material. The material properties also vary with the location in a plate that specimens extracted. The standard error of the mean of 7% indicates the accuracy of the sample mean to the experimental results mean of the UTS.

The findings of the fatigue experiment demonstrate that the N_f of the welded joint is influenced by an interaction between AC (WFS and travel speed) and BC (voltage and travel speed). The WFS is the most significant welding parameter that affects the N_f of the welded joint. Other welding parameters like voltage and travel speed are not significant for the N_f . Increasing WFS from level 1 to level 3 increases the N_f in the medium range (level 2) of travel speed while lower and higher range (i.e. level 1 and level 3) of travel speed increase the N_f to level 2 of WFS and then decrease to level 3 of WFS. Ghazvinloo and Shadfar (2010) observed that increasing current and voltage decreases the fatigue life of WM, but the fatigue life gradually increases with increasing the travel speed. There is a difference in analysis methods and different parameters are examined. Most studies on fatigue life are about the effect of weld bead geometry and the microstructure of the welded joint (Lee *et al.*, 2009; Chang Hee Suh, Rac Gyu Lee, Sang Kyun Oh, 2011; Ahiale and Oh, 2014), since geometry is the most significant factor influencing fatigue life. The statistical significance of the experimental results is usually not determined in their studies. As discussed by Dowling (2005), laboratory measurements of material parameters such as the N_f are often subjected to uncertainty. These results are further impacted by not perfect test specimen geometry, calibration errors, testing machine misalignment, and load accuracy. The standard error of the mean of 4% indicates the accuracy of the sample mean to the experimental results mean of the N_f .

4.3. Failure of welded joints

The results of the tensile and fatigue tests are discussed in this section. The acceptance testing criteria and the observed failure modes of the welded joints are discussed. Macrostructure examination and hardness test used for failure analysis of welded joints are also discussed.

4.3.1. Failure analysis of tensile tested specimens

The failure of the welded joint specimen should occur within gauge length to satisfy the acceptance testing criteria. If the specimens do not meet the specified requirements, the results are not considered. Figure 35 shows the accepted failure of the tensile specimen within the gauge length. All 81 tensile specimens failed within the gauge length.

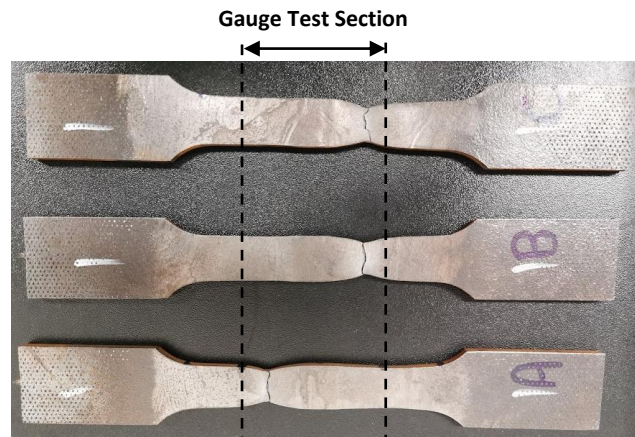


Figure 35: Specimen failure in gauge test section

The stress and strain curves of the tension test defined the material properties of the welded joints. The stress of the ductile specimen reaches a maximum point and subsequently declines before fracture, as in Figure 36, according to the stress-strain data that was collected at frequent intervals using a video extensometer and transferred via a digital computer. All the tensile tested specimens exhibited good ductility and follow the same ductile metal behaviour. The UTS was computed by dividing the maximum force being applied during the test by the initial cross-sectional area. Then the fracture strength was obtained from the force at the fracture dividing by the original cross-sectional area. The stress and strain curves for all 27 experiments are given in Appendix B.

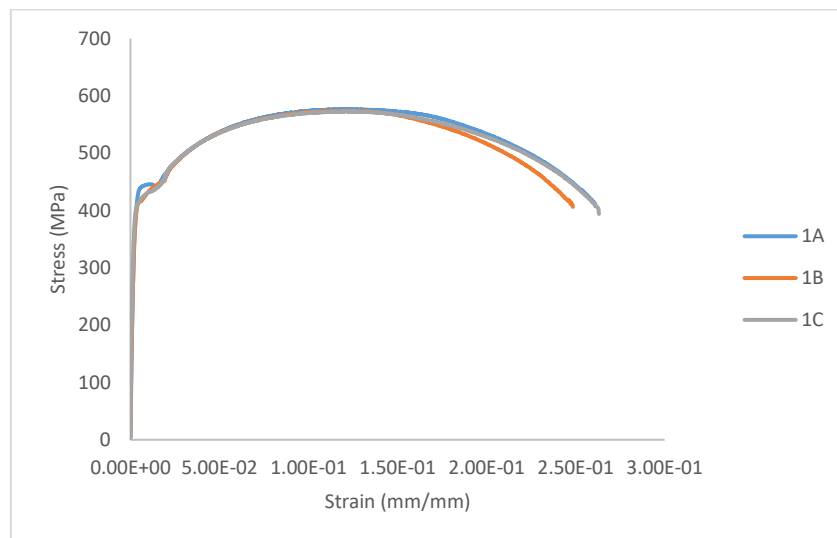


Figure 36: Stress - strain plot for three test specimens: 1A, 1B and 1C of the first experiment

This investigation found that, regardless of variation in welding parameters, the PM consistently experienced failure of the welded joints under tensile stress. This is comparable to findings reported by

Kumar and Shahi (2011) as well as Flores *et al.* (2016) that tensile specimens consistently fractured at the PM irrespective of variation in HI. This shows that the PM has lower UTS than the WM in each joint.

The shear band was identified as the common mode of failure of the tensile tests during visual examination of the specimens after fracture; this is illustrated in Figure 37 below.



Figure 37: Shear bands mode of fracture for tensile test

Callister (2017) stated that the ideal tensile fracture is the mixed mode of fracture (i.e. cup and cone). Kazasidis and Pantelis (2017) observed the intense bands of shear fracture in most tested specimens with a HI above 1 kJ/mm . There are similarities in the experimental findings, but different parameters were used. All the tensile specimens failed under shear with maximum stress at a 45-degree plane.

4.3.2. Failure analysis of fatigue tested specimens

The failure of the welded joint specimen should occur in the test section (i.e. reduced area) as shown in Figure 38 to satisfy the acceptance testing criteria. If the failure occurs on the specimen gripping section, the results are not considered. All 54 fatigue specimens failed within the testing section.



Figure 38: Fatigue tested specimen showing the location of fracture

The fracture surfaces for various welding parameters did not significantly differ from one another. All the specimens showed mainly transverse cracking and the crack initiation was within the test section.

Similar to the tensile specimens, the shear bands mode of fracture is the typical mode of failure for the fatigue-tested specimen. It was observed that 9% of the fatigue specimens fractured in the WM.

Most fatigue specimens consistently fractured at the PM irrespective of variation of welding parameters. Flores *et al.* (2016) observed that fatigue damage accumulation has no impact on the fracture location of the lower HI (1.1 kJ/mm) specimens because all specimens are fractured at the PM. However, it was found that high HI (1.6 kJ/mm) fracture took place in the WM. The fatigue failure of the welded joint is consistent with Flores *et al.* (2016) for HI between 1.1 and 1.6 kJ/mm . There is a difference between the experimental findings because of the different materials, methods, filler material, shielding gas and the number of passes per weld size used by other researchers.

4.3.3. Macrostructural examination

The three selected ruptured specimens were examined using a stereoscope to investigate the fracture location for tensile test specimens. The three specimens were selected based on HI and UTS which are experiments 3, 11 and 27. Experiment 3 has the lowest HI (1274 J/mm), experiment 27 has the high HI (1511 J/mm) and experiment 11 has the highest average UTS (591 MPa), and its HI (1404 J/mm) it is between the two selected experiments. The variation of grain size in different sub-zones such as WM, HAZ and PM for selected three ruptured specimens were examined. CGHAZ, FGHAZ, ICHAZ and SCHAZ next to the PM are the four sub-zones that make up the variation in grain size within the HAZ. The CGHAZ had the greatest peak temperature, which contributed to the sub-zone's increased grain size in the grain. The microstructure within FGHAZ and ICHAZ experienced low peak temperature compared to CGHAZ which caused the decrease in the grain size of the welded joint.

It is observed that the failure of the welded joint specimens is occurring in the PM away from the weld. The mechanical properties of the weld and HAZ are stronger than the parent metal of the welded joint. It was also observed that there is no correlation between the tensile failure of the welded joints with HI since all the tensile failures occur away from the weld and HAZ. However, the fracture location of welded joints 27A and 11C is close to the HAZ compared to 3A. Figure 39 to Figure 41 show the 2 mm stitched images of the stereoscope of the fractured specimens.

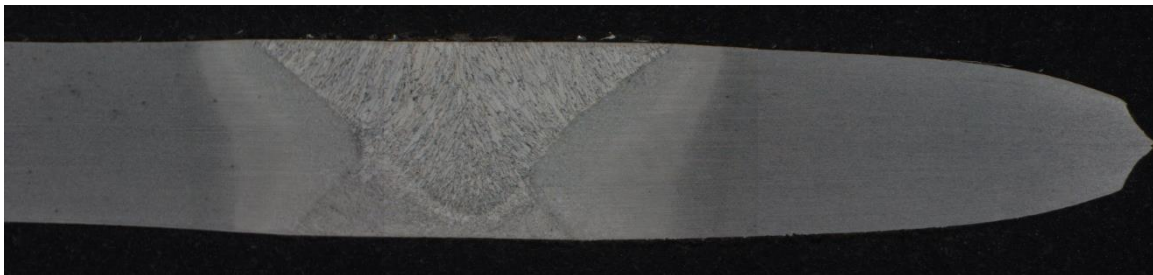


Figure 39: Welded joint 3A

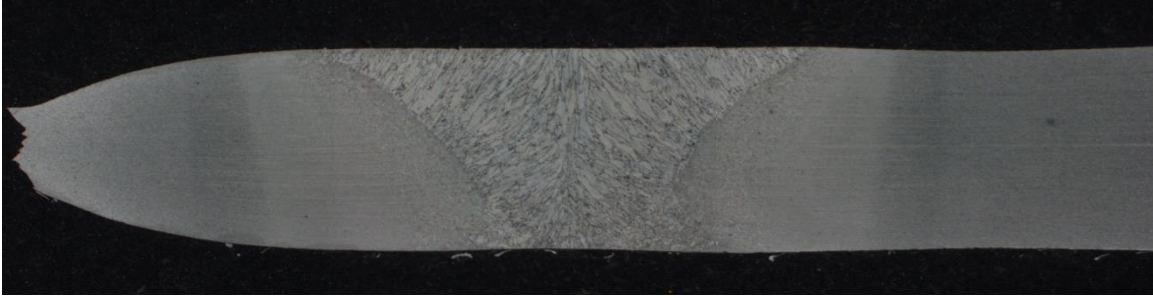


Figure 40: Welded joint 11C

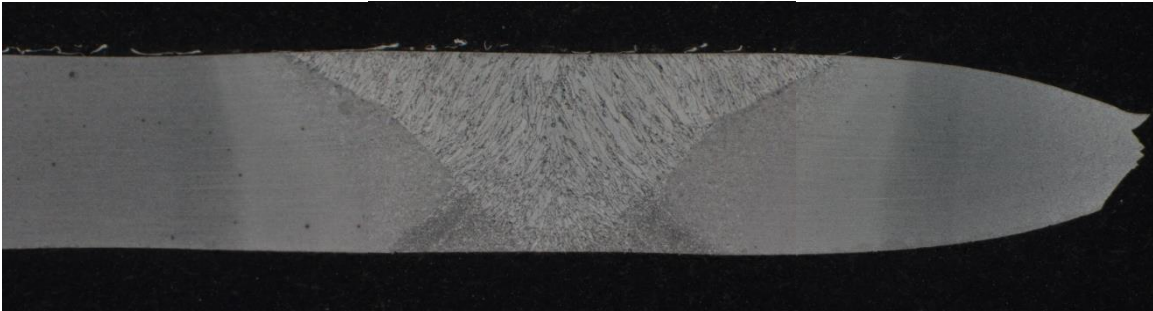


Figure 41: Welded joint 27A

As might be expected, the HI has a significant influence on the WM's macrostructure. The length of the HAZ increases with an increase in HI. The grain structure changes from the PM to HAZ and HAZ to the welded zone just like studies conducted by other researchers (Kumar and Shahi, 2011; Biswas *et al.*, 2018).

4.3.4. Hardness test

The hardness profile measurements were conducted to investigate the welded specimen failures using Vickers hardness test with a load of 0.5 kgf applied at 1 mm interval from the centreline of the weldments. The three selected experiments for macrostructural examination were analysed. Figure 42 shows hardness profile measurements of the three selected experiments from the centreline of the weldments. A logarithmic trendline was fitted to create the fitted curves. The WM and HAZ area are not the same sizes, due to different HIs applied within the three selected experiments. The HAZ for 3, 11 and 27 experiments start at the following distances: 3.5 , 2.5 and 5.5 mm respectively after the WM.

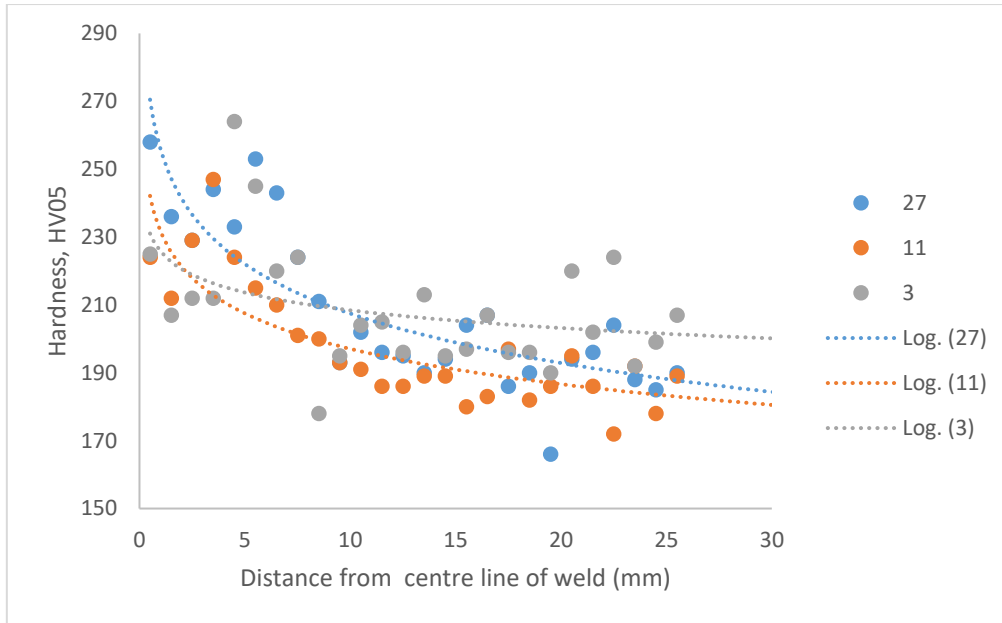


Figure 42: Hardness profile measurements of three selected experiments

Hardness is empirically correlated to the UTS of the welded specimens. The micro-Vickers hardness results revealed the hardness variation within the WM, HAZ and PM. It was observed that the hardness of the WM is more than that of the PM for the tested specimens. It was also observed that the hardness of the HAZ is more than that of the WM for experiments 3 and 11 but experiment 27 has more hardness in the WM than the HAZ. The experimental results showed that there is no significant difference between the PM hardness of the three selected specimens with respect to fracture point. The average hardness in the PM for experiments 3, 11 and 27 are 201, 187 and 193 *HV* respectively.

It was observed that HI affects the hardness of the WM, HAZ and PM as expected. The hardness experimental results are consistent with Kumar and Shahi (2011) findings that the low HI specimens have high hardness in the HAZ. High HI specimens have low hardness in the HAZ followed by medium HI specimens have medium hardness in the HAZ. There is a difference between the experimental findings because of the different number of passes per weld size. In multipass welded joints, the prior runs serve as pre-heat for the subsequent weld deposit that results in changed macrostructure and hardness (Murti *et al.*, 1993).

4.4. Non-destructive testing

NDT was conducted to detect the welding defects that might influence the mechanical properties of the welded joints without causing any physical damage to the testing specimen. Visual inspection was conducted to check for visible flaws like porosity, burn-through, undercut, underfill and incomplete root penetration during welding. MT is the NDT method that was utilised to detect surface and subsurface cracks of the welded joint.

Some experiments during welding of the root run had welding defects like burn-through, however, the filling run was welded to complete the weld joint. It was observed that the increase in voltage at low current causes burn-through of the welded joints because the WFS is too slow to feed wire. It was also observed that the increase in the WFS increases the bead height for the filling run. The results of the NDT test are displayed in Table 9.

Table 9: Non-destructive testing

Number of experiments	Visual testing	Magnetic particle testing
1	No weld imperfections	No weld imperfections
2	No weld imperfections	No weld imperfections
3	No weld imperfections	No weld imperfections
4	No weld imperfections	No weld imperfections
5	No weld imperfections	No weld imperfections
6	Burn-through (Root Run)	Pinhole
7	Burn-through (Root Run)	Pinhole
8	Burn-through (Root Run)	Pinhole
9	Burn-through (Root Run)	Pinhole
10	Porosity (Filling Run)	Porosity
11	No weld imperfections	No weld imperfections
12	No weld imperfections	No weld imperfections
13	No weld imperfections	No weld imperfections
14	No weld imperfections	No weld imperfections
15	Burn-through (Root Run)	Pinhole
16	No weld imperfections	No weld imperfections
17	Burn-through (Root Run)	Pinhole
18	Burn-through (Root Run)	Pinhole
19	No weld imperfections	No weld imperfections
20	No weld imperfections	No weld imperfections
21	No weld imperfections	No weld imperfections
22	No weld imperfections	No weld imperfections
23	No weld imperfections	No weld imperfections
24	No weld imperfections	No weld imperfections
25	No weld imperfections	No weld imperfections
26	No weld imperfections	No weld imperfections
27	Burn-through (Root Run)	Pinhole

Table 9 shows how the variation of welding parameters affects the weld quality. The experimental test results show the consistency of the nature of the welding defects produced during root run welding. Magnetic particle testing conducted showed that the same experiments which had burn-through root run have pinhole defects/lack of root fusion not permitted by Class B in terms of the ISO 5817 standard. The specimens with no indication of welding defects were used to conduct destructive tests such as tensile tests and fatigue tests. The extracted specimens from the welded plate with defects were discarded to avoid making the experimental results inconclusive. It has been proven by other scholars that the welding defects reduce the structural integrity of the welded joint (Madyira, Kumba and Kaymakci, 2017). Reduction in undesirable manufacturing defects and defect-free specimens yield better experimental test results to determine the effect of welding parameters on the UTS and fatigue life of the welded joint.

The effect of WFS, voltage, and travel speed on the welding defects identified in the specimens are illustrated in Figure 43. These plots illustrate the effect that changing the levels of the welding parameters has on the welding defects such as burn-through. It is observed that the number of welding defects of the welded joint decrease as WFS increase from level 1 to level 3, whereas increasing voltage

and travel speed from level 1 to level 3 increases the number of welding defects of the welded joint. Madyira, Kumba and Kaymakci (2017) observed that increasing travel speed affects the fatigue performance of the welded joints. According to Hussain *et al.* (2010), increasing travel speed causes the UTS of the welded joint to decrease, which in turn causes an increase in welding defects.

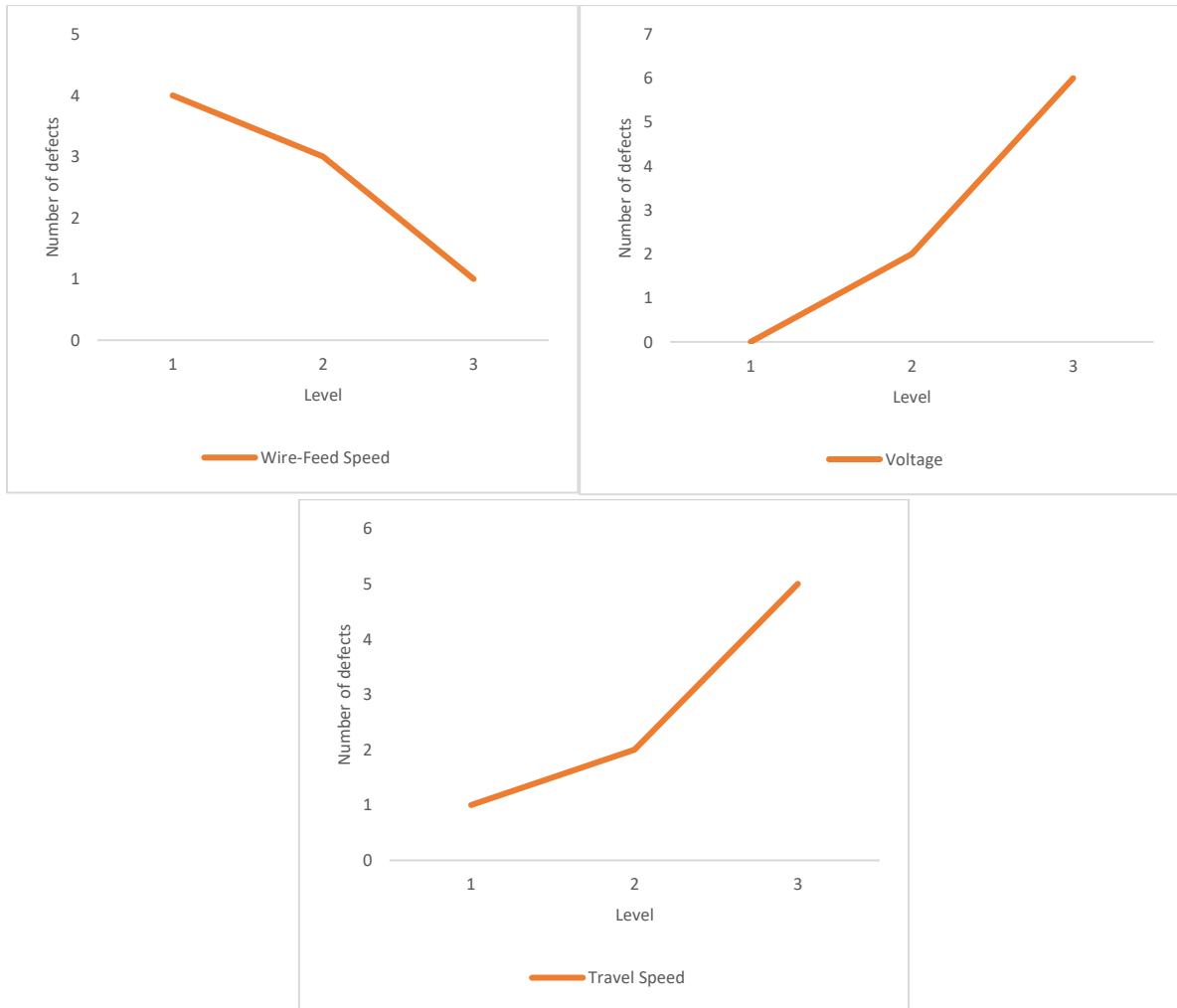


Figure 43: Effect of welding parameters vs. welding defects on each level

4.5. Effect of welding parameters on UTS and fatigue life of the welded joints

The effect of welding parameters on UTS and the N_f of the welded joint was ranked to determine the optimum levels. The position of the UTS and N_f relative to each other per experiment are compared in Table 10 below.

Table 10: Ultimate tensile strength and number of cycles to failure

No. of Exp.	Welding parameters levels			Ranking ultimate tensile strength and fatigue life		
	Wire-feed speed (A)	Voltage (B)	Travel speed (C)	UTS (MPa)	N_f (cycles)	Difference
1	1	1	1	11	22	11
2	1	1	2	15	21	6
3	1	1	3	18	18	0
4	1	2	1	13	17	4
5	1	2	2	17	25	8
6	1	2	3	10	19	9
7	1	3	1	21	14	7
8	1	3	2	24	27	3
9	1	3	3	3	12	9
10	2	1	1	2	7	5
11	2	1	2	1	16	15
12	2	1	3	16	20	4
13	2	2	1	26	1	25
14	2	2	2	19	26	7
15	2	2	3	9	4	5
16	2	3	1	27	3	24
17	2	3	2	4	11	7
18	2	3	3	5	15	10
19	3	1	1	23	23	0
20	3	1	2	14	5	9
21	3	1	3	12	6	6
22	3	2	1	20	10	10
23	3	2	2	7	9	2
24	3	2	3	6	13	7
25	3	3	1	25	8	17
26	3	3	2	8	2	6
27	3	3	3	22	24	2

The experimental results showed that variation of welding parameters produces welding defects. The number of welding defects of the welded joint decreases with increasing WFS and increases with increasing voltage and travel speed. The weld defects weaken the structural integrity of the welded joint. It was observed in Table 10 that the defect-free specimens that were extracted from the welded plates that had welding defects do not necessarily have weak structural integrity. The higher-ranking levels obtained are A2B1C1 (i.e. WFS level 2, voltage level 1 and travel speed level 1) for optimal UTS and fatigue life which corresponds to experiment 10. These optimal levels are achieved where welding defects are minimal. It was also observed that the experiments with lower ranking levels for optimal weld strength and fatigue life do not necessarily have weak structural integrity.

4.6. Conclusion

The experimental results from tensile and fatigue testing were used to evaluate the impact of welding parameters on the UTS and fatigue life, in order to establish the optimum combination of welding parameters on the UTS and fatigue life of the welded joint. Design of experiments was used to study the welding parameters by determining the relationship between controlled welding parameters affecting a process and the output of the process. ANOVA was used to interpret the impact of welding parameters on UTS and fatigue life. The statistical significance of the experimental results was tested by assuming the null hypothesis. The standard error mean of the experimental results was evaluated to measure the accuracy and consistency of the experimental results. The presence of interaction between welding parameters was also assessed. The effect of welding parameters of this study was compared to welding parameters from other studies.

The general mode of failure in this study for tensile is a shear bands mode of fracture. All tensile specimens exhibited good ductility and no correlation between the tensile failure of the welded joints with HI was observed, since all the tensile failure occurred away from the weld and HAZ. Most fatigue failures also occurred away from the weld, HAZ and no correlation between the fatigue failure of the welded joint with HI was observed. The interaction and main effect plots were employed to express how the welding parameters affect the UTS and fatigue life of the welded joint. The travel speed is the most significant welding parameter that has an influence on the weld strength of the welded joints. There is an interaction between voltage and travel speed that influence the UTS of the welded joints. The interaction effect plot between voltage and travel speed shows that the highest point observed of the UTS of 579 MPa is when the voltage is in the lower range (level 1) and travel speed is in the medium range (level 2), and when voltage is in the higher range (level 3) and travel speed is in the higher range (level 3), and when travel speed is in the medium range (level 2) and voltage is also in the medium range (level 2). The WFS is the most significant welding parameter that has an influence on the fatigue life of the welded joint. There is an interaction between WFS and travel speed, and voltage and travel speed that influence the N_f of the welded joints. The interaction effects plot between WFS and travel speed shows that the highest point observed of the N_f of 60845 cycles is when the travel speed is in the lower range (level 1) and WFS is in the medium range (level 2), and when WFS is in the medium range (level 2) and travel speed is in the lower range (level 1). The interaction effects plot between voltage and travel speed shows that the highest point observed in the N_f of 54785 cycles is when the travel speed is in the lower range (level 1) and voltage is in the higher range (level 3), and voltage is in the higher range (level 3) and travel speed is in the lower range (level 1). The optimum levels obtained are A2B1C1 (i.e. WFS level 2, voltage level 1 and travel speed level 1) for better weld strength and fatigue life.

5. Conclusion and recommendation

An experimental investigation was conducted to study the effect of welding parameters like WFS, voltage and travel speed on the UTS and fatigue life in robotic MIG welding for S355J2+N structural steel weld joints. The literature review in section 1.3 discussed the effect of welding parameters, HI, welding geometry, shielding gas, electrode, failure, and fracture of welded joints. The basic theories of static and fatigue loading of welded joints, testing methods and standards, and statistical analysis methods used to validate data of tensile and fatigue tests performed are discussed in chapter 2. The experimental methodology, material and welding parameter selection, specimen geometry and fabrication, experimental setup, and testing are discussed in chapter 3. The experimental results were discussed and analysed for both tensile and fatigue testing in chapter 4. Analysis of variance was used to draw a conclusion on the experimental results obtained from the experimental tests.

5.1. Conclusion

This study clearly showed that the tensile and fatigue testing results of S355J2+N welded joint specimens are dependent on the welding parameters (i.e. WFS, voltage and travel speed) and metallurgical structure per welding parameters specified. The experimental results obtained from both testing machines (i.e. MTS Criterion Model 45 Universal Testing Machine for tensile testing and Servo-Hydraulic Universal-Axial Testing machine PSA) showed consistency and repeatability. The variation in experimental results is attributed to several factors such as specimen fabrication (i.e. uniformity of the thickness of the plate, uniformity of the root face, bevel angle and root gap throughout the plates) and human error.

The effects of welding parameters on the UTS and fatigue life of the structural welded joints were analysed by varying the WFS, voltage and travel speed. The experimental results of the UTS showed that there is an interaction between the voltage and travel speed. The higher range of travel speed with increasing voltage is suitable for achieving maximum tensile strength. The UTS also increases with increasing travel speed at the medium and higher range of voltage. There is no statistically significant difference between the WFS and voltage with respect to levels being studied and the occurrence of the UTS. The experimental results of N_f showed that there is an interaction between WFS and travel speed, and voltage and travel speed. The medium range of travel speed with increasing WFS increases the N_f . The N_f is also increased with increasing voltage at the lower range of travel speed. There is no statistically significant difference between the voltage and travel speed with respect to levels being studied and the occurrence of the N_f .

Instead of only designing for static failure, this extensive knowledge can be put to use in practice to design against fatigue failure and static failure. It was observed that variation of welding parameters affects the weld quality, the weld defects are caused by an increase in voltage and travel speed at lower WFS. There is no correlation between the tensile and fatigue failure of the welded joints with HI from the parameter values being studied.

The strength and fatigue life of any structure are essentially reduced by welding, according to the literature. The designers of rolling stock are interested in achieving suitable levels of weld performance and economy, while also assuring the safety and durability of the welded components. This study will improve the production of rolling stock components by minimising the number of welding defects

produced by variation of welding parameters. The welding defects introduce additional stress concentrations into the weld that affects the structural integrity of welded joints. The optimum welding parameters selection for UTS and fatigue life will improve the welded joint design life and strength of rolling stock components.

5.2. Contribution and limitations

This study can be utilised as a part of an ongoing investigation into the effect of welding parameters on UTS and fatigue life of welded joints produced by different welding processes with different joint designs. The contribution of this study includes the following.

- Understanding the impact of welding parameters of the welded joint under static and fatigue loading.
- The optimum welding parameters selection for UTS and fatigue life can be developed.
- Undesirable welding defects that affect the structural integrity of the welded joint can be minimised to improve weld quality, increase productivity, and reduce reworks.
- Improve welding parameters allowable range limitation.

The limitations experienced during this study are due to limited resources and time constraints.

- A transverse weld tension test is unacceptable for evaluating YS and elongation due of the unevenly distributed strain through the gauge length during yielding. The actual YS and elongation could not be obtained.
- High cyclic fatigue testing could not be investigated as it requires more time than could made available for a master's degree study during the COVID-19 pandemic.
- Testing more than three specimens would provide more accurate experimental results with lower standard error of the specimen mean.

5.3. Recommendations for future work

Various welding parameters of welding processes have an influence on the UTS and fatigue life of the welded joint. A need exists to further experimentally investigate tensile and fatigue testing to build upon the existing experimental data. Future work with regards to the effect of welding parameters on mechanical properties could include the following:

- Extensive research focussing on precise controlled welding parameters to improve weld quality without producing welding defects should be investigated.
- Different weld joint designs with different welding processes should be examined.
- The effect of various steel materials and dissimilar welding steel materials should be studied.
- Development in the prediction of welding distortions and residual stress should be investigated.
- Formulae to predict optimum welding parameters without the fabrication process and welding process limitations should be investigated.
- Various stress ratios should be considered.
- Effect of applied stress ratio and frequency on the fatigue life of the welded joint should be studied.

- Round welded bar should be used to study the effect of welding parameters on the fatigue life since it is difficult to obtain adequate surface finish in welded plates.

6. References

- Ahiale, G.K. and Oh, Y.J. (2014) 'Microstructure and fatigue performance of butt-welded joints in advanced high-strength steels', *Materials Science and Engineering A*, 597, pp. 342–348. Available at: <https://doi.org/10.1016/j.msea.2014.01.007>.
- Amraei, M., Ahola, A., Afkhami, S., Björk, T., Heidarpour, A. and Zhao, X.L. (2019) 'Effects of heat input on the mechanical properties of butt-welded high and ultra-high strength steels', *Engineering Structures*, 198(August), p. 109460. Available at: <https://doi.org/10.1016/j.engstruct.2019.109460>.
- ASTM E1382 (2004) 'Standard Test Methods for Determining Average Grain Size Using Semiautomatic and Automatic Image Analysis', 97(November 2004), pp. 1–21. Available at: <https://doi.org/10.1520/E1382-97R10.Section>.
- ASTM E3 – 11 (2011) 'Standard Practice for Preparation of Metallographic Specimens', *ASTM Standards*, pp. 1–12.
- ASTM E384 (2002) 'Standard Test Method for Microindentation Hardness of Materials ASTM E384', *ASTM Standards*, pp. 1–24.
- ASTM E4-03 (2010) 'Standard Practices for Force Verification of Testing Machines', *Quality Assurance Journal*, 13(3–4), pp. 41–56.
- ASTM E466-15 (2015) 'Practice for conducting force controlled constant amplitude axial fatigue tests of metallic materials', *ASTM Book of Standards*, pp. 1–6. Available at: <https://doi.org/10.1520/E0466-15.2>.
- ASTM E739-91 (2009) 'Standard Practice for Statistical Analysis of Linear or Linearized Stress-Life (S-N) and Strain-Life (ϵ -N) Fatigue Data', *Statistical Analysis of Fatigue Data*, (Reapproved 2004), pp. 1–7. Available at: <https://doi.org/10.1520/stp29332s>.
- ASTM E8 (2006) 'Standard Test Methods for Tension Testing of Metallic Materials 1', i, pp. 1–24.
- Avazkonandeh-Gharavol, M.H., Haddad-Sabzevar, M. and Haerian, A. (2009) 'Effect of copper content on the microstructure and mechanical properties of multipass MMA, low alloy steel weld metal deposits', *Materials and Design*, 30(6), pp. 1902–1912. Available at: <https://doi.org/10.1016/j.matdes.2008.09.023>.
- AWS B4.0 (2016) 'Standard Methods for Mechanical Testing of Welds', *American Welding Society (AWS)*, pp. 2–12.
- AWS D1.1/D1.1M (2015) *Structural Welding Code – Steel*.
- Basak, S., Pal, T.K. and Shome, M. (2016) 'High-cycle fatigue behavior of MIG brazed galvanized DP600 steel sheet joint—effect of process parameters', *International Journal of Advanced Manufacturing Technology*, 82(5–8), pp. 1197–1211. Available at: <https://doi.org/10.1007/s00170-015-7451-1>.
- Basim, N.A., Rahul Raj, N., Sajin, S.J., Pradeep, W.V. and Nagaraj, S.V. (2017) 'Experimental Investigation of MIG Welding Parameters and its Mechanical Properties on Dissimilar Steels', *International Journal of Engineering Science and Computing*, 7(4), pp. 9989–9991. Available at: <http://ijesc.org/>.
- Bęczkowski, R. and Gucwa, M. (2014) 'The Effect of Heat Input on the Geometric Properties of Welded Joints', *Archives of Foundry Engineering*, 14(9), pp. 127–130.
- Biswas, A.R., Chakraborty, S., Ghosh, P.S. and Bose, D. (2018) 'Study of Parametric Effects on Mechanical Properties of Stainless Steel (AISI 304) and Medium Carbon Steel (45C8) Welded Joint Using GMAW', *Materials Today: Proceedings*, 5(5), pp. 12384–12393. Available at:

<https://doi.org/10.1016/j.matpr.2018.02.217>.

Brooke, M.H. and Miller, R. (1990) 'Fatigue testing', *Muscle & Nerve*, 13(1 S), pp. S35–S37. Available at: <https://doi.org/10.1002/mus.880131311>.

BS EN 10025-2 (2004) 'Hot rolled products of structural steels— Part 2: Technical delivery conditions for non-alloy structural steels', *Bs En 10025-2:2004*, 3, p. 36. Available at: <https://bsol.bsigroup.com/en/Bsol-Item-Detail-Page/?pid=000000000030157914>.

BS EN 1011-1 (1998) 'Welding - Recommendations for welding of metallic materials - Part 1: General guidance for arc welding', pp. 1–10.

BS EN 1291 (1998) 'British Standard Non-destructive testing of welds — Magnetic particle testing of welds — Acceptance levels'.

BS EN 13749 (2011) 'Railway applications — Wheelsets and bogies — Method of specifying the structural requirements of bogie frames'.

BS EN ISO 14341 (2011) 'Welding consumables - Wire electrodes and weld deposits for gas shielded metal arc welding of non alloy and fine grain steels - Classification (ISO 14341:2010)'.

BS EN ISO 15614-1 (2012) 'Specification and qualification of welding procedures for metallic materials - Welding procedure test'.

BS EN ISO 17638 (2009) 'Non-destructive testing of welds — Magnetic particle testing (ISO 17638)'.

BS EN ISO 4136 (2012) 'Destructive tests on welds in metallic materials - Transverse tensile test'.

Budynas–Nisbett (1997) 'Discourse: The new critical idiom', *Shigley's Mechanical Engineering Design* [Preprint]. Available at: <https://doi.org/10.1007/s13398-014-0173-7.2>.

Callister, W. (2017) *Materials Science and Engineering An Introduction, 10th Edition* by David G. Rethwisch and William Callister.

Celik, S. and Ersozlu, I. (2009) 'Investigation of the mechanical properties and microstructure of friction welded joints between AISI 4140 and AISI 1050 steels', *Materials and Design*, 30(4), pp. 970–976. Available at: <https://doi.org/10.1016/j.matdes.2008.06.070>.

Cerón-Bretón, J.G., Cerón-Bretón, R.M., Rangel-Marrón, M., Muriel-García, M., Cordova-Quiroz A.V. and Estrella-Cahuich, A. (2011) 'A new prediction of the fatigue limit based on Brinell hardness and ultimate strength for high strength steels', 5(3), pp. 328–336.

Chang Hee Suh, Rac Gyu Lee, Sang Kyun Oh, Y.-C.J. (2011) 'Effect of welding heat input on fatigue life of quenched boron steel and FB steel lap joint', *Journal of Mechanical Science and Technology*, 25(7), pp. 1727–1735. Available at: <https://doi.org/10.1007/s12206-011-0424-x>.

Chotai, A.P.H. (2011) 'A Review on Parameters Controlling Gas Metal Arc Welding (GMAW) Process', pp. 8–10.

Devore, J.L., Farnum, N.R. and Doi, J.A. (2001) *Applied Statistics for Engineers and Scientists, Technometrics*. Available at: <https://doi.org/10.1198/tech.2001.s554>.

Dowling, N.E. (2005) *Mechanical behavior of materials: Engineering methods for deformation, fracture, and fatigue*, Pearson. Available at: <https://doi.org/10.1017/CBO9780511810930>.

EN ISO 17637 (2016) 'Non-destructive testing of welds - Visual testing of fusion - welded joints', pp. 2–7.

Flores, R.B., Ruíz, A., Rubio-González, C., *et al.* (2016) 'Effect of heat input and accumulated fatigue damage on mechanical properties of dissimilar AL-6XN/316L welded joints', *Materials Characterization*, 112, pp. 41–50. Available at: <https://doi.org/10.1016/j.matchar.2015.11.029>.

- Ghazvinloo, H.R. and Shadfar, N. (2010) 'Effect of arc voltage , welding current and welding speed on fatigue life , impact energy and bead penetration of AA6061 joints produced by robotic MIG welding', 5356(February).
- Gonçalves, T.S., de Faria, G.L., de Siqueira, R.H.M. and de Lima, M.S.F. (2020) 'Weldability and mechanical behavior of laser-welded TRIP 750 steel sheets', *International Journal of Advanced Manufacturing Technology*, 107(5–6), pp. 2807–2815. Available at: <https://doi.org/10.1007/s00170-020-05223-y>.
- Guo, W., Crowther, D., Francis, J.A., Thompson, A., Liu, Z. and Li, L. (2015) 'Microstructure and mechanical properties of laser welded S960 high strength steel', *Materials and Design*, 85(November 2017), pp. 534–548. Available at: <https://doi.org/10.1016/j.matdes.2015.07.037>.
- Hobbacher, A. (2008) *IIW document IIW-1823-07 Fatigue Design of Welded Joints and Components*.
- Hussain, A.K., Lateef, A., Javed, M. and Pramesh, T. (2010) 'Influence of Welding Speed on Tensile Strength of Welded Joint in TIG Welding Process', 1(3), pp. 518–527.
- Ibrahim, I.A., Mohamat, S.A., Amir, A. and Ghalib, A. (2012) 'The Effect of Gas Metal Arc Welding (GMAW) processes on different welding parameters', 41(Iris), pp. 1502–1506. Available at: <https://doi.org/10.1016/j.proeng.2012.07.342>.
- ISO 1099 (2006) 'Metallics materials-Fatigue testing-Axial force-controlled method.PDF', p. 28.
- ISO 15609-1 (2004) 'Specification and qualification of welding — Welding procedure specification — procedures for metallic materials — Part 1: Arc welding', 2004, pp. 2–7.
- ISO 17640 (2010) 'Non-destructive testing of welds — Ultrasonic testing — Techniques , testing levels , and assessment (ISO 17640 : 2010)'.
- ISO 5725 (1994) 'Accuracy (Trueness and Precision) of Measurement Methods and Results'.
- ISO 5817 (2014) 'Welding — Fusion-welding joints in steel , nickel , titanium and their alloys (beam welding excluded) — Quality levels for imperfections', 2014.
- ISO 9692-1 (2013) 'Welding and allied processes — Types of joint preparation — Part 1: Manual metal arc welding, gas- shielded metal arc welding, gas welding, TIG welding and beam welding of steels', 2013.
- Jagtap, K.R., Rojekar, M.S., Dravid, S. V and Deshpande, A.R. (2017) 'ScienceDirect Effect of Welding Parameters on Tensile & Yield Strength of IS 2062 grade Steel Using Design of Experiment Approach', *Materials Today: Proceedings*, 4(8), pp. 7875–7883. Available at: <https://doi.org/10.1016/j.matpr.2017.07.123>.
- Jenney, C.L. and O'Brien, A. (1969) *Welding Handbook, Welding Handbook*. Available at: <https://doi.org/10.1007/978-1-349-00324-2>.
- Jenney, C.L. and O'Brien, A. (1991) *Welding handbook-II part I, American Welding Society*.
- Kaçar, R. and Kökemli, K. (2005) 'Effect of controlled atmosphere on the mig-mag arc weldment properties', *Materials and Design*, 26(6), pp. 508–516. Available at: <https://doi.org/10.1016/j.matdes.2004.07.027>.
- Kalpajian, S. and Schmid, S.R. (2013) *Manufacturing Engineering and Technology, Bulletin of Science, Technology & Society*. Available at: <https://doi.org/10.1177/0270467687007005-605>.
- Kang, L., Ge, H. and Kato, T. (2015) 'Experimental and ductile fracture model study of single-groove welded joints under monotonic loading', *Engineering Structures*, 85, pp. 36–51. Available at: <https://doi.org/10.1016/j.engstruct.2014.12.006>.
- Karadeniz, E., Ozsarac, U. and Yildiz, C. (2007) 'The effect of process parameters on penetration in

- gas metal arc welding processes', *Materials and Design*, 28(2), pp. 649–656. Available at: <https://doi.org/10.1016/j.matdes.2005.07.014>.
- Kazasidis, M.E. and Pantelis, D.I. (2017) 'The effect of the heat input energy on the tensile properties of the AH-40 fatigue crack arrester steel, welded by the use of the robotic metal-cored arc welding technique', *International Journal of Advanced Manufacturing Technology*, 93(9–12), pp. 3967–3980. Available at: <https://doi.org/10.1007/s00170-017-0761-8>.
- Kihl, D.P. and Sarkani, S. (1999) 'Mean stress effects in fatigue of welded steel joints', *Probabilistic Engineering Mechanics*, 14(1–2), pp. 97–104. Available at: [https://doi.org/10.1016/S0266-8920\(98\)00019-8](https://doi.org/10.1016/S0266-8920(98)00019-8).
- Kim, H.J., Lee, C.S., Park, S.H. and Shin, D.H. (2004) 'Quantitative analysis on low cycle fatigue damage: A microstructural model for the prediction of fatigue life', *Materials Science and Engineering A*, 379(1–2), pp. 210–217. Available at: <https://doi.org/10.1016/j.msea.2004.01.044>.
- Kim, I.S., Son, J.S., Kim, I.G., Kim, J.Y. and Kim, O.S. (2003) 'A study on relationship between process variables and bead penetration for robotic CO₂ arc welding', *Journal of Materials Processing Technology*, 136(1–3), pp. 139–145. Available at: [https://doi.org/10.1016/S0924-0136\(02\)01126-3](https://doi.org/10.1016/S0924-0136(02)01126-3).
- Kolhe, K.P. and Datta, C.K. (2008) 'Prediction of microstructure and mechanical properties of multipass SAW', *Journal of Materials Processing Technology*, 197(1–3), pp. 241–249. Available at: <https://doi.org/10.1016/j.jmatprotec.2007.06.066>.
- Kumar, A., Khurana, M.K. and Yadav, P.K. (2016) 'Optimization of Gas Metal Arc Welding Process Parameters', *IOP Conference Series: Materials Science and Engineering*, 149(1). Available at: <https://doi.org/10.1088/1757-899X/149/1/012002>.
- Kumar, S. and Shahi, A.S. (2011) 'Effect of heat input on the microstructure and mechanical properties of gas tungsten arc welded AISI 304 stainless steel joints', *Materials and Design*, 32(6), pp. 3617–3623. Available at: <https://doi.org/10.1016/j.matdes.2011.02.017>.
- Laitinen, R., Valkonen, I. and Kömi, J. (2013) 'Influence of the base material strength and edge preparation on the fatigue strength of the structures made by high and ultra-high strength steels', *Procedia Engineering*, 66, pp. 282–291. Available at: <https://doi.org/10.1016/j.proeng.2013.12.083>.
- Lee, C.H., Chang, K.H., Jang, G.C. and Lee, C.Y. (2009) 'Effect of weld geometry on the fatigue life of non-load-carrying fillet welded cruciform joints', *Engineering Failure Analysis*, 16(3), pp. 849–855. Available at: <https://doi.org/10.1016/j.engfailanal.2008.07.004>.
- Lee, J.H., Park, S.H., Kwon, H.S., Kim, G.S. and Lee, C.S. (2014) 'Laser, tungsten inert gas, and metal active gas welding of DP780 steel: Comparison of hardness, tensile properties and fatigue resistance', *Materials and Design*, 64, pp. 559–565. Available at: <https://doi.org/10.1016/j.matdes.2014.07.065>.
- Li, M., Sun, F., Li, D.F., O'Donoghue, P.E., Leen, S.B. and O'Dowd, N.P. (2018) 'The effect of ferrite phases on the micromechanical response and crack initiation in the intercritical heat-affected zone of a welded 9Cr martensitic steel', *Fatigue and Fracture of Engineering Materials and Structures*, 41(6), pp. 1245–1259. Available at: <https://doi.org/10.1111/ffe.12768>.
- Long, H., Gery, D., Carlier, A. and Maropoulos, P.G. (2009) 'Prediction of welding distortion in butt joint of thin plates', *Materials and Design*, 30(10), pp. 4126–4135. Available at: <https://doi.org/10.1016/j.matdes.2009.05.004>.
- Maddox, S.J. (2000) 'Fatigue design rules for welded structures', pp. 102–109.
- Madyira, D.M., Kumba, T. and Kaymakci, A. (2017) 'Influence of Manufacturing Conditions on Fatigue Life of Welded Joints', 8(October 2016), pp. 665–672. Available at: <https://doi.org/10.1016/j.promfg.2017.02.085>.

- Marines, I., Dominguez, G., Baudry, G., *et al.* (2003) 'Ultrasonic fatigue tests on bearing steel AISI-SAE 52100 at frequency of 20 and 30 kHz', *International Journal of Fatigue*, 25(9–11), pp. 1037–1046. Available at: [https://doi.org/10.1016/S0142-1123\(03\)00161-0](https://doi.org/10.1016/S0142-1123(03)00161-0).
- Mercan, S., Aydin, S. and Özdemir, N. (2015) 'Effect of welding parameters on the fatigue properties of dissimilar AISI 2205-AISI 1020 joined by friction welding', *International Journal of Fatigue*, 81, pp. 78–90. Available at: <https://doi.org/10.1016/j.ijfatigue.2015.07.023>.
- Mishra, B., Panda, R.R. and Mohanta, D.K. (2014) 'Metal Inert Gas (Mig) Welding Parameters Optimization', *International Journal of Multidisciplinary and Current Research*, 2(June), pp. 637–639.
- Murti, V.S.R., Srinivas, P.D., Banadeki, G.H.D. and Raju, K.S. (1993) 'Effect of heat input on the metallurgical properties of HSLA steel in multi-pass MIG welding', *Journal of Materials Processing Tech.*, 37(1–4), pp. 723–729. Available at: [https://doi.org/10.1016/0924-0136\(93\)90131-O](https://doi.org/10.1016/0924-0136(93)90131-O).
- Ottersböck, M.J., Leitner, M., Stoschka, M. and Maurer, W. (2016) 'Effect of Weld Defects on the Fatigue Strength of Ultra High-strength Steels', *Procedia Engineering*, 160(Icmfm Xviii), pp. 214–222. Available at: <https://doi.org/10.1016/j.proeng.2016.08.883>.
- Patil, S.R. and Waghmare, C.A. (2013) 'Optimization of Mig Welding Parameters for Improving Strength of Welded Joints', *International Journal of Advanced Engineering Research and Studies*, II(July-Sept.), pp. 14–16. Available at: <https://doi.org/10.1007/s00170-009-1931-0.K.Y>.
- Pawaria, N., Kataria, S., Goyal, A. and Sharma, S. (2013) 'Effect of Heat Input and Shielding Gas on Hardness , Tensile and Impact Strength of 2 . 25 Cr-1Mo Steel Weld Metals in GMAW', 5762(February), pp. 266–269.
- Pirinen, M. (2013) *The Effects of Welding Heat Input on the Usability of High Strength Steels in Welded Structures, Doctor of Science Thesis. Lappeenranta University of Technology.*
- Ragu Nathan, S., Balasubramanian, V., Malarvizhi, S. and Rao, A.G. (2015) 'Effect of welding processes on mechanical and microstructural characteristics of high strength low alloy naval grade steel joints', *Defence Technology*, 11(3), pp. 308–317. Available at: <https://doi.org/10.1016/j.dt.2015.06.001>.
- Reddy Vempati, S., Brahma Raju, K. and Venkata Subbaiah, K. (2018) 'Optimization of Welding Parameters of Ti 6al 4v Cruciform shape Weld joint to Improve Weld Strength Based on Taguchi Method', *Materials Today: Proceedings*, 5(2), pp. 4948–4957. Available at: <https://doi.org/10.1016/j.matpr.2017.12.072>.
- Sakai, T., Sato, Y., Nagano, Y., Takeda, M. and Oguma, N. (2006) 'Effect of stress ratio on long life fatigue behavior of high carbon chromium bearing steel under axial loading', *International Journal of Fatigue*, 28(11), pp. 1547–1554. Available at: <https://doi.org/10.1016/j.ijfatigue.2005.04.018>.
- Sankar, B.V., Lawrence, I.D. and Jayabal, S. (2018) 'Experimental Study and Analysis of Weld Parameters by GRA on MIG Welding', *Materials Today: Proceedings*, 5(6), pp. 14309–14316. Available at: <https://doi.org/10.1016/j.matpr.2018.03.013>.
- Schijve, J. (2008) *Fatigue of structures and materials, Fatigue of Structures and Materials.* Available at: https://doi.org/10.1007/978-1-4020-6808-9_12.
- Shinde, A.P., Deshpande, A.R., Chinchankar, S.S. and Kulkarni, A.P. (2017) 'ScienceDirect Evaluation of Tensile Strength of a Butt-Welded Joint Considering the Effect of Welding Parameters Using Response Surface Methodology', *Materials Today: Proceedings*, 4(8), pp. 7219–7227. Available at: <https://doi.org/10.1016/j.matpr.2017.07.049>.
- Shoeb, M. (2013) 'Effect of Mig Welding Input Process Parameters on Weld Bead Geometry on Hsla Steel', *International Journal of Engineering & Technology*, 5(01), pp. 200–212.

Singh, R. (2022) *Arc Welding Processes Handbook, Arc Welding Processes Handbook*. Available at: <https://doi.org/10.1002/9781119819080>.

Sittichai, K., Santirat, N. and Sompong, P. (2012) 'A Study of Gas Metal Arc Welding Affecting Mechanical Properties of Austenitic Stainless', *World Academy of Science, Engineering and Technology*, 6(1), pp. 402–405.

Stoschka, M., Leitner, M., Posch, G. and Eichlseder, W. (2013) 'Effect of high-strength filler metals on the fatigue behaviour of butt joints', *Welding in the World*, 57(1), pp. 85–96. Available at: <https://doi.org/10.1007/s40194-012-0010-6>.

Svoboda, H.G. and Nadale, H.C. (2015) 'Fatigue Life of GMAW and PAW Welding Joints of Boron Microalloyed Steels', *Procedia Materials Science*, 9, pp. 419–427. Available at: <https://doi.org/10.1016/j.mspro.2015.05.012>.

Tong, L., Niu, L., Ren, Z. and Zhao, X.L. (2021) 'Experimental investigation on fatigue behavior of butt-welded high-strength steel plates', *Thin-Walled Structures*, 165(March), p. 107956. Available at: <https://doi.org/10.1016/j.tws.2021.107956>.

Ullah, N., Rajput, S.K., Gupta, V., Verma, V. and Soota, T. (2019) 'ScienceDirect To study mechanical properties and microstructures of MIG welded high strength low alloy steel', *Materials Today: Proceedings*, 18, pp. 2550–2555. Available at: <https://doi.org/10.1016/j.matpr.2019.07.112>.

Vanaja, T. (2017) 'Optimization of Mig Welding Process Parameters for Improving Welding Strength of', 50(1), pp. 26–33.

Wang, H., Xu, S., Wang, Y. and Li, A. (2018) 'Effect of pitting degradation on ductile fracture initiation of steel butt-welded joints', *Journal of Constructional Steel Research*, 148, pp. 436–449. Available at: <https://doi.org/10.1016/j.jcsr.2018.06.001>.

Wang, Y., Kannan, R. and Li, L. (2016) 'Characterization of as-welded microstructure of heat-affected zone in modified 9Cr-1Mo-V-Nb steel weldment', *Materials Characterization*, 118, pp. 225–234. Available at: <https://doi.org/10.1016/j.matchar.2016.05.024>.

Zhao, X., Dongpo, W., Deng, C., Liu, Y. and Zongxian, S. (2012) 'The fatigue behaviors of butt welds ground flush in the super-long life regime', *International Journal of Fatigue*, 36(1), pp. 1–8. Available at: <https://doi.org/10.1016/j.ijfatigue.2011.09.009>.

Zolfaghari, Abolfazl, Zolfaghari, Amin and Kolahan, F. (2018) 'Reliability and sensitivity of magnetic particle nondestructive testing in detecting the surface cracks of welded components', *Nondestructive Testing and Evaluation*, 33(3), pp. 290–300. Available at: <https://doi.org/10.1080/10589759.2018.1428322>.

Appendix A: Manufacturing process of welded joint specimen

The fabrication of the specimens was accomplished by cutting the steel plates with specified dimensions of $350\text{ mm} \times 125\text{ mm} \times 6\text{ mm}$ and bevelled into the required dimensions (i.e. root face of 0 mm and bevel angle of 32°). The plates were cut and bevelled using a waterjet cutting machine.



Figure 44: Waterjet cut steel plates

The area near the welding surface was ground and, wire-brushed to remove oil, dirt, cracks, and any other defects that might adversely affect the quality of the weld. Then the edges of the bevelled plates with a single V configuration were tacked together to maintain the root gap of 2.4 mm . Subsequently, the tacks were ground to a smooth surface and the welding area was wire brushed to ensure good root penetration. Finally, the removable ceramic backing bar was placed on the back of the plate to ensure that the root edges were completely fused.

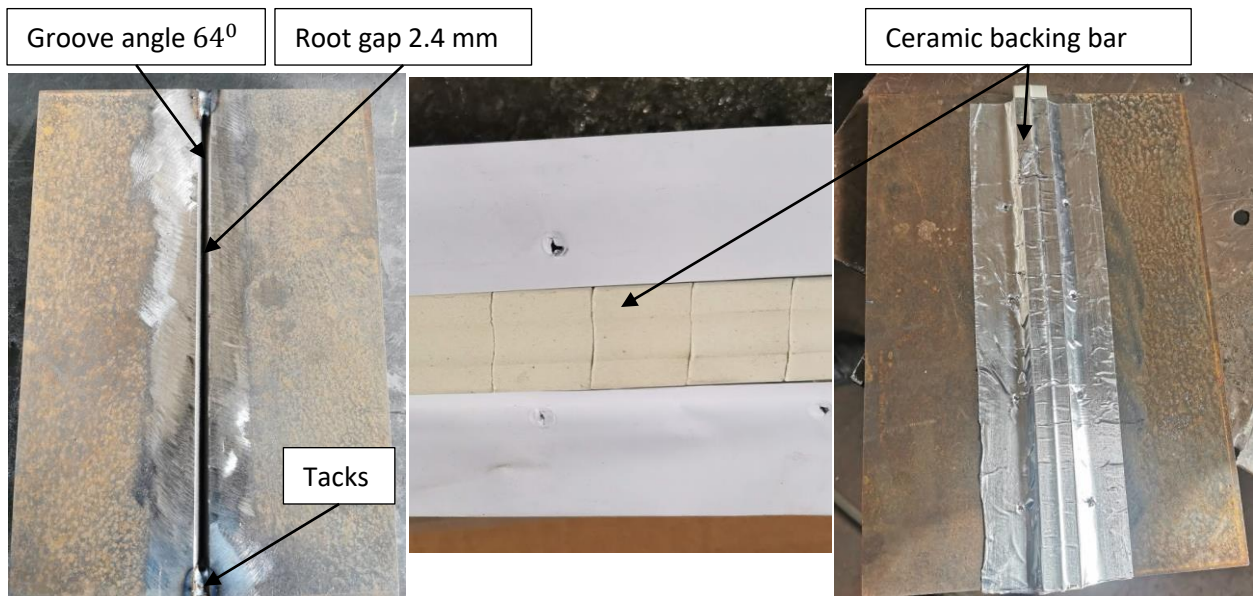


Figure 45: Tacked plate

The tacked steel plate was properly placed in the welding fixture stand to ensure repeatability of the experimental investigation and to reduce distortion of the welded plate.



Figure 46: Fixture arrangement for fixing specimen

Thereafter the start/stop points and the sequences of movements were programmed in the welding pendant interface for the robot to automatically follow the weld path during welding.



Figure 47: Welding pendant

The welding parameter values of the root run and capping run were set in the SKS Q80 process controller and pendant of the robot. The welding parameters such as WFS, voltage, wire diameter, and gas quality were set on the SKS Q80 controller and the travel speed was set on the pendant of the robot.

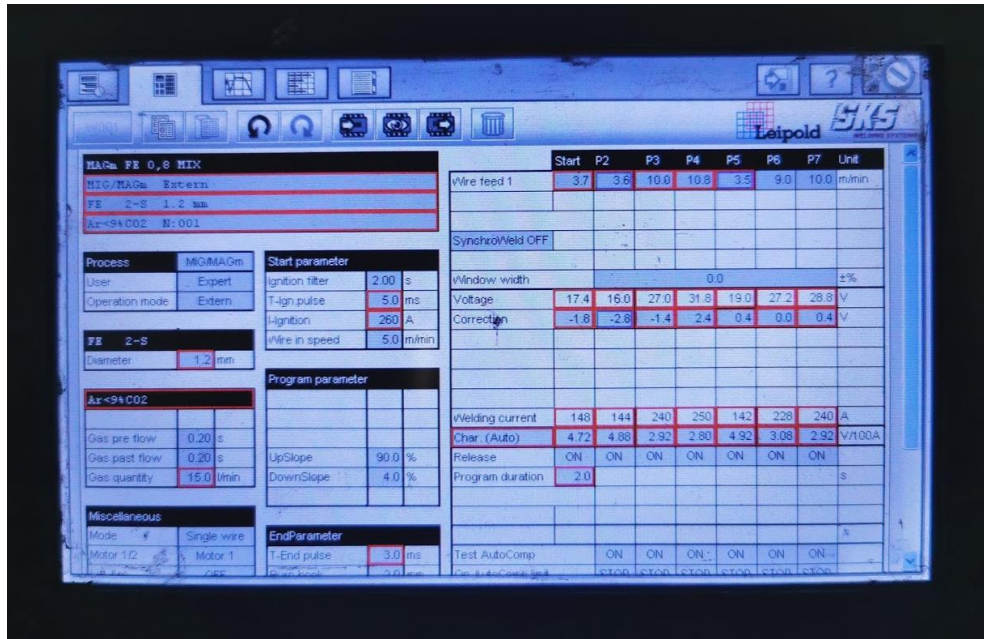


Figure 48: Programming SKS Q80 controller

The root run and capping run was welded, and the welded plate was wire brushed between the welding runs. The same process was followed for all 27 experiments. The welding gun nozzle was cleaned with spatter release spray between experiments to avoid unnecessary welding defects.



Figure 49: Robot welding

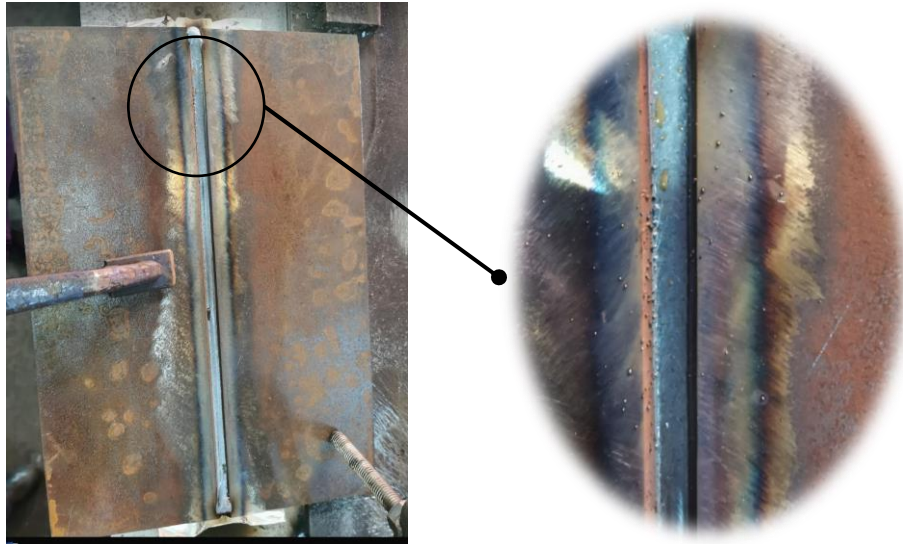


Figure 50: Root run

Finally, the welded joint plate was removed from the welding fixture and the removable ceramic weld backing bar was removed. The welded joint plate was marked for the identification of experiments.

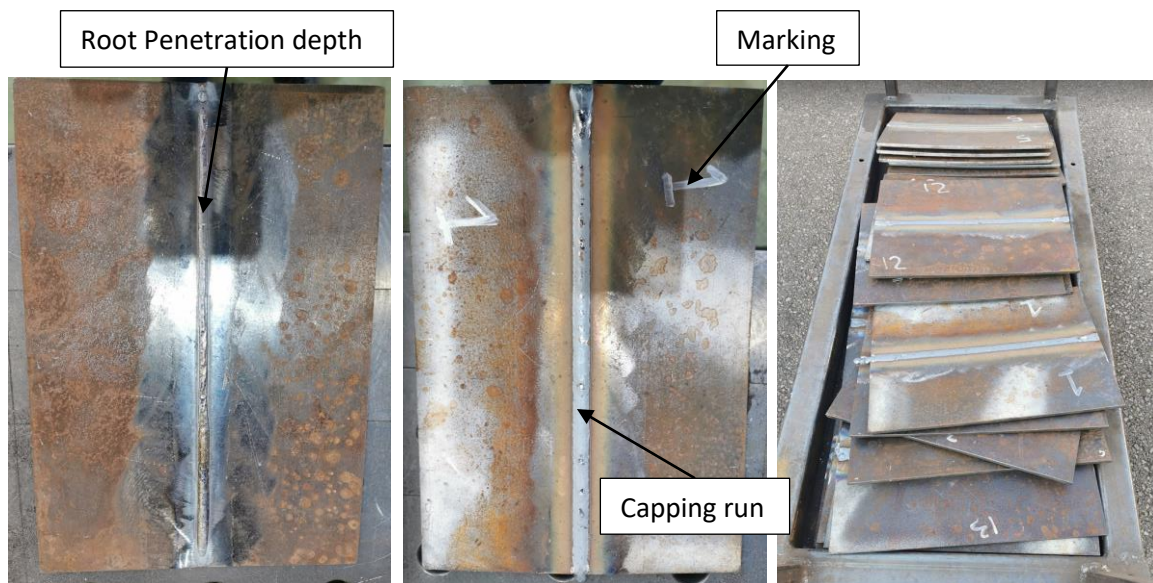


Figure 51: Welded plate

The SKS welding system records the welding parameters during the welding process. The graphs show the welding parameters such as voltage, current, wire feed and time during welding. The influence of the welding parameters on arc stability can be observed in the graphs.



Figure 52: Welding parameters graphs for root run and capping run

The visual inspection was conducted to check for visible flaws like cavities and cracks. Thereafter, the welds were ground flush to the thickness of the base material to minimise the geometric notch effect. The welding surface of the welded plate was prepared by grinding the welding irregularities like spatters. Magnetic particle testing was used to detect surface and subsurface cracks of the welded joint. The white contrast paint was applied by spraying as a background on the welded joint plate. Then a black magnetic ink composed of iron powder particles in a liquid form was applied by spraying and the hand-held electromagnetic yoke magnetising was used for magnetising the welded plate to detect defects.

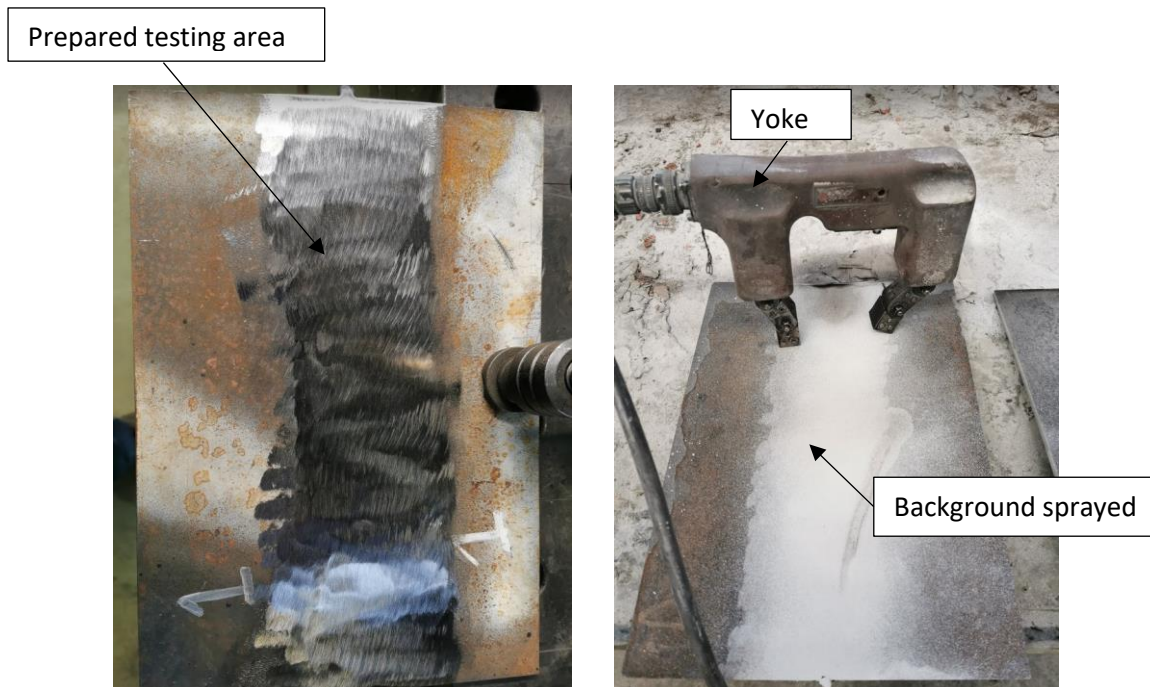


Figure 53: MT preparation

To ensure the detection of imperfections in all orientations, the weld was magnetized in two directions that are perpendicular and parallel to the weld joint in the direction of the rolling directions. The acceptance criteria specified by ISO 5817 and BS EN 1291 were used to evaluate the completeness of the fusion of the root run and capping run. The welding defects were marked, and defect-free specimens were extracted from the welded joint plate. The test welded joint plate was demagnetised after conducting the test.



Figure 54: MT performed on the welded

Thereafter the specimens were extracted from the welded plate using a waterjet cutting machine. The specimens were extracted 25 mm away from the edge of the welded plate to avoid imperfections and defects such as crater cracks. The surface finish for all the specimens extracted from the test welded joint plates will be the same since the same machining rate and cutting wire are used. The welded plates were wire brushed to remove any rust and oil films on the specimen's surfaces. Thereafter the welded plates were polished with the sanding flap disc. Then the extracted specimens were marked for each experiment and packed together.

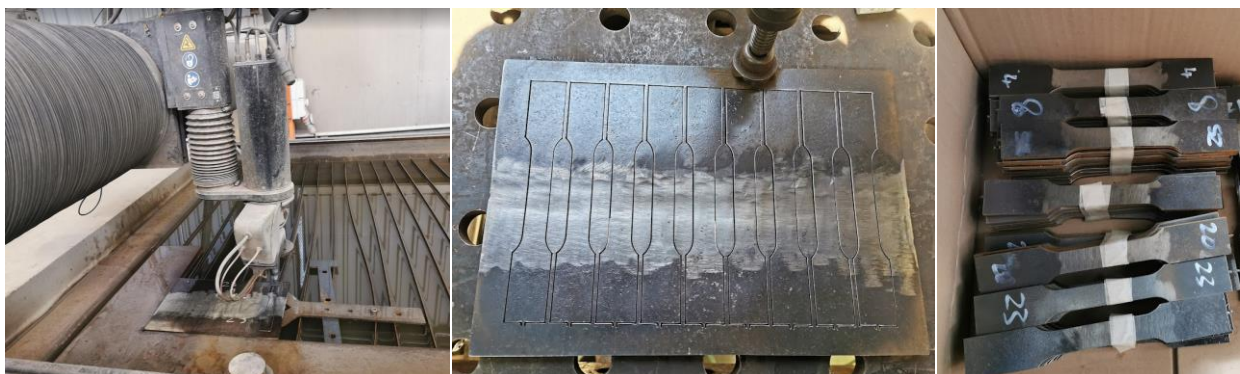


Figure 55: Manufactured specimens

Appendix B: Experimental results and analysis summary

B.1 Tension testing results

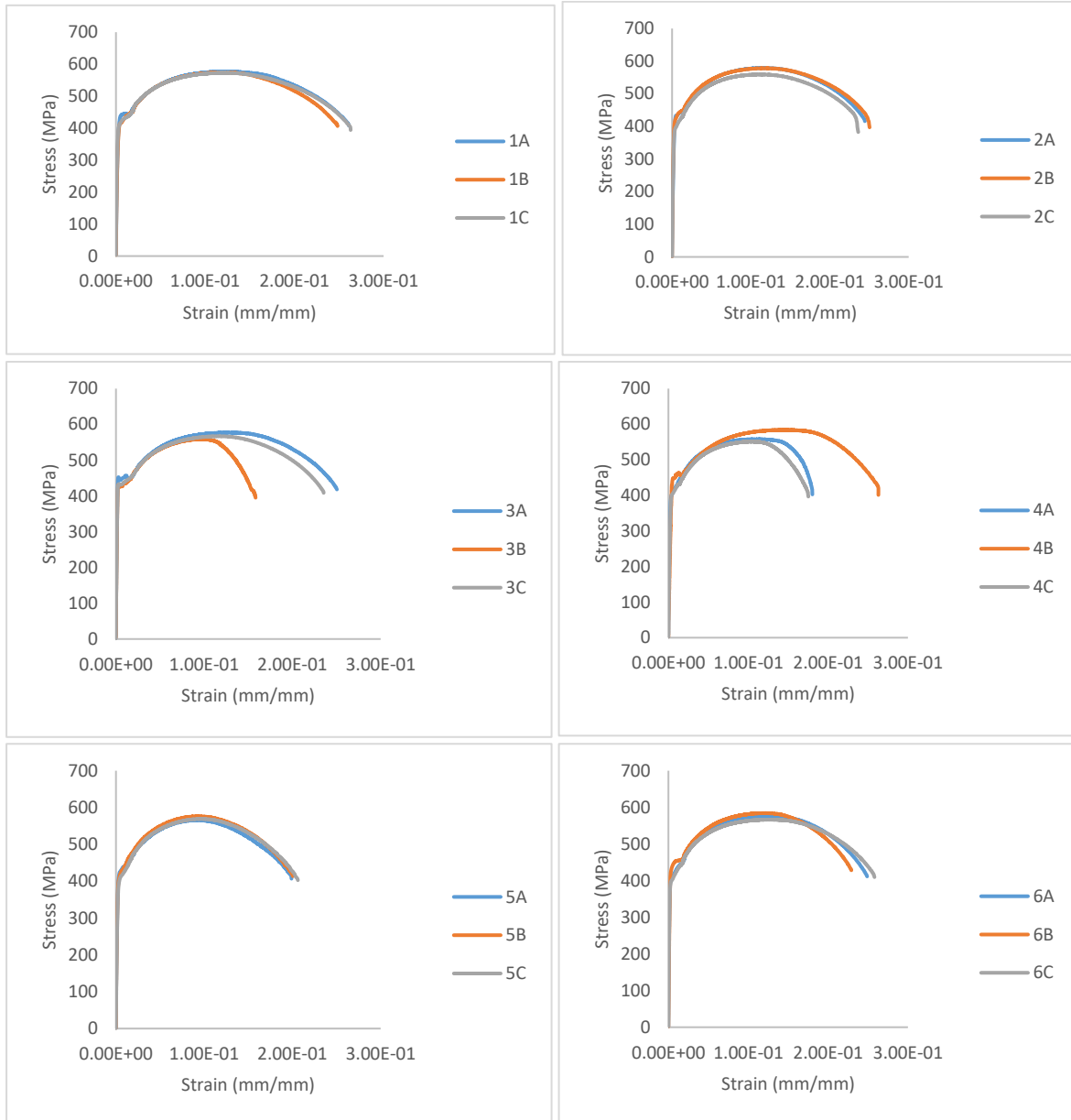


Figure 56: Stress - strain plot for three test specimens of experiments number 1 to 6

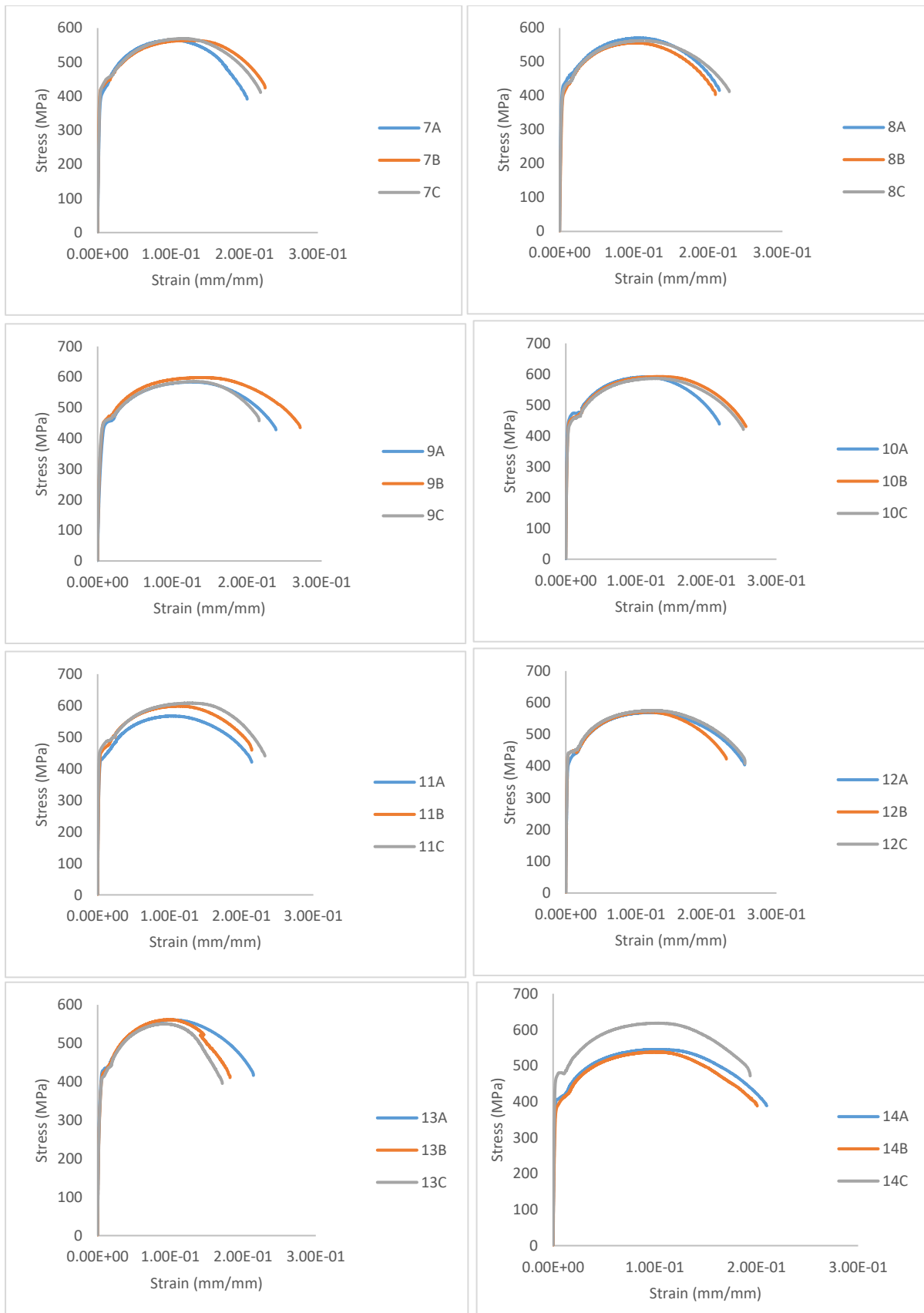


Figure 57: Stress - strain plot for three test specimens of experiments number 7 to 14

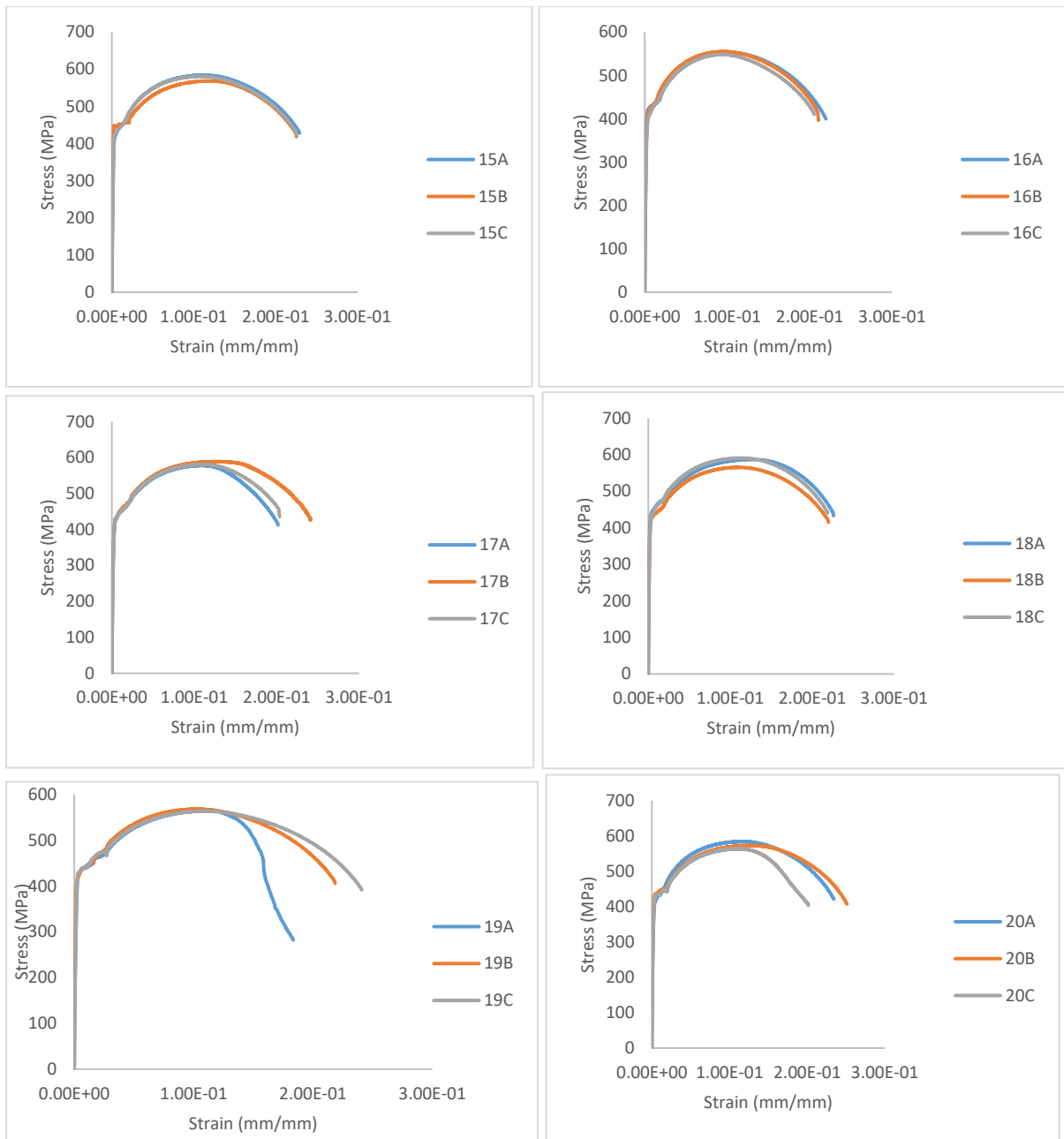


Figure 58: Stress - strain plot for three test specimens of experiments number 15 to 20

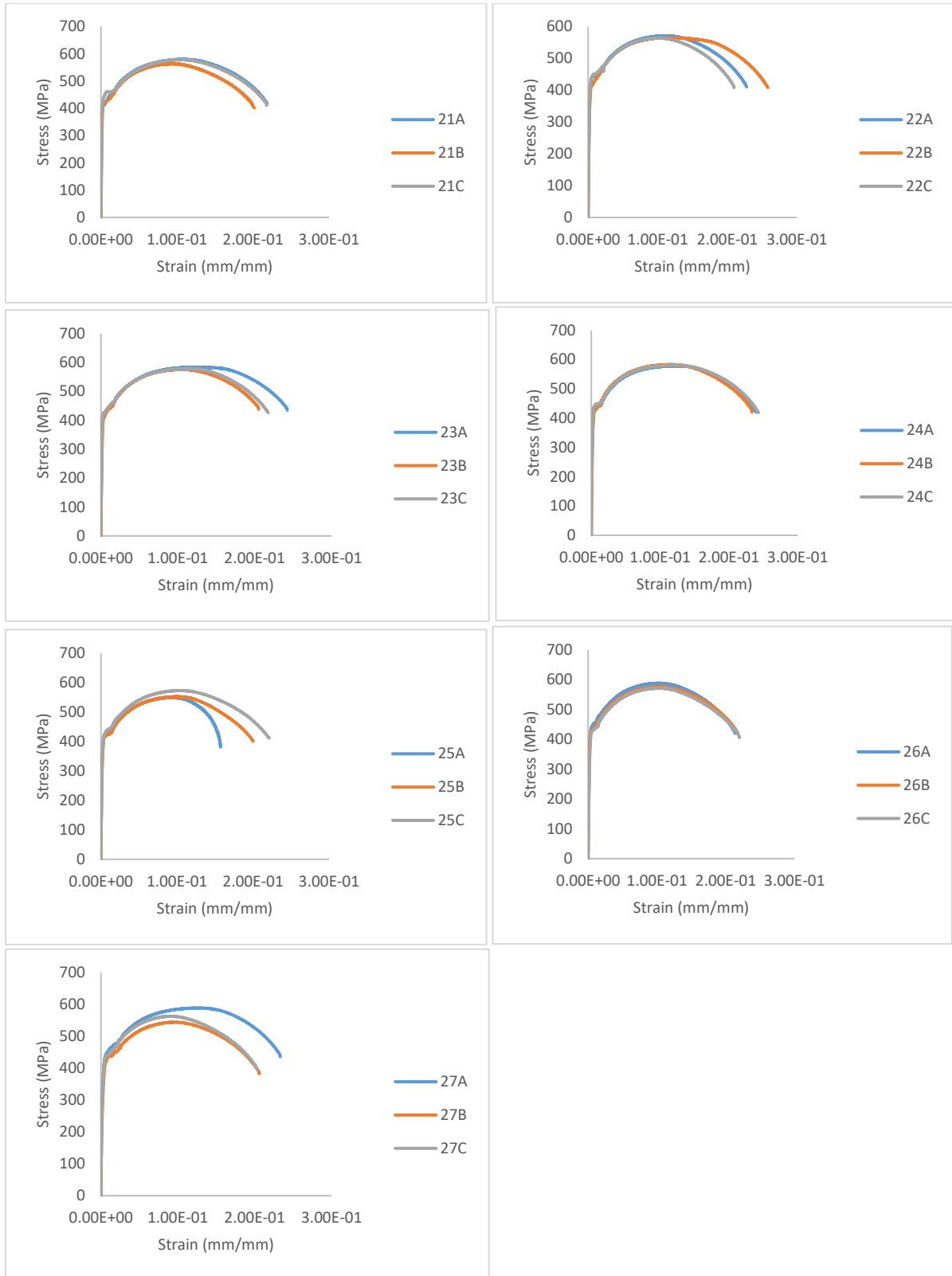


Figure 59: Stress - strain diagram for three test specimens of experiments number 21 to 27

B.2 Tensile experimental data analysis

Table 11: Ultimate tensile strength data analysis

	B1				B2				B3			
	C1	C2	C3	Sum X_{ij}	C1	C2	C3	Sum X_{ij}	C1	C2	C3	Sum X_{ij}
A1	577	579	577	5143	580	566	575	5158	565	571	584	5156
	574	578.3	558.7		583.8	576.3	584.2		563.9	556.4	598.4	
	572.8	559.2	566.9		558	569.2	566.5		569	562.7	585.6	
Mean X_{ijk}	574	572	568		574	570	575		566	563	589	
Sum X_{ijk}	1723	1717	1703		1721	1711	1726		1698	1690	1768	
SS X_{ijk}	989928	982608	966450		988007	976127	992722		960743	951797	1042183	
A2	591	582	569	5258	561	545	584	5108	554	579	587	5150
	592	584	571		562	538	569		555.2	589	566	
	586	608	575		551	618	581		549	581	591	
Mean X_{ijk}	590	591	572		558	567	578		552	583	581	
Sum X_{ijk}	1770	1773	1715		1673	1701	1734		1657	1749	1744	
SS X_{ijk}	1043730	1048627	980315		932827	968409	1002157		915462	1019725	1013639	
A3	565	584	580	5139	571	583	578	5180	549	588	589	5105
	567.8	573	563.6		565.7	575.5	582.7		551.8	576.7	544.4	
	563.4	563.4	578.7		563.9	578.1	580.9		572.5	571.5	562.7	
Mean X_{ijk}	565	574	574		567	579	581		558	579	565	
Sum X_{ijk}	1696	1721	1722		1701	1737	1742		1673	1736	1696	
SS X_{ijk}	958590	987155	988939		964041	1005755	1011415	26827220	933311	1005057	959806	
Total X_k	5189	5211	5140	15539	5095	5149	5201	15445	5028	5175	5208	15411
Grand Mean	573											

B.3 Fatigue experimental data analysis

Table 12: Number of cycles to failure data analysis

	B1				B2				B3			
	C1	C2	C3	Sum X_{ij}	C1	C2	C3	Sum X_{ij}	C1	C2	C3	Sum X_{ij}
A1	26408	56638	50698		49020	34215	41174		48591	24803	55475	
	55915	26003	38068	253730	43633	42570	43044	253656	49716	47673	42924	269181
Mean X_{ijk}	41161	41321	44383		46326	38393	42109		49153	36238	49199	
Sum X_{ijk}	82323	82641	88766		92653	76785	84218		98307	72476	98399	
SS X_{ijk}	3823831391	3884028546	4019438161		4306795210	2982905605	3548068596		4832760456	2887880073	4919909909	
A2	54847	45822	38718		71240	36585	70251		56569	49004	51379	
	56110	47287	44336	287121	61865	37807	50144	327892	64438	50054	45581	317025
Mean X_{ijk}	55479	46555	41527		66552	37196	60198		60503	49529	48480	
Sum X_{ijk}	110957	93109	83054		133105	74392	120395		121007	99058	96960	
SS X_{ijk}	6156529390	4335740439	3464792169		8902371304	2767828615	7449650964		7352256782	4906804689	4717471675	
A3	43444	51755	56596		36237	43937	42800		42681	68336	47075	
	35383	65734	58244	311156	63098	56334	55582	297988	66716	57715	30500	313023
Mean X_{ijk}	39413	58744	57420		49667	50135	49191		54699	63026	38787	
Sum X_{ijk}	78827	117489	114840		99335	100271	98382		109397	126051	77575	
SS X_{ijk}	3139322530	6999520011	6595488591		5294448741	5103975778	4921172612		6272692769	8000845381	3146297116	
Total X_k	272106	293239	286660	852006	325092	251448	302995	879536	328711	297585	272934	899229
Grand Mean	48718											

B.4 Stereoscope for tension test

The 5 mm images of the stereoscope of the fractured specimens are depicted below.



Figure 60: Welded joint 3A

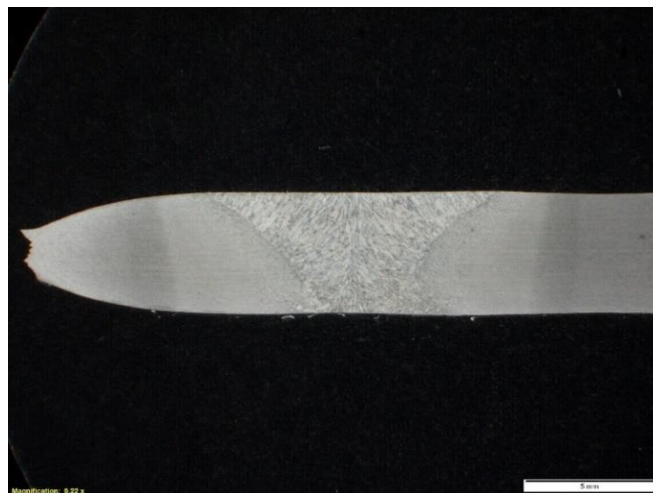


Figure 61: Welded joint 11C



Figure 62: Welded joint 27A